

1-1-2010

# Enzymology And Medicinal Chemistry Of N5-Carboxyaminoimidazole Ribonucleotide Synthetase : A Novel Antibacterial Target

Hanumantharao Paritala  
*Wayne State University*

Follow this and additional works at: [http://digitalcommons.wayne.edu/oa\\_dissertations](http://digitalcommons.wayne.edu/oa_dissertations)

---

## Recommended Citation

Paritala, Hanumantharao, "Enzymology And Medicinal Chemistry Of N5-Carboxyaminoimidazole Ribonucleotide Synthetase : A Novel Antibacterial Target" (2010). *Wayne State University Dissertations*. Paper 26.

This Open Access Dissertation is brought to you for free and open access by DigitalCommons@WayneState. It has been accepted for inclusion in Wayne State University Dissertations by an authorized administrator of DigitalCommons@WayneState.

**ENZYMOLOGY AND MEDICINAL CHEMISTRY OF N<sup>5</sup>-  
CARBOXYAMINOIMIDAZOLE RIBONUCLEOTIDE SYNTHETASE:  
A NOVEL ANTIBACTERIAL TARGET**

by

**HANUMANTHARAO PARITALA**

**DISSERTATION**

Submitted to the Graduate School

of Wayne State University,

Detroit, Michigan

in partial fulfillment of the requirements

for the degree of

**DOCTOR OF PHILOSOPHY**

2010

MAJOR: PHARMACEUTICAL SCIENCES

Approved by:

\_\_\_\_\_  
Advisor

\_\_\_\_\_  
Date

\_\_\_\_\_

\_\_\_\_\_

\_\_\_\_\_

\_\_\_\_\_

## **DEDICATION**

To my parents and brothers.

## **ACKNOWLEDGMENTS**

I would like to take this opportunity to thank so many people without whom it would have been impossible to complete this work. I owe deepest gratitude to my advisor Prof. Steven Firestine. His philosophical, conceptual, financial as well as moral support helped me to make this graduate study an outstanding experience. His conversations with me are always thought provoking and inspiring. I think I learnt not only the research but also the way of life from him. His suggestions and guiding principles are more valuable to me. I thank him from the core of my heart.

Besides my advisor, I would like to thank the rest of my dissertation committee: Prof. Patrick Woster, who gave me invaluable suggestions; Prof. Anjaneyulu Kowluru, for his timely suggestions and prompt reviewing of my work; and Prof. Christine Chow, for her insightful comments and suggestions for my dissertation.

I also wish to thank Dr William Lindblad, Dr Hanley Abramson and Dr David Oupicky for their help as graduate officers.

I would like to acknowledge Prof. Hazel Holden of University of Wisconsin, Madison, for her collaboration on this research and for her suggestions.

I am thankful to Wayne State University for providing me the graduate research assistance throughout my research; American Chemical Society, Medicinal Chemistry Division for travel award.

Special thanks go to Dr George Corcoran, chairman, Department of Pharmaceutical Sciences for creating such a wonderful environment to work.

I would like to extend my thanks to all the faculty, staff and colleagues of the department for their help and support, directly or indirectly.

I would also like to thank Firestine lab members Dr. Mahender Dewal, for his insightful discussions on various projects and for his friendship; Dr Shahid Islam for his suggestions and friendship. I thank past Firestine lab members Dr Sreeman Kumar Mamidyala for his valuable suggestions and help during my initial stages of dissertation and Dr Sunil Vooturi for his support.

Words are not enough to express my profound gratitude towards my parents, for their love, support and blessings. I am grateful to my brothers for their love and support. My special thanks to my wife, Sireesha, for her love and support on personal front.

Finally, I am thankful to the *almighty* for guiding me and showing me the right path.

## TABLE OF CONTENTS

Dedication.....	ii
Acknowledgements.....	iii
List of Tables.....	viii
List of Figures.....	ix
List of Schemes.....	xi

### CHAPTER 1 – INTRODUCTION

1.1. Introduction.....	1
1.2. Purine biosynthetic pathway.....	4
1.2.1. Salvage pathway.....	5
1.2.2. The “classical” <i>de novo</i> purine biosynthetic pathway.....	5
1.2.2.1. Divergence in <i>de novo</i> purine biosynthesis.....	10
1.2.3. Structure and function similarities among purine biosynthetic enzymes.....	14
1.2.3.1. Class I and Class II PurEs.....	14
1.2.3.2. ATP-grasp superfamily enzymes in purine biosynthesis.....	15
1.2.4. Genetic studies support <i>de novo</i> purine biosynthesis as an antimicrobial target.....	16

## CHAPTER 2- RESULTS

2.1.1. Site-directed mutagenesis on the AIR binding site.....	19
2.1.1. A. ATP binding site.....	20
2.1.1. B. AIR binding site.....	21
2.1.1. C. Kinetic and thermodynamic characterization of site-directed mutants	24
2.1.1. D. Bicarbonate-dependent ATPase activity of the enzyme.....	27
2.1.2. Modeling carboxyphosphate into the active site of N <sup>5</sup> -CAIR synthetase...	28
2.1.2. A. Computational studies on carboxyphosphate.....	29
2.1.2. B. Modeling of carboxyphosphate in the N <sup>5</sup> -CAIR synthetase active site	31
2.1.3. Proposed mechanism of N <sup>5</sup> -CAIR synthetase.....	36
2. 2. Discovery of selective N <sup>5</sup> -CAIR synthetase inhibitors.....	37
2. 2.1. Assay development for high-throughput screening.....	38
2. 2. 2. Screening compound libraries.....	39
2. 2. 3. Classification of the hits.....	40
2. 2. 3. A. Class I compounds inhibit N <sup>5</sup> -CAIR synthetase by reacting with AIR	40
2. 2. 3. B. Class II compounds are non-competitive inhibitors of N <sup>5</sup> -CAIR synthetase.....	44
2. 2. 3. C. Investigation of class III compounds.....	45

2. 2. 3. D. Class II compounds do not inhibit AIR carboxylase or SAICAR.....	46
synthetase	
2. 2. 4. Class II compounds inhibit <i>E. Coli</i> growth.....	47
2. 2. 5. Design and synthesis of a class II based photoreactive agent.....	47
2. 2. 5. A. Kinetic characterization of the photo reactive agent.....	49
2. 2. 6. Photo crosslinking studies.....	49
2. 2. 7. Study of photochemical properties of isatin.....	51
2. 2. 8. HPLC and GC/MS analysis of UV irradiated isatin and understanding The isatin photochemistry.....	53
2. 2. 9. LC-MS/MS analysis of the photo crosslinked protein.....	59
<b>CHAPTER 3 –DISCUSSION.....</b>	<b>63</b>
<b>CHAPTER 4 – CONCLUSIONS AND FUTURE DIRECTIONS.....</b>	<b>83</b>
<b>CHAPTER 5 – MATERIALS AND METHODS.....</b>	<b>87</b>
Appendix : List of Abbreviations.....	103
References .....	104
Abstract.....	120
Autobiographical Statement.....	123



## LIST OF TABLES

Table 1. List of abbreviations utilized for purine biosynthetic pathway intermediates.....	7
Table 2. Enzymes of purine biosynthetic pathway.....	8
Table 3. Kinetic and thermodynamic parameters determined for site-directed mutants.....	25
Table 4. Hits from HTS.....	41

## LIST OF FIGURES

Figure 1. <i>De novo</i> purine biosynthetic pathway.....	6
Figure 2. Divergence in purine biosynthetic pathway.....	13
Figure 3. Crystal structure of the N <sup>5</sup> -CAIR synthetase dimer from <i>Aspergillus clavatus</i> .....	19
Figure 4. N <sup>5</sup> -CAIR synthetase monomer from <i>Aspergillus clavatus</i> .....	20
Figure 5. ATP binding site of N <sup>5</sup> -CAIR synthetase.....	21
Figure 6. AIR binding site.....	23
Figure 7. The coupled N <sup>5</sup> -CAIR synthetase assay.....	25
Figure 8. Bicarbonate-dependent ATPase activity of N <sup>5</sup> -CAIR synthetase.....	28
Figure 9. Phosphoryl transfer onto bicarbonate.....	29
Figure 10. Computational studies on the conformations of carboxyphosphate....	31
Figure 11. ADP and Pi binding site of <i>E. coli</i> N <sup>5</sup> -CAIR synthetase.....	32
Figure 12. The model of the active site of <i>Aspergillus</i> N <sup>5</sup> -CAIR synthetase with ADP, AIR and carboxyphosphate bound.....	33
Figure 13. Close-up view of <i>Aspergillus clavatus</i> N <sup>5</sup> -CAIR synthetase active site with carboxyphosphate modeled into the site.....	34
Figure 14. Synthesis of N <sup>5</sup> -CAIR by N <sup>5</sup> -CAIR synthetase in the absence of ATP.	36
Figure 15. Proposed mechanism for N <sup>5</sup> -CAIR synthetase.....	37
Figure 16. Phosphomolybdate and malachite green assay for N <sup>5</sup> -CAIR synthetase.....	39
Figure 17. Michaelis-Menten plot of N <sup>5</sup> -CAIR synthetase in the presence of <b>1</b> ....	42

Figure 18. Kinetic characterization of class II inhibitors.....	45
Figure 19. Kinetic characterization of compound <b>13</b> .....	46
Figure 20. Kinetic characterization of compound <b>14</b> .....	46
Figure 21. Designed class II diazirine based photoreactive agent.....	48
Figure 22. Kinetic characterization of <b>15</b> .....	49
Figure 23 .Photocrosslinking studies of N <sup>5</sup> -CAIR synthetase with compound <b>15</b> .	50
Figure 24. Time dependent enzyme inactivation by <b>7</b> .....	52
Figure 25. HPLC analysis of the UV irradiated N-methyl isatin.....	54
Figure 26. (Top) Gas chromatogram of UV irradiated N-methyl isatin; (Middle) Mass spectra of 6.49 peak; (Bottom) Mass spectra of 7.23 peak.....	55
Figure 27. GC/MS analysis of N-methyl isatin irradiated in THF.....	57
Figure 28. GC analysis of the reaction shown in Scheme 8.....	59
Figure 29. N <sup>5</sup> -CAIR synthetase with the missing peptides shown in red. Ser227 is shown in green.....	61
Figure 30. Mechanism of biotin carboxylase and carbamoylphosphate Synthetase and N <sup>5</sup> -CAIR synthetase.....	64
Figure 31. Possible fate of carboxyphosphate during carboxylation reaction.....	65
Figure 32. Biotin carboxylase with bicarbonate and ADP in the crystal structure.....	71
Figure 33. Proposed mechanism for the formation of isatoic anhydride from isatin.....	80

## LIST OF SCHEMES

Scheme 1. Nonenzymatic production of N <sup>5</sup> -CAIR.....	11
Scheme 2. Proposed hypothesis for PurK and PurE biochemistry in eukaryotes.	12
Scheme 3. The proposed carboxyphosphate and acylphosphate intermediates in the reactions catalyzed by PurD, PurK, PurT and PurP.....	16
Scheme 4. Reaction of class I inhibitors.....	43
Scheme 5. Synthesis of compound <b>15</b> .....	49
Scheme 6. Photochemical turnover of <i>N</i> -methyl isatin to <i>N</i> -methyl isatoic anhydride.....	58
Scheme 7. Proposed transformation of <b>15</b> upon UV irradiation of <b>15</b> in water....	58
Scheme 8. Reaction of isatoic anhydride with benzyl alcohol.....	59

## CHAPTER 1.

### INTRODUCTION

#### 1.1. Introduction:

Arguably, one of the most significant discoveries in medicine was the discovery of penicillin by Alexander Fleming in 1921.<sup>1</sup> Since then, antibiotics have saved millions of lives and by the end of the 1960s the pharmaceutical industry had stockpiled such a large number of different antibiotics that it was possible to conclude that mankind had solved the problem of infectious disease.<sup>2</sup> However, almost from the first, resistance to antibiotics was detected in patients.<sup>3</sup> At first, resistance to antibiotics was not a major concern because numerous other antibiotics were available for use in treating resistant organisms. Yet, the continued increase in antibiotic-resistant pathogens has now become so pronounced that antibiotic resistance threatens to undermine public health. To demonstrate this, a recent report by Klevens *et al.* showed that the most common antibiotic-resistant pathogen, methicillin resistant *Staphylococcus aureus* (MRSA), caused approximately 19000 deaths in 2006 in USA.<sup>4</sup> This death toll is greater than that from AIDS in that year. MRSA infections have continued to increase. In the mid 1970s, MRSA infections constituted only 2% of all infections; yet, three decades later, MRSA accounts for 63% of *Staphylococcus* infections.<sup>4</sup> In a separate study conducted at the Detroit Receiving Hospital, the cost of hospitalization for treating MRSA bacteremia is double that for methicillin-sensitive *Staphylococcus aureus* (\$21,577 vs. \$11,668, respectively).<sup>5</sup>

There are three major classes of pathogens that represent the greatest threat from antibiotic resistance. The first is the multiple-antibiotic-resistant Gram positive pathogens, which include MRSA and vancomycin-resistant *Staphylococcus aureus* (VRSA) strains. Studies have shown that these strains add an additional three to four billion dollars to the national health care costs. The second class is the pandrug<sup>6</sup>-resistant Gram negative bacteria, which include *Acinobacter baumannii* and *Pseudomonas aeruginosa*. While the numbers of infections due to these pathogens are smaller than those from Gram positive microbes, they are more challenging to treat because of their unique cell wall and the presence of active efflux pumps. The final class of pathogens is the extensively drug-resistant *Mycobacterium tuberculosis*. Currently, the treatment for this pathogen includes a multi-drug regimen which must be given for about six months. The long treatment period leads to compliance problems which in turn leads to more resistant mycobacterium.<sup>7</sup>

The rise of antibiotic-resistant infections has placed pressure to develop new antibiotics. Historically, novel antibiotics have come from elaboration and modification of existing antibiotic scaffolds. These scaffolds (penicillins, cephalosporins, quinolones, macrolides and tetracyclines), discovered between the 1940 and 1960s, have formed the basis for most currently used antibiotics. This approach has been successful and has contributed to the large commercial market for antibiotics. For example, the early modifications of penicillin resulted in significantly better compounds with greater spectrum, potency, resistance to  $\beta$ -

lactamases, and better pharmacokinetics. Ampicillin, with an expanded spectrum and methicillin, with increased resistance to  $\beta$ -lactamases are successful examples of this approach. While making incremental changes on existing drugs may be a good short-term strategy, there is clearly a need to discover novel antibiotics with new mechanisms of action.

Unfortunately, despite the increase in infections due to resistant pathogens, the rate of new drugs entering the market is very low.<sup>7, 8</sup> Since 1995 only three new classes of antibiotics have been introduced. The first class is the oxazolidinones (linezolid), which inhibit protein synthesis. The second class is the lipopeptides, represented by daptomycin, which are believed to act by inhibiting plasma membrane functions. Finally, the third class of compounds are mutlins, which exert their action by inhibiting the 50s ribosomal subunit by binding to an unique binding site.<sup>7</sup> What is most worrisome about these new drugs is the fact that despite their recent introduction to the clinic, resistance to these agents has already been detected. For example, an *Enterococci* species resistant to linezolid was detected in 2003<sup>9</sup> and a *Corynebacterium jeikeium* strain resistant to daptomycin was discovered in 2009.<sup>10</sup>

One of the more important objectives for future antibiotic drug discovery is to identify new, validated targets. Attractive targets are gene products that must be expressed for the survival of the organism. These targets can be broadly distributed into generic classes such as DNA replication, RNA synthesis, protein biosynthesis, cell integrity, aromatic amino acid biosynthesis, cell division, two

component signal transduction, fatty acid biosynthesis, and isoprenoid biosynthesis.<sup>11-14</sup> These general categories have been validated, since commercially available antibiotics exist for each.<sup>11-14</sup> One unexplored pathway for antimicrobial drug design is *de novo* purine biosynthesis. As revealed in studies conducted in the 1980s, bacteria, yeast, and fungi synthesize the purine intermediate inosine monophosphate (IMP) via 11 enzymatic steps, whereas in humans, only 10 steps are required (Figure 1). The differences in pathways between microbes and humans indicate that purine biosynthesis may be an ideal target for antibiotic drug discovery.

#### 1.2. Purine biosynthetic pathway:

The purines, adenine and guanine, are essential chemical components utilized in various biochemical reactions in the cell. For example, these nucleotides are used for both DNA and RNA synthesis and they are used as precursors to second messengers in the cell. These nucleotides are essential carriers of chemical energy and they are components of the cofactors NAD, FAD, S-adenosylmethionine, and coenzyme A.

Given the importance of the purines, there are two pathways for their synthesis. The first, called the salvage pathway, prepares new purine nucleotides by recycling existing purine bases. The second pathway, *de novo* purine biosynthesis, prepares purine metabolites from non-purine precursors. This pathway is necessary for the cell division and is required for rapidly dividing cells.<sup>15, 16</sup>



### 1.2.1. Salvage pathway<sup>16</sup>:

Free purine bases are constantly released in cells during the metabolic degradation of nucleotides. To utilize these bases, the salvage pathway converts them into the corresponding nucleotide. One of the primary salvage pathways consists of a single reaction catalyzed by adenosine phosphoribosyltransferase, in which free adenine reacts with phosphoribosyl pyrophosphate (PRPP) to yield the corresponding adenine nucleotide. Free guanine and hypoxanthine (the deamination product of adenine) are salvaged in a similar fashion by the activity of the enzyme guanine phosphoribosyltransferase.

The amount of nucleotides produced from the salvage pathway is quite low, roughly 1% or less of the amount required for synthesizing the cell's DNA. Therefore, cells must continue to synthesize nucleotides by the *de novo* purine biosynthetic pathway so that nucleic acids can be synthesized.<sup>15, 16</sup>

### 1.2.2. The "classical" *de novo* purine biosynthetic pathway<sup>15, 17</sup>:

*De novo* purine biosynthesis was elucidated in the 1950s by Buchanan and co-workers.<sup>15</sup> They determined that the pathway contained 10 enzymatic steps which converted PRPP into Inosine monophosphate (IMP). The pathway was believed to be universal in all organisms.<sup>15</sup>

In *de novo* purine biosynthesis PRPP provides the foundation on which the bases are constructed step by step (Figure 1).<sup>1</sup>

---

<sup>1</sup> The naming of the purine biosynthetic enzymes and intermediates can be confusing. To aid the reader, tables 1 and 2 contain a complete list of acronyms of the purine biosynthetic enzymes, intermediates and abbreviations for those intermediates.



**Table 1.** List of abbreviations utilized for purine biosynthetic pathway intermediates.

Abbreviation of intermediate	Expanded name
PRPP	5-Phosphoribosylpyrophosphate
PRA	5-Phospho-D-ribosylamine
GAR	Glycinamide ribonucleotide
FGAR	N-Formylglycinamide ribonucleotide
FGAM	N-Formylglycinamide ribonucleotide
AIR	Aminoimidazole ribonucleotide
N <sup>5</sup> -CAIR	N <sup>5</sup> -Carboxyaminoimidazole ribonucleotide
CAIR	Carboxyaminoimidazole ribonucleotide
SAICAR	Succino 5-aminoimidazole-4-carboxamide ribonucleotide
AICAR	Aminoimidazole-4-carboxamide ribonucleotide
FAICAR	5-Formamido-4-imidazolecarboxamide ribonucleotide
IMP	Inosine monophosphate

**Table 2.** Enzymes of Purine biosynthetic pathway:

Gene name	Enzyme name
PurF	Amidophosphoribosyltransferase
PurD	Glycinamide ribonucleotide (GAR) synthetase
PurN	Glycinamide ribonucleotide (GAR) transformylase
PurT (prokaryotic)	Formylglycinamide ribonucleotide(FGAR) synthetase
PurL	Formylglycinamide ribonucleotide (FGAR) synthetase
PurM	Aminoimidazole ribonucleotide (AIR) synthetase
PurE (Class II)	Aminoimidazole ribonucleotide (AIR) carboxylase
PurK (prokaryotic)	N <sup>5</sup> -Carboxyaminoimidazole ribonucleotide (N <sup>5</sup> -CAIR) synthetase
PurE (Class I) (prokaryotic)	N <sup>5</sup> -Carboxyaminoimidazole ribonucleotide (N <sup>5</sup> -CAIR) mutase
PurC	N-Succinyl-5-aminoimidazolyl-4-carboxamide ribonucleotide (SAICAR) synthetase
PurB	SAICAR lyase
PurH	5-Aminoimidazole-4-carboxamide ribonucleotide (AICAR) transformylase
PurP (prokaryotic)	Flavin 5-aminoimidazole-4-carboxamide ribonucleotide (AICAR) synthetase
PurJ	Inosine monophosphate (IMP) cyclohydrolase
PurO (prokaryotic)	Inosine monophosphate (IMP) cyclohydrolase

The first step, which is the committed step, is the displacement of pyrophosphate from PRPP by ammonia to produce 5-phosphoribosylamine (PRA). Amidophosphoribosyltransferase (PurF) catalyzes this reaction. In the second step, glycine is coupled to the amine group of PRA to produce glycinamide ribonucleotide (GAR). GAR synthetase (PurD) catalyzes this reaction. The next reaction is the transfer of a formyl group from N<sup>10</sup>-formyltetrahydrofolate to the amino group of GAR to form N<sup>10</sup>-formyl glycinamide ribonucleotide (FGAR). This step is catalyzed by GAR transformylase (PurN). In the fourth step, the enzyme formylglycinamidase synthetase converts FGAR to FGAM. Aminoimidazole ribonucleotide (AIR) is synthesized in the fifth step by the action of the enzyme aminoimidazole ribonucleotide synthetase (PurM). This step results in the synthesis of the first heterocycle of the pathway. AIR and CO<sub>2</sub> are directly converted to CAIR by the enzyme AIR carboxylase.

In the seventh step, the carboxyl group of CAIR is phosphorylated and the phosphate is displaced by the amino group of aspartate to produce succinylaminoimidazole carboxamide ribonucleotide (SAICAR). This step is catalyzed by SAICAR synthetase (PurC). In the eighth step, fumarate, an intermediate in the citric acid cycle, is eliminated from SAICAR to yield aminoimidazole 4-carboxamide ribonucleotide (AICAR). This step is catalyzed by SAICAR lyase. AICAR is converted to formamidoimidazole carboxamide ribonucleotide (FAICAR) with the help of N<sup>10</sup>-formyltetrahydrofolate and AICAR

transformylase (PurH). The final intermediate cyclizes with the loss of water by a cyclohydrolase to form IMP<sup>18</sup>.

#### 1.2.2.1. Divergence in *de novo* purine biosynthesis:

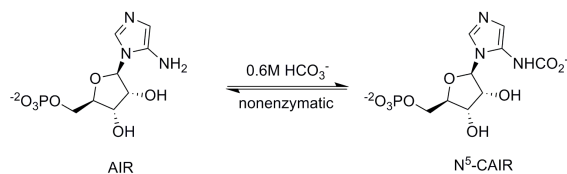
The only carbon-carbon bond forming reaction in *de novo* purine biosynthesis occurs in the sixth step (Figures 1, 2). In this reaction, AIR carboxylase catalyzes the conversion of AIR to CAIR. Studies of the step in bacteria, yeast and fungi were initiated by attempting to identify the AIR carboxylase gene in these microbes. In these single-cell organisms, the gene is encoded by the PurE locus. In the late 1980s, genomic sequence analysis experiments conducted by Zengado *et al.* and Watanabe *et al.* identified two distinct genes within this locus and they termed these PurE and PurK.<sup>19</sup> In seminal experiments conducted by Zalkin using chicken liver cDNA, he found a 429 amino acid protein that corresponded to PurE locus.<sup>19, 20</sup> This protein appeared to have functions similar to bacterial PurE-PurC, yet surprisingly, no enzyme with a PurK-like sequence was identified. This suggested that the chicken AIR carboxylase was similar to the bacterial PurE protein, yet there appeared to be no PurK protein. Thus, at the completion of these studies, an unanswered question remained regarding the role of PurK in the sixth step of the pathway.<sup>20</sup>

To address this question, both PurK and PurE gene products from bacteria were purified to homogeneity and their physical and catalytic properties were thoroughly studied by Firestine *et al.* and Mueller *et al.*<sup>19-23</sup> These groups observed that homogeneous PurE was capable of catalyzing the carboxylation of AIR to

CAIR; however, a high non-physiological concentration of  $\text{HCO}_3^-$  was required (0.18 M) to observe a reaction. Initial studies on PurK revealed that it had the ability to catalyze the hydrolysis of ATP to ADP and Pi. This ATPase activity, however, only occurred in the presence of AIR. Experiments designed to look for the production of CAIR concomitant with this AIR-dependent ATP hydrolysis were all negative. Experiments in which both proteins were included revealed the conversion of AIR to CAIR in the presence of “low” concentrations of  $\text{HCO}_3^-$  (100  $\mu\text{M}$ ), but only in the presence of ATP. Furthermore, every molecule of AIR consumed is accompanied by production of an equivalent amount of ADP and Pi were produced.<sup>23</sup> These studies revealed that both PurE and PurK appeared to be involved in the conversion of AIR to CAIR. PurE appeared to be the catalytic subunit based upon sequence alignments with AIR carboxylase from other organisms. The function of PurK was unknown, but was believed to be involved in the utilization of bicarbonate.<sup>19, 20</sup>

To explain the function of PurK, the Stubbe lab<sup>23</sup> took advantage of the work done by Alenin et al on the chemistry of AIR.<sup>24</sup> Alenin *et al* found that incubation of AIR with sub molar concentrations of bicarbonate lead to the non-enzymatic production of a new species. Subsequent studies indicated the new compound to be the N5-carbamate, which was named as N<sup>5</sup>-CAIR (Scheme 1).<sup>23</sup>

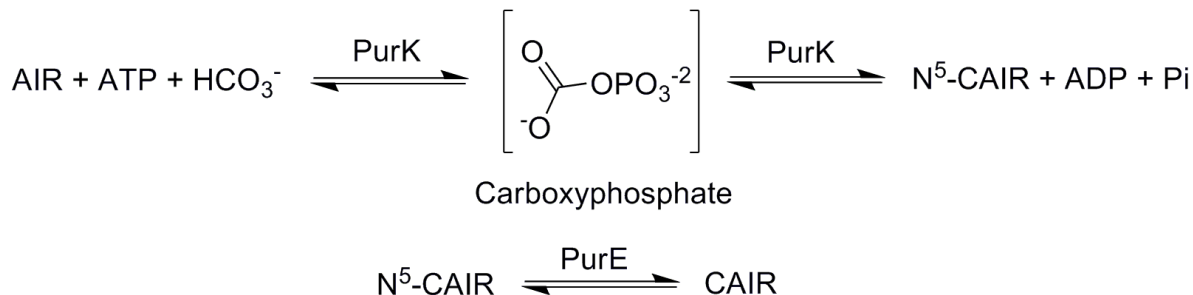
**Scheme 1.** Non enzymatic production of N<sup>5</sup>-CAIR



These studies revealed that at higher concentrations of bicarbonate, AIR is converted into N<sup>5</sup>-CAIR, and this result suggested that N<sup>5</sup>-CAIR might be the true substrate for PurE. Additional studies including NMR spectroscopy and kinetic analysis showed that this was the case.<sup>23</sup>

What is the function of PurK? Stubbe *et al.* hypothesized that the role of PurK was to produce N<sup>5</sup>-CAIR under low bicarbonate conditions. Subsequent NMR spectroscopic and kinetic analysis confirmed this hypothesis (Scheme 2). An investigation of the mechanism of the reaction by positional isotope studies suggested that the reaction proceeded via the formation of carboxyphosphate. Whether carboxyphosphate dissociated to give carbon dioxide, which is then attacked by AIR to form N<sup>5</sup>-CAIR or whether carboxyphosphate is directly attacked by AIR was unsolved at the time.<sup>23</sup>

**Scheme 2.** Proposed hypothesis for PurK and PurE biochemistry in eukaryotes





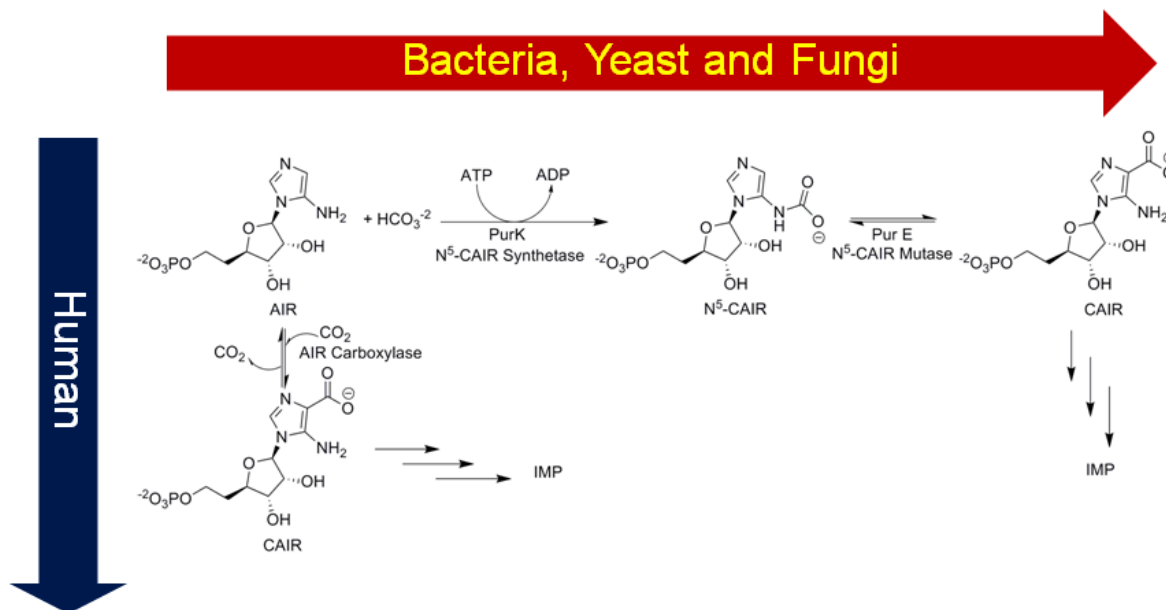


**Figure 2.** Divergence in purine biosynthetic pathway

The observed biochemical divergence in the pathway is echoed in the genetic and protein organization of the pathway. In higher eukaryotes, the de novo pathway uses a variety of multifunctional proteins in which multiple enzymatic activities are included within the same polypeptide. For example, steps 2, 3 and 5 are catalyzed by a trifunctional protein, while steps 6 and 7 are catalyzed by a bifunctional protein. Other multifunctional proteins are involved for other steps in the pathway. However, there exist at least three monofunctional enzymes (glutamine PRPP amidotransferase (PurF) (step 1), Flavin GAR amidotransferase (PurL) (step 4) and SAICAR lyase (PurH) (step 8)) that are needed as well. The fusion of multiple enzymes into one polypeptide chain has suggested that substrate channeling could be important; however, repeated efforts to identify channeling have failed. Recently work from the Benkovic lab demonstrated that a large, multiprotein complex called the purinosome forms

under low purine conditions.<sup>25</sup> This complex requires the presence of other cellular proteins which provides some rationale for why complexes were not previously observed. Lower eukaryotes have some multifunctional proteins, but not as many as seen in higher eukaryotes. In prokaryotes, such as *Escherichia coli*, monofunctional enzymes are found throughout this pathway, with the sole exception for the bifunctional enzyme which ends the pathway (aminoimidazolecarboxamide ribonucleotide transformylase (PurP) (step 10) and IMP cyclohydrolase (PurO) (step 11)).

### 1.2.3. Structure and function similarities among purine biosynthetic enzymes:

The crystallographic structures of all known purine biosynthetic enzymes have been solved<sup>17</sup>. The availability of these structures gives us the opportunity to study the structure-function similarities between the enzymes, and these relationships have important implications for the evolution of the proteins and the pathway.

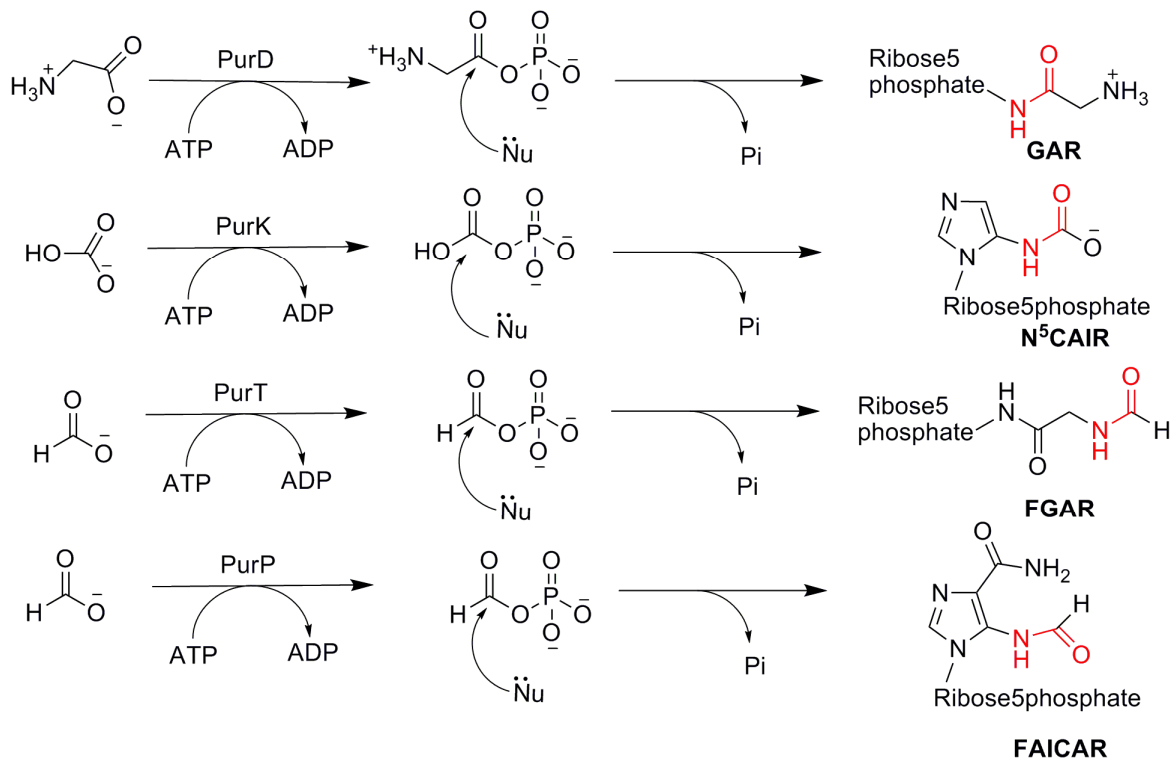
#### 1.2.3.1. Class I and Class II PurEs:

Class I and Class II PurEs represent an example of structurally and functionally similar enzymes in purine biosynthetic pathway. Class II enzymes catalyze the direct carboxylation of AIR to form CAIR, while class I enzymes require N<sup>5</sup>-CAIR, which is the product of PurK. Even though both of these enzymes are evolutionarily related, they are specific for their substrates.<sup>17, 26</sup>

### 1.2.3.2. ATP-grasp superfamily enzymes in purine biosynthesis:

There are four ATP-grasp superfamily enzymes in the purine biosynthetic pathway. These are PurD, PurT, PurK, and PurP. There are three other enzymes, PurL, PurM, and PurC in the purine biosynthetic pathway that utilize ATP, but do not belong to the ATP-grasp superfamily of enzymes. ATP-grasp enzymes are characterized by a unique three domain structure and the name of the superfamily is derived from the specific arrangement of domains needed to bind ATP. The three domains are usually called the A, B, and C domains. The A and B domains constitute the core of the protein and provide the binding sites for the substrates. The ATP binding site is located in the B domain. The phosphate chain of ATP is firmly anchored into a well-defined pocket created by the P-loop in the B domain. The P-loop is thought to provide critical residues needed for the stabilization of the intermediates during catalysis. All four purine enzymes share a highly homologous three-dimensional structure and are believed to proceed through a carboxyphosphate intermediate or acylphosphate intermediate to catalyze the reaction between the carboxylate and the amine as shown in Scheme 3. These similarities are also found in other enzymes that are not part of purine biosynthesis. For example, biotin carboxylase, D-alanine-D-alanine ligase, and carbamoyl phosphate synthetase all belong to the ATP-grasp superfamily. All of these enzymes proceed through similar reaction mechanisms as outlined in Scheme 4.<sup>17, 23</sup>

**Scheme 3.** The proposed acylphosphate and carboxyphosphate intermediates in the reactions catalyzed by PurD, PurK, PurT, and PurP. The amide group formed in each reaction is indicated in red color.



#### 1.2.4. Genetic studies support de novo purine biosynthesis as an antimicrobial target:

The purine and pyrimidine biosynthetic pathways of an organism have been shown to be linked to its virulence within the host.<sup>27, 28</sup> In fact, one antifungal agent, flucytosine, has already exploited the unique enzymes in the pyrimidine pathway of *Candida* and *Cryptococcus* spp. to inhibit effectively the growth of these yeasts *in vivo*.<sup>29</sup> An association between decreased virulence and purine auxotrophy in bacteria and fungi is also well documented. As early as 1950, Bacon *et al.* reported that *Salmonella* strains carrying a mutation in the purine biosynthetic pathway were markedly less virulent than the wild-type strain in

mice.<sup>30</sup> The decrease in the virulence of purine auxotrophs has also been found in *Salmonella typhimurium*<sup>27</sup>, *Salmonella dublin*<sup>27</sup>, *Klebsiella pneumoniae*<sup>31</sup>, *Bacillus anthracis*<sup>32</sup>, *Yersinia pestis*<sup>33</sup>, and *Candida albicans*.<sup>28, 34</sup> The association of decreased virulence and purine auxotrophy presumably results from the inability of the organism to multiply sufficiently in the host environment, reflecting the limited availability of nutrients or the inability to use exogenous metabolites from the host.<sup>35</sup> In a study carried out by Perfect *et al.*, the importance of an intact purine metabolic pathway in *C. neoformans* was examined using a meningitis animal model.<sup>29</sup> The inactivation of the phosphoribosylaminoimidazole carboxylase gene (Class II PurE or ADE2) in *C. neoformans* by mutagenesis and subsequent restoration by transformation were used to correlate directly the functional activity of this gene with the yeast's ability to grow within the subarachnoid space.<sup>29</sup> They found that the *C. neoformans ade2* auxotroph was not able to replicate, while complemented *C. neoformans ade2* restored the virulence and growth of the organism.<sup>29</sup> In an interesting study aimed at identifying the virulence factors in *Streptococcus pneumonia*, various purine enzymes including PurE, PurK, PurC, and PurL were identified as the virulence genes.<sup>36</sup>

Genetic studies conducted by Donovan *et al.* also confirmed that the *ADE2* gene and de novo purine biosynthesis were required for *Candida* pathogenicity.<sup>37</sup> In this study, the virulence of a *ade2*- *C. albicans* strain was evaluated in an immunosuppressed model of systemic candidiasis. The *ade2*- strain was unable to proliferate in the kidney and was nonpathogenic compared to its parent strain. The

reduced virulence of the strain resulted directly from the block in de novo purine biosynthesis and the inability of the organism to scavenge purines from the host. Further, they identified that only a single copy of the ADE2 gene was required to restore wild-type virulence.<sup>37</sup>

Analysis of virulence and inflammatory potential of *Shigella flexneri* purine biosynthesis mutants revealed that PurE and PurK genes are necessary for the virulence in animal models of shigellosis.<sup>38</sup> In their experiments, Cersini *et al*, constructed *S. flexneri* mutants of PurE and PurK. These mutant were shown to have no virulence, and the bacterial growth of these strains was very low in contrast to the unmodified strains of *S. flexneri*.<sup>38</sup>

In summary, PurK (N<sup>5</sup>-CAIR synthetase) is a purine biosynthetic enzyme that is unique to bacteria, yeast and fungi. Humans do not have this enzyme and have no homologs of this enzyme. Various genetic and biochemical studies have proved that PurK gene is a virulence factor.<sup>28, 29, 36-39</sup>

These studies indicate that N<sup>5</sup>-CAIR synthetase is a validated target for the development of novel antibiotics. In this thesis, I will present biochemistry, enzymology, and medicinal chemistry studies on N5-CAIR synthetase with the goal of understanding the mechanism of the enzyme and the identification of inhibitors of the enzyme.

## Chapter 2.

### RESULTS

#### 2.1.1. Site-directed mutagenesis on the AIR binding site:

The crystal structures of N<sup>5</sup>-CAIR synthetase from *Aspergillus clavatus* and *E. coli* with various substrates bound were obtained in collaboration with Professor Hazel Holden of the University of Wisconsin, Madison. Structural studies on N<sup>5</sup>-CAIR synthetase, as well as solution phase experiments, indicate that the enzyme exists as a dimer (Figure 3).<sup>40-42</sup> Each subunit of the dimer folds into three domains that are referred to as the A, B, and C domains. Domain A extends from Met1 to Ala119. Domain B is defined as the region from Glu120 to Trp183, while domain C is composed of amino acids from Ala184 to Arg382 (Figure 4). The A and C domains contribute to the subunit-subunit interface, while the B domain is oriented away from the main body of the molecule.<sup>42</sup>

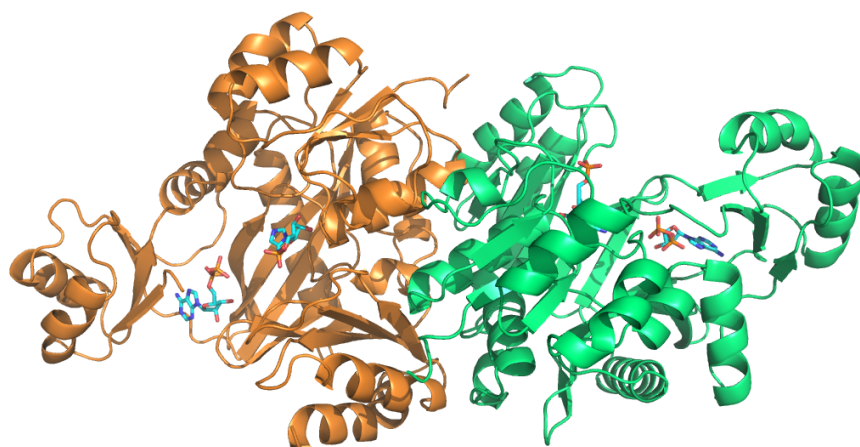


**Figure 3.** Crystal structure of the N<sup>5</sup>-CAIR<sup>41</sup> synthetase dimer from *Aspergillus clavatus* (PDB number: 3K5I). The two monomers of N<sup>5</sup>-CAIR synthetase dimer are shown in green and orange colors, respectively. Bound ADP and AIR ligands are shown in stick representation with blue color carbon atoms.

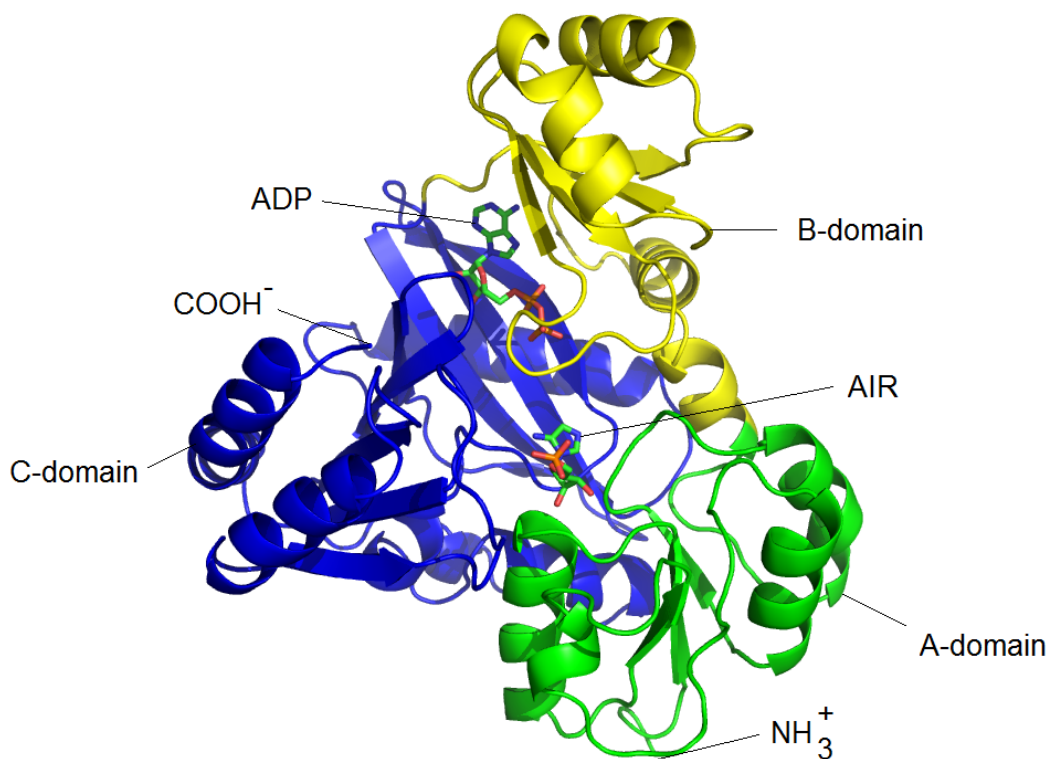


**Figure 4.**  $N^5$ -CAIR synthetase monomer from *Aspergillus clavatus*. Domain A is shown in green, domain B is shown in yellow, and domain C is shown in blue. Stick representations of AIR and ATP are shown in their respective binding sites.

#### 2.1.1. A. ATP binding site:

All of the residues responsible for binding ATP are contributed by the B and C domains (Figure 5).<sup>41</sup> There are two magnesium ions and both are octahedrally coordinated. One of the magnesium ions is surrounded by Glu254, Glu267, and the  $\alpha$ - and  $\gamma$ -phosphoryl oxygens. The other magnesium ion is coordinated by Glu267, and the  $\beta$ - and  $\gamma$ -phosphoryl oxygens of ATP. Glu267 also serves to bridge the two ions. The binding site contains two positively charged amino acids, Lys104 and Lys146, which neutralize the negatively charged phosphoryl groups of ATP. The adenine ring is bound by hydrogen bonds with Lys146 and Glu181, and



with the carbonyl oxygen of Lys182 and the backbone amide nitrogen of Ala184. The 2' and 3' hydroxyl groups hydrogen bond to the carboxylate of Glu189. The phenyl ring of Phe183 forms a T-shaped stacking interaction with the adenine ring.<sup>41</sup>

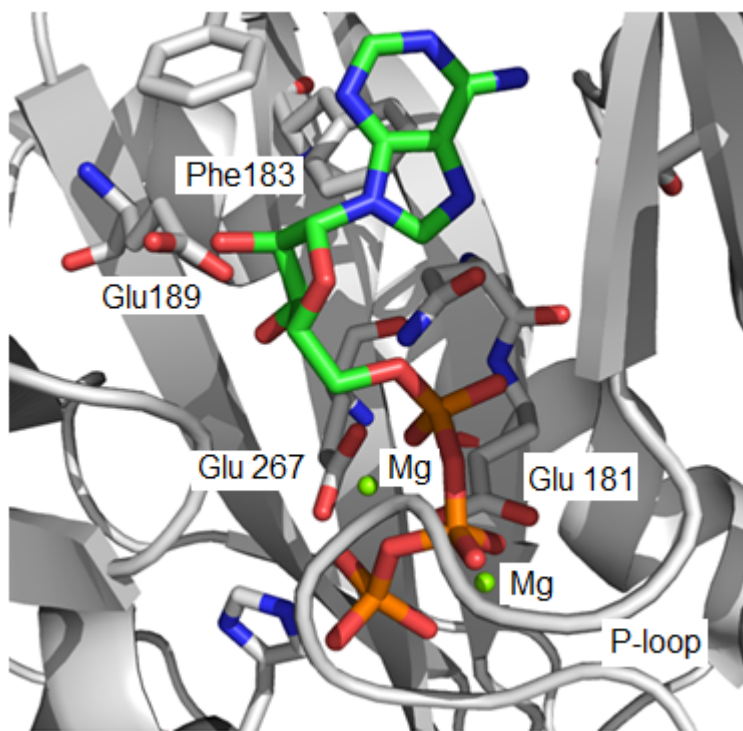


**Figure 5.** ATP binding site of N<sup>5</sup>-CAIR synthetase. The green spheres represent the Mg ions. Glu267 and Glu181 and the P-loop coordinate with the phosphate side chain of ATP. Glu189 hydrogen bonds to the ribose hydroxyl groups. Phe183 makes a T shaped  $\pi$ - $\pi$  interactions with adenine moiety of ATP.

#### 2.1.1. B. AIR binding site (Figure 6):

The crystal structure of N<sup>5</sup>-CAIR synthetase complexed with Mg:ADP and AIR is also a dimer. The two ligands are separated by 8 Å. The 5-aminoimidazole heterocycle of AIR is hydrogen bonded to the carboxylate of Asp153. Glu73 forms a hydrogen bond to the 2' and 3' hydroxyl groups of the ribose, whereas the

positively charged side chains of Arg155, Lys345, and Arg352 participate in electrostatic interactions with the 5' phosphate of AIR. An additional hydrogen bond is formed between Tyr152 and the phosphoryl oxygen of the AIR. Tyr152 also forms a stacking interaction with the aromatic imidazole ring of the substrate. Lys353 and Arg271, which are present within the active site, do not appear to interact directly with AIR. Rather, Lys353 hydrogen bonds to Asp153 and presumably stabilizes the conformation of the aspartic acid. The function of Arg271 is unknown; however, given its location, it is reasonable to speculate that Arg271 may play a role in bicarbonate binding and utilization.

The availability of the Mg:ADP:AIR structure provided us with the necessary information to begin to assess the function of amino acids located in the AIR binding site. Given the structural information, the investigations reported here focused on five residues (Glu73, Tyr152, Asp153, Arg155, and Lys353) for site-directed mutagenesis and analysis. Although Lys353 does not appear to directly contact AIR, we choose to investigate this residue because of its close proximity to Asp153. Each residue was mutated to alanine, and the resulting proteins were purified as His<sub>6</sub>-tagged proteins using a metal chelate column. The resulting purified proteins were judged to be at least 95% pure by gel electrophoresis. To investigate the role of each residue in AIR binding, each mutated protein was analyzed by steady-state kinetics and equilibrium dialysis.<sup>41</sup>

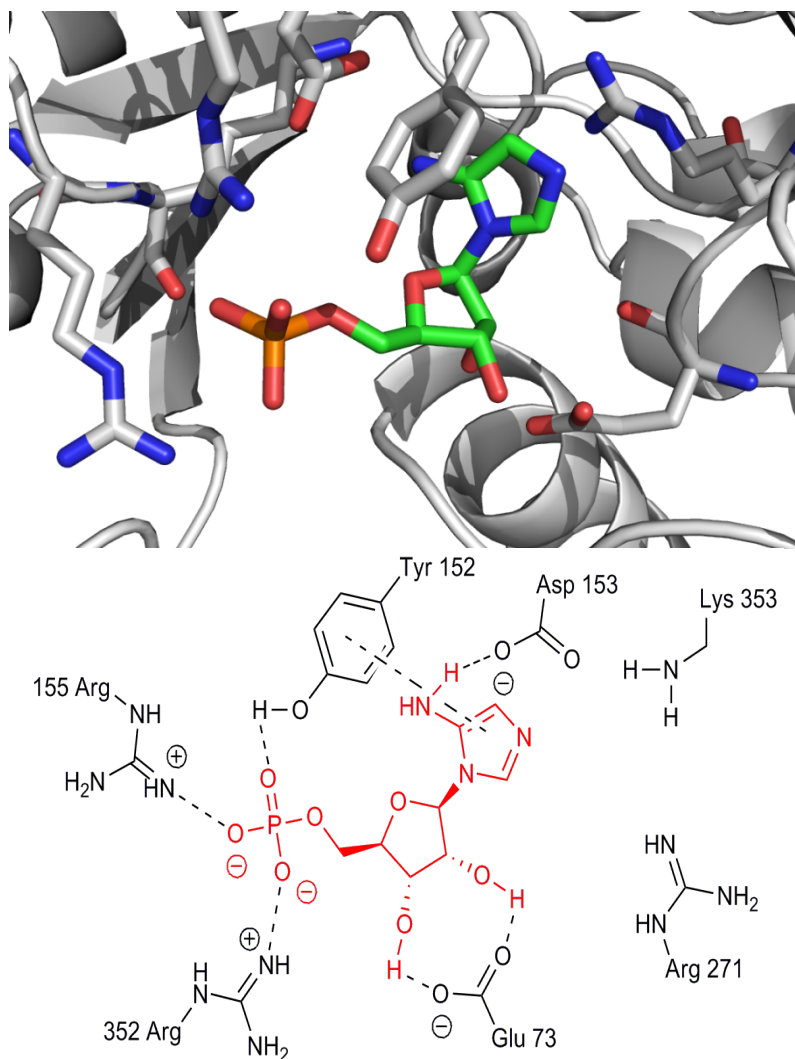


**Figure 6.** AIR binding site. Top: Close-up view of the AIR binding site from *Aspergillus*. The protein is shown in ribbon form and AIR is depicted in stick representation. Critical residues (see bottom portion of figure) are also shown in stick representation. Bottom: Detailed model of the AIR binding site. Asp153 interacts with the N5 of AIR via hydrogen bonding. The hydroxyl group of tyrosine hydrogen bonds to the phosphoryl oxygen of AIR while the phenyl ring forms an aromatic stacking interaction with the imidazole ring of AIR. Glu73 interacts with the 2' and 3' hydroxyl groups of ribose. Arg352 and Arg155 neutralize the negative charge of the phosphate of AIR.

### 2.1.1. C. Kinetic and thermodynamic characterization of site-directed mutants:

Kinetic characterization of the site-directed mutants was accomplished using the previously reported ADP-coupled pyruvate kinase and lactate dehydrogenase assay (Figure 7).<sup>43</sup> The initial velocity versus substrate concentration was fitted to the Michalis-Menten equation using Kaleidagraph to determine the kinetic parameters  $V_{max}$  and  $K_m$ . The catalytic turnover of the enzyme,  $k_{cat}$ , was determined from the equation  $k_{cat} = V_{max}/[E]$ .<sup>18</sup> The molecular weight of the dimer (89,486 daltons) was used for calculating the enzyme concentration.

It is well known that  $K_m$  cannot be used as an accurate determination of the dissociation constant ( $K_d$ ) for substrate binding, since  $K_m$  depends up on multiple rate constants. To determine  $K_d$ , we used equilibrium dialysis. This experiment was done by placing the enzyme (10-12  $\mu$ M) inside a dialysis bag and individual bags were dialysed against six different concentrations of AIR ranging from 1 to 300  $\mu$ M. The bound AIR was determined spectrophotometrically from the absorbance of the solution at 250 nm ( $\epsilon$  3,270  $M^{-1} cm^{-1}$ ). The concentration of AIR bound was plotted against the total amount of AIR added and the  $K_d$  was determined by fitting the data to the quadratic equation (Table 3 and Equation 1).

$$AIR_{bound} = \frac{[E_T + AIR_T + K_d - \sqrt{(E_T + AIR_T + K_d)^2 - 4E_T AIR_T}]}{2E_T} \quad (1)$$

For Equation 1,  $E_T$  is the total enzyme concentration,  $AIR_T$  is the total AIR concentration,  $AIR_{bound}$  is the amount of AIR bound to the enzyme, and  $K_d$  is the dissociation constant.

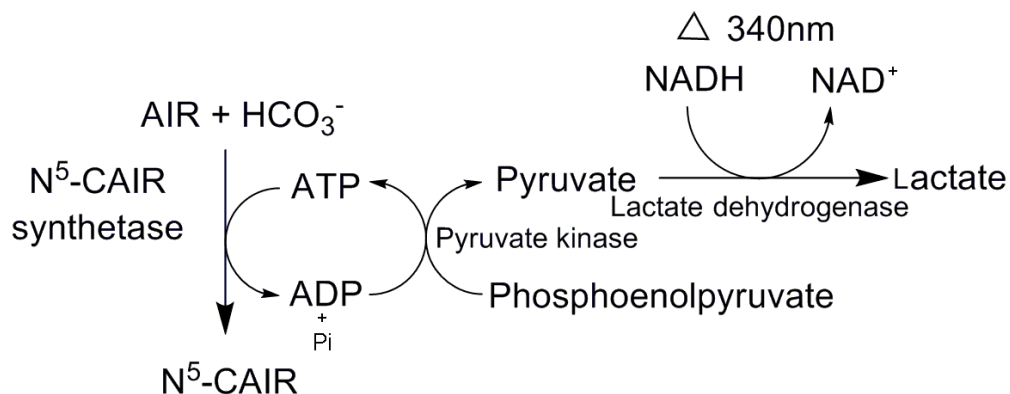


**Figure 7.** The coupled N<sup>5</sup>-CAIR synthetase assay

**Table 3.** Kinetic and thermodynamic parameters<sup>a</sup> determined for site-directed mutants.

Mutant	$V_{max}^b$ ( $\mu\text{M} \cdot \text{min}^{-1} \cdot \text{mg}^{-1}$ )	$K_m^b$ ( $\mu\text{M}$ )	$K_d^c$ ( $\mu\text{M}$ )	$k_{cat}^d$ ( $\text{min}^{-1}$ )	$k_{cat}/K_m$ ( $\mu\text{M}^{-1} \cdot \text{min}^{-1}$ )
Wild type	50±3	25±5	20±8	4140±250	330±70
D 153A	0.03±0.001	40±7	20±3	2.50±0.05	0.12±0.02
R 155A	6±0.5	180±40	1.6±0.5	510±40	6.0±1
Y 152A	1±0.2	460±120	50±20	110±20	0.50±0.2
E 73A	0.03±0.003	140±40	9±4	2.5±0.3	0.04±0.01
K 353A	inactive <sup>e</sup>	NA	20±5	NA	NA

<sup>a</sup>Reported errors are those obtained from curve fitting the appropriate data set. <sup>b</sup>Steady-state values were determined using the ATP-coupled assay system with the concentration of ATP and bicarbonate fixed and the concentration of AIR varied. <sup>c</sup>Calculated from equilibrium dialysis experiments using eq 1. <sup>d</sup>Calculated using the molecular weight of the dimer. Calculations were conducted assuming that 100% of the protein was active. <sup>e</sup>No measurable activity up to a protein concentration of 725  $\mu\text{g}/\text{mL}$ .

A comparison of the kinetic parameters for the wild-type enzyme versus the mutated enzymes revealed that all of the mutations decreased the catalytic proficiency of the enzyme by 50-8,000 fold (Table 3). The  $K_m$  of AIR for the mutant

proteins increased, yet surprisingly, for most, the  $K_d$  of AIR remained either unchanged or decreased. We expected that mutations in the substrate binding site would weaken the binding of AIR.

Mutation of Tyr152 resulted in a significant increase in  $K_m$  and only a moderate increase in  $K_d$ . This residue is of particular interest given the recent discovery that substitution of a tyrosine at this location in the *E. coli* PurT-encoded glycinamide transformylase confers  $N^5$ -CAIR synthetase activity to the enzyme<sup>44</sup>. As mentioned above, Tyr152 forms a hydrogen bond to the phosphate group of AIR and also has stacking interactions with the imidazole ring of the substrate. These interactions might be responsible for locking AIR into a specific conformation. We believe that in the absence of the Tyr152, AIR adopts a different conformation that is non-productive, thus resulting in the drastic decrease in enzyme proficiency ( $k_{cat}/K_M$ ) observed in this mutant.

The Glu 73A mutant displayed a 1,400 fold decrease in catalytic efficiency, yet structural information indicates that this residue is distal to the site for catalysis. We are uncertain why Glu73 has such a profound effect on catalysis. One possible explanation is that this residue is important in optimizing the alignment of AIR into the active site. Mutation to this residue did not directly alter the affinity of AIR binding, but instead may alter the alignment of AIR for nucleophilic attack.

One critical question regarding the mechanism of  $N^5$ -CAIR synthetase is the identity of the active site base that removes the proton from the exocyclic amine of AIR. Analysis of the crystal structures of the enzyme reveal that Lys 353

is  $\sim 4$  Å from the exocyclic amine of AIR, whereas Asp153 is only 3 Å distant. Replacement of Asp153 with alanine results in an enzyme with essentially the same  $K_m$  and  $K_d$  as the wild-type enzyme, but with a  $k_{cat}$  value more than 1,600-fold lower. Clearly, Asp153 is involved in catalysis, but not substrate binding. Mutation of Lys 353 to alanine generated an inactive enzyme. The mutant protein, however, was capable of binding AIR with the same affinity as the wild-type enzyme. On the basis of our structural information, we suggest that Lys 353 is too distant to function as the catalytic base and likely plays another role in catalysis. However, we realize that the existing kinetic information cannot definitively rule out Lys353 as the catalytic base.

#### 2.1.1. D. Bicarbonate-dependent ATPase activity of the enzyme:

To determine whether N<sup>5</sup>-CAIR synthetase can catalyze the half reaction (that is attack by bicarbonate onto ATP to generate carboxyphosphate), we determined the rate of ATP consumption in the presence of added bicarbonate, but in the absence of AIR. We measured ATP consumption via the pyruvate kinase and lactate dehydrogenase system. Incubation of 28 µg of enzyme with various concentrations of bicarbonate generated a dose-dependent increase in ATP consumption as shown Figure 8. This data indicates that N<sup>5</sup>-CAIR synthetase is capable of catalyzing the attack of ATP by bicarbonate. This half-reaction has also been observed for other ATP-grasp carboxylation enzymes.<sup>45</sup> The data were fitted to the Michelis-Menten equation to generate a  $K_{m\ app}$  of 3.2mM and  $V_{max}$  of

0.09  $\mu\text{mol}/\text{min}\cdot\text{mg}$ . The  $V_{\text{max}}$  for the half reaction is 800 times lower than for the full reaction ( $V_{\text{max}}$  for full reaction is 73  $\mu\text{mol}/\text{min}\cdot\text{mg}$ ).

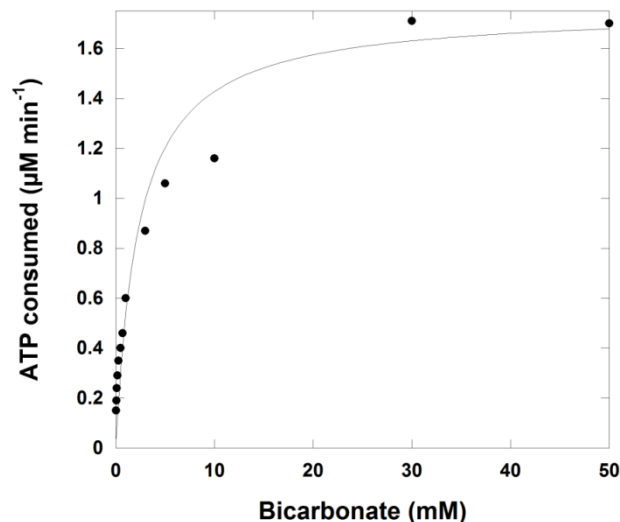


**Figure 8.** Bicarbonate dependent ATPase activity of  $\text{N}^5$ -CAIR synthetase. The ability of the enzyme to catalyze the attack of ATP by bicarbonate in the absence of AIR was measured using the coupled assay shown in figure 7. The curve shown is the fit of the data to the Michaelis-Menten equation.

#### 2.1.2. Modeling carboxyphosphate into the active site of $\text{N}^5$ -CAIR synthetase:

$\text{N}^5$ -CAIR synthetase in the presence of AIR, ATP, and  $[^{18}\text{O}]$ -bicarbonate catalyzes quantitative transfer of  $^{18}\text{O}$  from bicarbonate to inorganic phosphate.<sup>23</sup>  $\text{N}^5$ -CAIR synthetase also shows bicarbonate-dependent ATPase activity. These observations suggest that bicarbonate reacts with ATP to generate the highly reactive intermediate carboxyphosphate.<sup>23</sup> Carboxyphosphate has been implicated in the mechanism of other ATP-grasp enzymes including biotin carboxylase and carbamoyl phosphate synthetase.<sup>42, 46-50</sup> Carboxyphosphate, unfortunately, is highly unstable and has a predicted half life of 70 milliseconds.<sup>23</sup>



Indeed, direct experimental evidence for this intermediate has only been determined once for one enzyme.<sup>51</sup>

Since carboxyphosphate is critical to the mechanism of the enzyme, it would be of great utility to have the structure of this intermediate bound to the enzyme. Carboxyphosphate, however, is very unstable and is a transient intermediate in the reaction. Thus, a crystal structure of this intermediate bound to the enzyme is not possible. To circumvent this problem, we sought to generate a molecular model of carboxyphosphate bound to the enzyme from the available crystal structures.

#### 2. 1. 2. A. Computational studies on carboxyphosphate:

The use of bicarbonate as a nucleophile in phosphoryl transfer reactions was extensively investigated by Herschlag *et al.*<sup>52-54</sup> These studies revealed that phosphoryl transfer proceeds with the aid of an intramolecular hydrogen bond. This hydrogen bond seems to orient the negatively charged oxygens of bicarbonate away from the negatively charged phosphate group. The reaction and the proposed transition state is shown in Figure 9.<sup>52</sup>

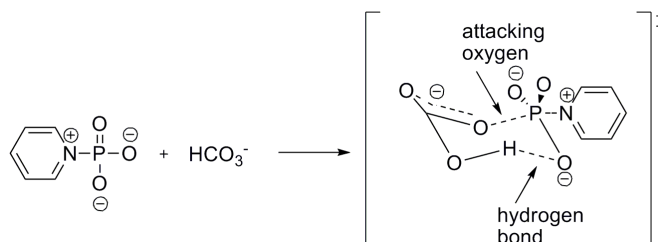


**Figure 9.** Phosphoryl transfer onto bicarbonate. In this reaction, pyridine phosphate is attacked by bicarbonate. Physical chemistry studies on this reaction reveal that the reaction proceeds via an intramolecular hydrogen bond.

Using this information, we modeled carboxyphosphate in both the pseudo-chair and extended conformations and subjected each conformation to quantum mechanical calculations (as executed by Gaussian) to determine the most stable conformation.<sup>41, 55</sup> The computational studies revealed that the pseudo-chair conformation is 13 kcal/mole more stable than the extended conformation (Figure 10). Given this and the physical chemistry studies by Herschlag and colleagues, it is logical to assume that during catalysis by N<sup>5</sup>-CAIR synthetase, the pseudo-chair conformation of carboxyphosphate is also formed.<sup>40</sup> The pseudo-chair conformation is in part stabilized by a hydrogen bond between the proton on the acid and one of the oxygens on the phosphate. In this arrangement, it is possible for the phosphate group in carboxyphosphate to act as a base to remove the proton. Such an intramolecular proton has been observed in the decomposition of carbamoyl phosphate.<sup>56</sup> To determine the relative energy difference between two pseudo-chair structures, we conducted quantum mechanical calculations. These calculations reveal that carboxyphosphate with the proton on the phosphate is more stable by 4.8 kcal/mole. The result of these two calculations suggested that carboxyphosphate adopts a conformation that allows rapid, non-enzyme mediated transfer of the proton from bicarbonate onto phosphate.

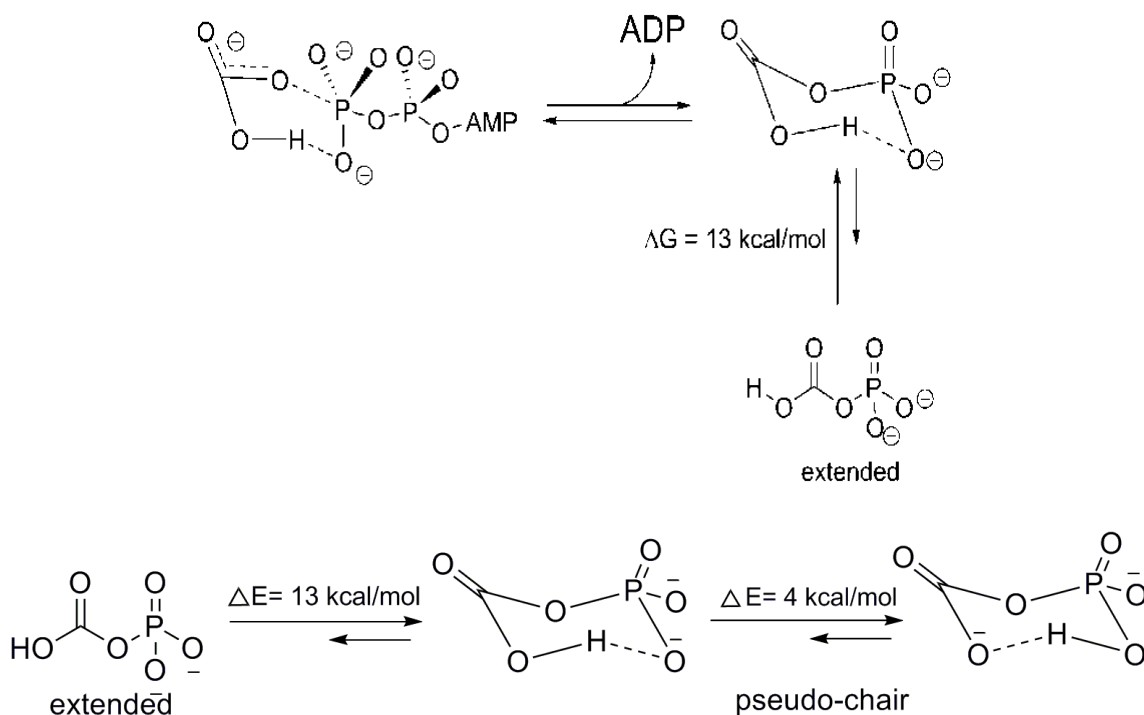


**Figure 10.** Top: Computational studies on the conformations of carboxyphosphate. Quantum mechanical calculations (Gaussian, B-3LYP-G\* basis set) showed that the pseudo-chair conformation is more stable than the extended conformation.

Bottom: Semi-empirical calculations on the conformation and hydrogen transfer of carboxyphosphate.

### 2.1.2. B. Modeling of carboxyphosphate in the N<sup>5</sup>-CAIR synthetase active site:

In order to model the pseudo-chair conformation of carboxyphosphate into the active site of N<sup>5</sup>-CAIR synthetase, we need to know the location of the carboxyphosphate binding site. To identify this site, we took advantage of the N<sup>5</sup>-CAIR synthetase:ADP:Pi:Mg crystal structure (Figure 11, PDB: 3ETJ). This structure was obtained when crystals of *E. coli* N<sup>5</sup>-CAIR synthetase were incubated with AIR and ATP.<sup>40</sup> The formation of ADP and Pi indicates that the enzyme is active in the crystal. This, in turn, suggests that the location of the

inorganic phosphate represents the site of carboxyphosphate binding since this phosphate group must come from this highly unstable intermediate. Superposition of the phosphate group of the pseudo-chair carboxyphosphate model with the phosphate of the crystal structure should provide a logical model for this intermediate bound to the enzyme. The resulting model can be found in Figures 12 and 13.

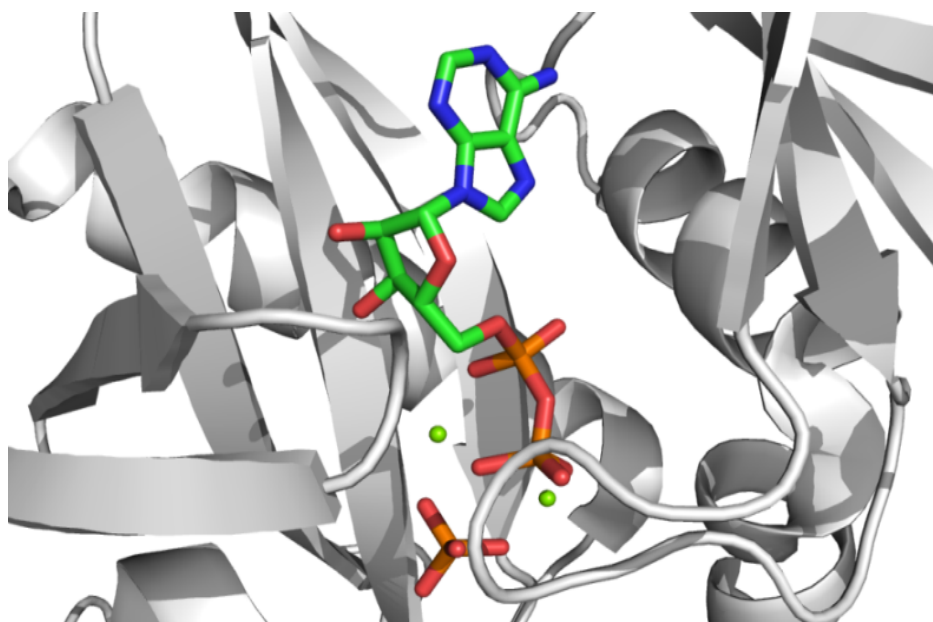


**Figure 11.** ADP and Pi binding site of *E. coli* N<sup>5</sup>-CAIR synthetase. The protein is shown as a grey ribbon, while the location of ADP and Pi is shown in stick representation with green carbon, orange phosphorous, blue nitrogen and red oxygen atoms. Mg<sup>2+</sup> atoms are shown as light green spheres.

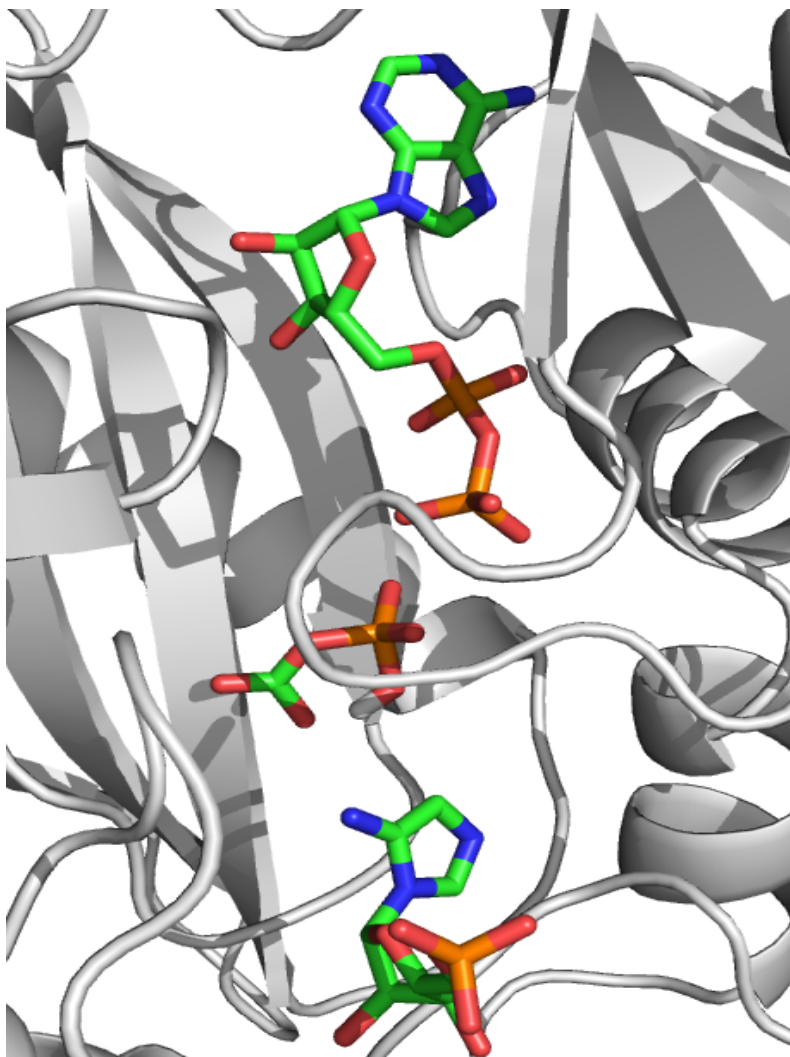


**Figure 12.** The model of the active site of *Aspergillus* N<sup>5</sup>-CAIR synthetase with ADP, AIR, and carboxyphosphate bound. Carboxyphosphate was modeled onto the location of Pi determined from the crystal structure of *E. coli* N<sup>5</sup>-CAIR synthetase (PDB: 3ETJ).<sup>41</sup> The location of ADP and AIR are experimentally determined (PDB: 3K5I).<sup>41</sup> The protein is shown as a grey ribbon with the molecules shown in stick representation with green carbon, orange phosphorous, blue nitrogen, and red oxygen atoms.

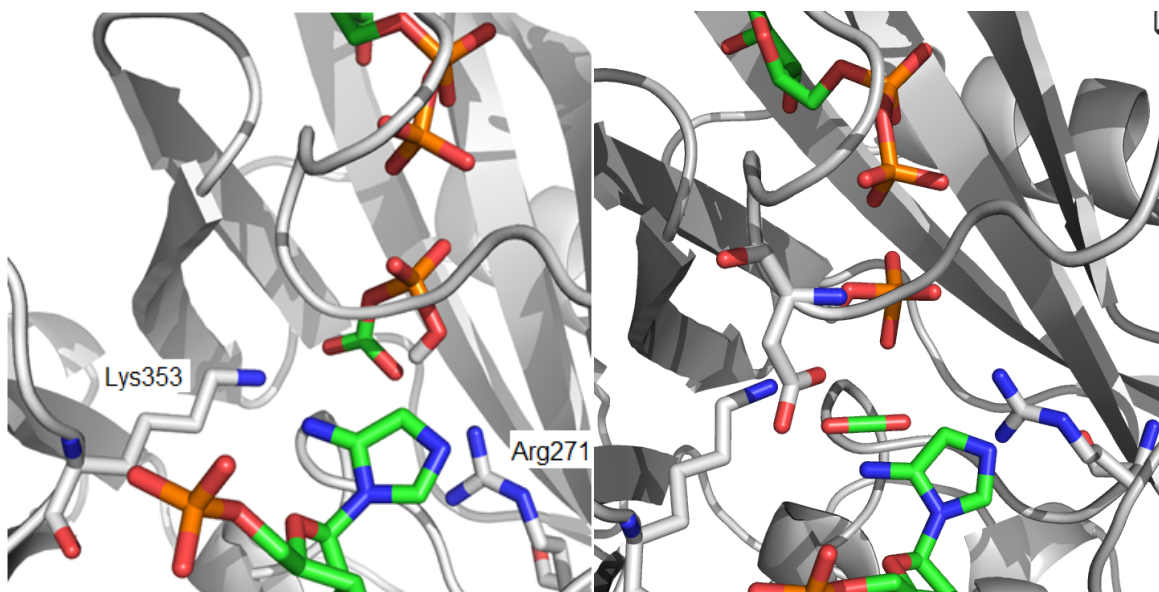


**Figure 13. (left).** Close-up view of *Aspergillus clavatus* N<sup>5</sup>-CAIR synthetase active site with carboxyphosphate modeled into the site. The picture shows the carbonyl oxygen atoms of carboxyphosphate are nicely placed between Arg271 and Lys353. The representations within the figure are the same as those found in Figure 10. **(Right)** The carbondioxide produced upon dissociation of carboxyphosphate is shown in the model.

An examination of the model (Figure 13) reveals that the two carbonyl oxygen atoms of carboxyphosphate are beautifully placed between Arg271 and Lys353. Thus, it is logical to conclude that these residues could aid in the formation or breakdown of this intermediate. Previous researchers have speculated that carboxyphosphate is the electrophile in other carboxylation enzymes (*i.e.* carbamoyl phosphate synthetase).<sup>51</sup> However, in our model, the distance between the exocyclic amine of AIR and the carbonyl carbon of carboxyphosphate is ~4 Å and the angle of approach is incorrect. This suggests that AIR does not directly attack carboxyphosphate. Instead, we propose that carboxyphosphate decomposes to CO<sub>2</sub> and HPO<sub>4</sub><sup>-</sup>. Decarboxylation of

carboxyphosphate may be catalyzed by an intramolecular proton abstraction by the phosphate group to yield  $\text{HPO}_4^-$ . This proposal is based upon computational studies, which show that the proton in carboxyphosphate prefers to be located on the phosphoryl group and the fact that  $\text{HPO}_4^-$  is the form of phosphate that is released by another ATP-grasp carboxylation enzyme, biotin carboxylase.<sup>23, 52, 57</sup> This reaction could also be aided by both Arg271 and Lys353.

The above hypothesis suggests that  $\text{N}^5$ -CAIR synthetase may have the ability to bind and stabilize  $\text{CO}_2$ . To investigate this hypothesis, we conducted an experiment to determine if  $\text{N}^5$ -CAIR synthetase is able to synthesize  $\text{N}^5$ -CAIR in the absence of ATP. Addition of 112  $\mu\text{g}$  of enzyme to a solution containing AIR and 20 mM  $\text{HCO}_3^-$  resulted in a decreased absorbance at 250 nm due to  $\text{N}^5$ -CAIR synthesis. Reactions conducted in the absence of the enzyme or in the presence of BSA instead of  $\text{N}^5$ -CAIR synthetase resulted in no  $\text{N}^5$ -CAIR production (Figure 14). This experiment provides definitive evidence that the enzyme utilize  $\text{CO}_2$  as a substrate.

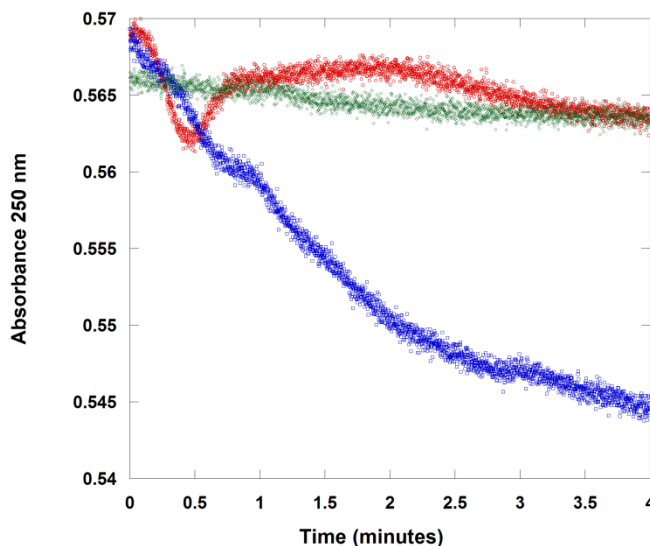


**Figure 14.** Synthesis of  $N^5$ -CAIR by  $N^5$ -CAIR synthetase in the absence of ATP. Red: AIR and bicarbonate, no enzyme; Green: AIR, bicarbonate and BSA instead of  $N^5$ -CAIR synthetase; Blue: AIR, bicarbonate and  $N^5$ -CAIR synthetase.

### 2.1.3. Proposed mechanism of $N^5$ -CAIR synthetase:

Our proposed mechanism is shown in Figure 15. In this mechanism, we start after the formation of carboxyphosphate. Carboxyphosphate is stabilized by Arg271 and Lys353, where each residue forms hydrogen and electrostatic bonds with the oxygen atoms of carboxyphosphate. Carboxyphosphate decomposes to  $HPO_4^{-2}$  and  $CO_2$  via intramolecular hydrogen abstraction. The resulting  $CO_2$  group is now positioned between Lys353 and Arg271. These residues, which likely are positively charged, should enhance the electrophilicity of  $CO_2$  by drawing electrons away from the carbon atom. An examination of the  $CO_2$  model indicates that  $CO_2$  is  $\sim 2.7 \text{ \AA}$  away from the amine of AIR and there is optimal alignment for nucleophilic attack by the exocyclic amine. Catalysis likely occurs in a concerted



fashion such that the amine of AIR attacks the carbon of CO<sub>2</sub> as Asp153 removes the proton from the amine. The resulting negative charge on the oxygen atom of the carbamate is stabilized by either Arg271 or Lys353.

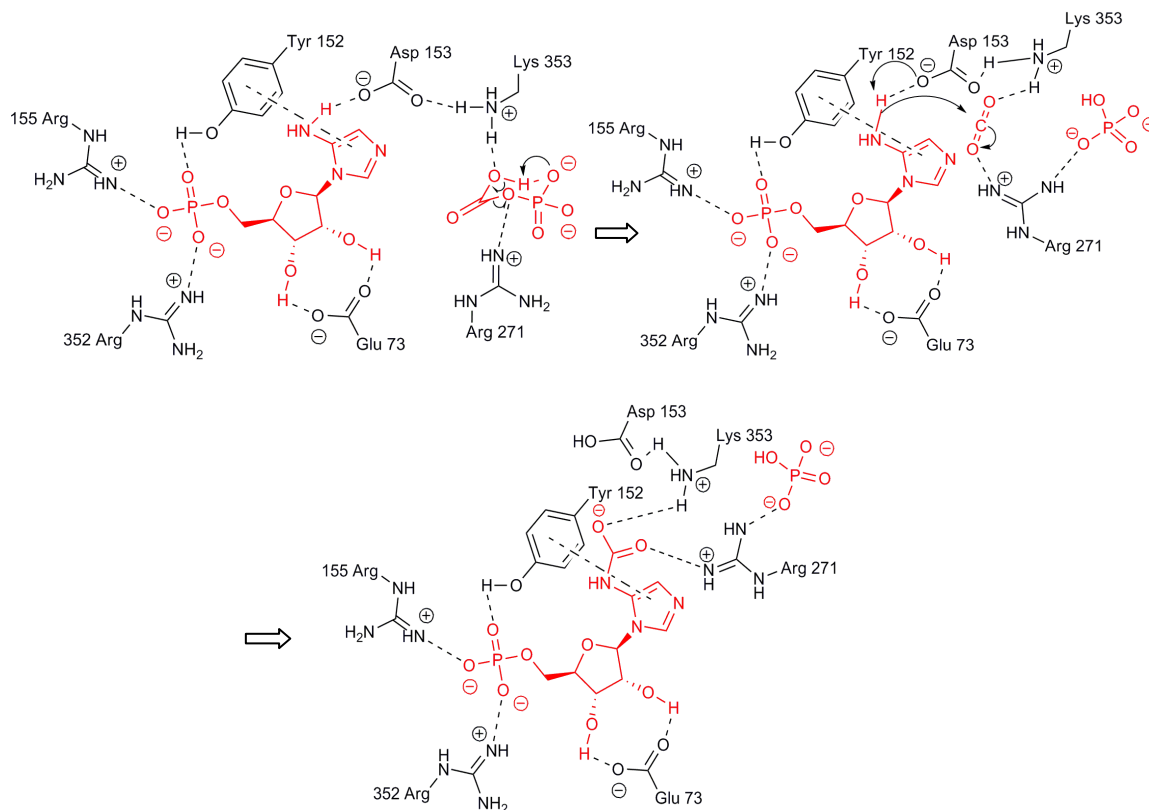


**Figure 15.** Proposed mechanism for N<sup>5</sup>-CAIR synthetase. AIR and carboxyphosphate are shown in red. The functional groups of the side chains of amino acids believed to be involved in the mechanism are shown along with the residue number.

## 2.2. Discovery of selective N<sup>5</sup>-CAIR synthetase inhibitors:

The evidence presented in the introduction indicates that N<sup>5</sup>-CAIR synthetase is an important target for the design of antibacterial and antifungal agents. Unfortunately, at the start of this project, no small molecule inhibitors of the enzyme were known. To correct this problem, we initiated a high-throughput

screening (HTS) study on the enzyme. HTS was carried out at the Center for Chemical Genomics located at the University of Michigan, Ann Arbor. The results of assay development, HTS screening, hit identification, and kinetic characterization of the hits are presented in the following sections.

#### 2. 2.1. Assay development for high-throughput screening:

The published assay for N<sup>5</sup>-CAIR synthetase (Figure 7) relies upon the measurement of ADP using a system in which ADP production is coupled to the reduction of pyruvate. While this assay is well known, it suffers from the problem that false hits could be generated due to inhibition of the coupling enzymes rather than N<sup>5</sup>-CAIR synthetase. Thus, additional screening would have to be done to identify the true target of any inhibitor identified in the assay.

To circumvent this problem, we utilized the well-known malachite green/phosphomolybdate assay to detect the AIR-dependent production of phosphate by the enzyme. In this assay, the phosphate produced complexes with molybdate to form a colorless complex, which upon reaction with malachite green generates a blue color that can be measured at 600 nm (Figure 16). We observed that this assay worked well for N<sup>5</sup>-CAIR synthetase, could easily be run in 384-well plates and is highly reproducible (Z' score of 0.7).

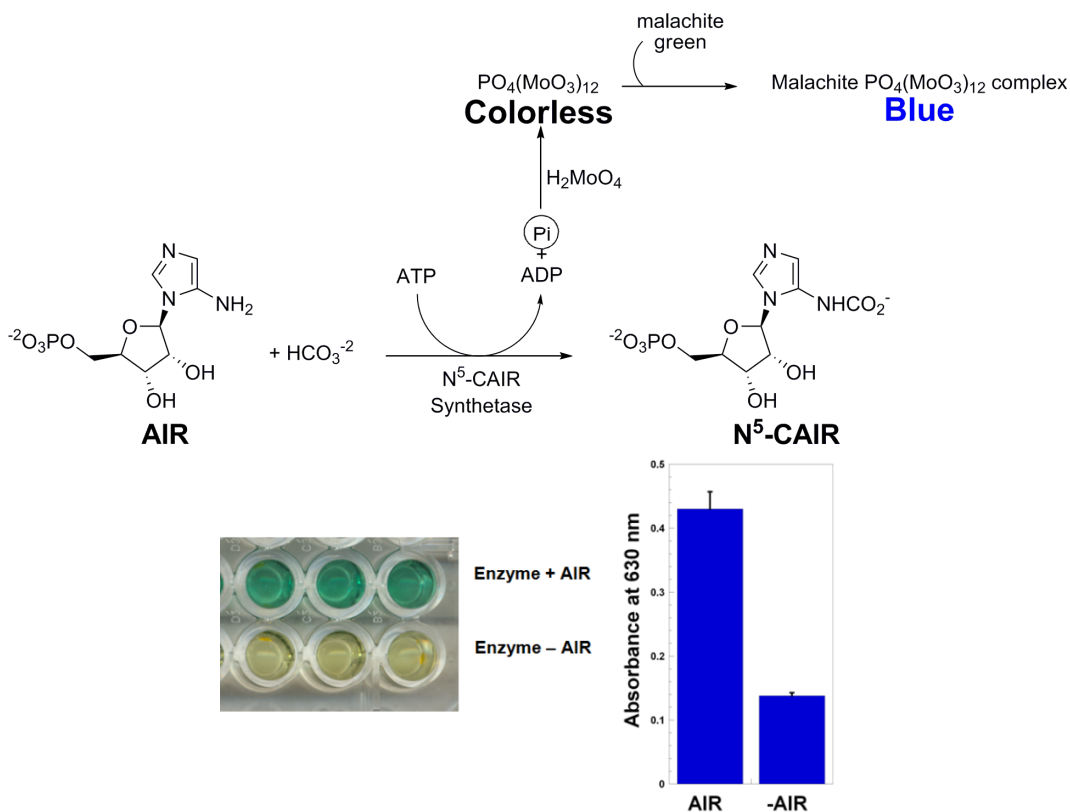


**Figure 16.** Phosphomolybdate and malachite green assay for N<sup>5</sup>-CAIR synthetase (top). The assay allows for easy analysis by measurement of absorbance at 630 nm (bottom).

### 2. 2. 2. Screening compound libraries:

Using this assay, 48,000 drug-like, commercially available compounds collected from the Maybridge Hit-Finder library (Maybridge), ChemDiv corporation, Chembridge corporation and the MS Spectrum library were screened at a single inhibitor concentration ranging from 5 to 27  $\mu$ M (depending upon supplier). We found 212 potential inhibitors (hit rate: 0.44%). Dose–response curves, using the phosphate assay, were generated for the most potent 107 compounds as determined from the primary screen. Of these, only 14 displayed a dose–response

relationship (hit rate: 0.03%). Importantly, none of these 14 was identified as hits in the PubChem database indicating that our compounds display some measure of selectivity.

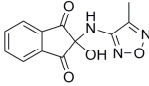
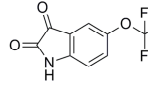
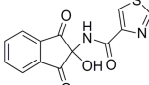
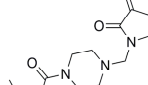
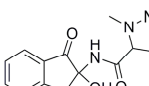
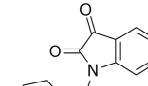
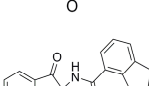
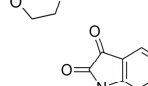
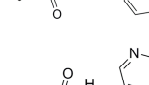
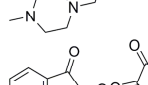
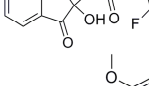
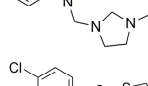
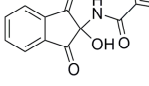
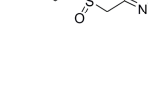
### 2. 2. 3. Classification of the hits:

The structures of the 14 compounds are shown in Table 4 along with their  $IC_{50}$  values. The hits identified can be classified into three classes based on chemical structure. Class I contains compounds with an indenedione core. Class II compounds contain an isatin core, while class III contains compounds that are structurally unrelated to any other inhibitor. We determined the Michaelis–Menten kinetics for five compounds (**1**, **2**, **7**, **13**, and **14**) using the standard  $N^5$ -CAIR synthetase assay shown in Figure 7.

#### 2. 2. 3. A. Class I compounds inhibit $N^5$ -CAIR synthetase by reacting with AIR:

The Michaelis–Menten plot of **1** and **2** versus AIR concentration revealed a biphasic relationship in which there was a lag followed by an increase in velocity as the concentration of AIR increased (Figure 17). Examination of the data revealed that the breakpoint between the lag versus turnover always occurred when the concentration of AIR was twice that of the inhibitor. This suggested that the inhibitor reacts with AIR and once the inhibitor is consumed, additional AIR is available for turnover by the enzyme. Such a result is odd for two reasons. First, in these reactions, the substrate and the inhibitor are added at the same time to the enzyme. Thus, the reaction between the inhibitor and AIR had to occur faster than the conversion of AIR to  $N^5$ -CAIR. Thus, the reaction between the inhibitor and

Table 4. Hits from HTS

No.	Compound	IC <sub>50</sub> <sup>a</sup>	K <sub>i</sub> <sup>b</sup>	type <sup>c</sup>	No.	Compound	IC <sub>50</sub> <sup>a</sup>	K <sub>i</sub> <sup>b</sup>	type <sup>c</sup>
1		2.3	NA	R	8		19	ND	NA
2		5.6	NA	R	9		21.9	ND	NA
3		7.76	NA	R	10		23	ND	NA
4		8.7	ND	NA	11		37	ND	NA
5		17	ND	NA	12		69	ND	NA
6		17.38	ND	NA	13		10	62 <sup>d</sup> 43 <sup>e</sup>	C U
7		10.47	29 <sup>d</sup> 40 <sup>e</sup>	NC NC	14		20	81 <sup>d</sup> 122 <sup>e</sup>	NC NC

<sup>a</sup> IC<sub>50</sub> values determined from dose–response curves using the phosphate assay. <sup>b</sup> K<sub>i</sub> values determined using the ATPase assay with variable amounts of either AIR or ATP at a fixed concentration of bicarbonate. Values determined by curve fitting data using various models of inhibition. <sup>c</sup> Type of inhibition determined by fitting data to the modified Michaelis–Menten equations for the presence of different types of inhibitors. Equations that produced the best fit to the data were used to determine the type of inhibition. Results of these curve fits were validated by Lineweaver–Burke plots. R: reacts with substrate; NC: noncompetitive; C: competitive; U: uncompetitive.

<sup>d</sup> Obtained using variable concentrations of AIR and fixed ATP and bicarbonate concentrations.

<sup>e</sup> Obtained using variable concentrations of ATP and fixed AIR and bicarbonate concentrations.

AIR had to occur faster than the conversion of AIR to N<sup>5</sup>-CAIR. Second, the structures of the class I inhibitors do not display any obvious reactive groups.

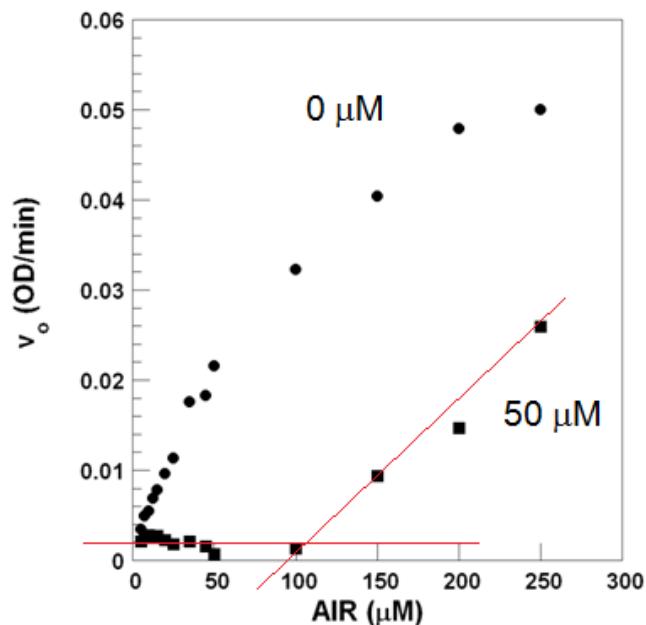


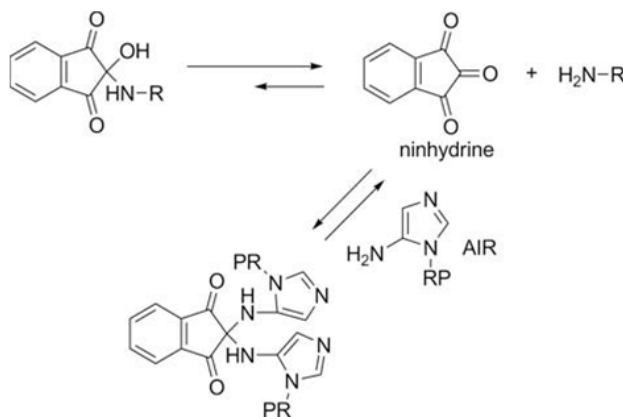
**Figure 17.** Michaelis-Menten plot of N<sup>5</sup>-CAIR synthetase in the presence (■) and absence (●) of **1**. The initial velocity of the reaction in the presence or absence of the inhibitor was determined for the first two minutes of the reaction using the couple assay system. The breakpoint (intersection of the two red lines) always appears at twice the concentration of AIR.

An answer to this conundrum raised in the previous section can be found in a retrosynthetic analysis of these inhibitors. Class I compounds are prepared by reaction of ninhydrine with an amine or an amide. Given this, we hypothesized that these molecules may be unstable and could decompose to the 1, 2, 3-triketoidane (the dehydrated form of ninhydrin) and either the amine or amide (Scheme 4). If such a reaction occurred, the 1,2,3-triketoidane present in the

reaction mixture could react with the amine of AIR thereby preventing AIR from binding to the enzyme.

We examined aqueous solutions of **1** and **2** by TLC and found that the compounds decomposed to generate ninhydrin. The rate of decomposition was dependent upon the chemical nature of the compound. Studies on **1** revealed that this compound completely decomposed to ninhydrin after approximately 30 min while decomposition of **2** took around 45 min. This decomposition was not observed in DMSO solutions of the compounds indicating that a proton (presumably from water) was necessary for the reverse reaction.

**Scheme 4.** Reaction of class I inhibitors.



To assess the rate of the reaction, we incubated ninhydrin with AIR and observed a very rapid reaction ( $\leq 20$  s) as determined by TLC analysis. Experiments utilizing TLC and UV spectroscopy indicated that the enzyme did not catalyze a reaction between AIR and ninhydrin. To determine if the reaction between AIR and ninhydrin was responsible for the kinetics observed for **1** and **2**, we obtained a Michaelis–Menten plot with variable AIR and ninhydrin. Once again,

we observed the same kinetic results as for **1** and **2**; namely, no reaction until the concentration of AIR exceeded that of ninhydrin. This suggested that ninhydrin was responsible for the observed inhibition by removing available substrate from solution. To confirm this, we examined whether DMSO solutions of **1** or **2** were capable of inhibiting N<sup>5</sup>-CAIR synthetase. We found that upon addition of these non-aqueous solutions, neither compound resulted in inhibition of the enzyme. Thus, our data suggest that compounds belonging to class I are not true inhibitors of N<sup>5</sup>-CAIR synthetase, but rather inhibit the reaction by reacting with the substrate. Given this mechanism of action, class I compounds do not represent viable lead agents for the development of antimicrobial agents.

2. 2.3.B. Class II compounds are non-competitive inhibitors of N<sup>5</sup>-CAIR synthetase:

We determined the Michaelis–Menten kinetics of compound **7** (Figure 18), which is the most potent member of the class II family of inhibitors. Kinetic analysis reveals that **7** is non-competitive with both AIR and ATP. N<sup>5</sup>-CAIR synthetase has no known allosteric regulators; however, HTS of other enzymes related to N<sup>5</sup>-CAIR synthetase has identified non-competitive inhibitors as well.<sup>58</sup> Given the structural similarity between **7** and the other class II inhibitors, we anticipate that all compounds belonging to this class will be non-competitive inhibitors of the enzyme.



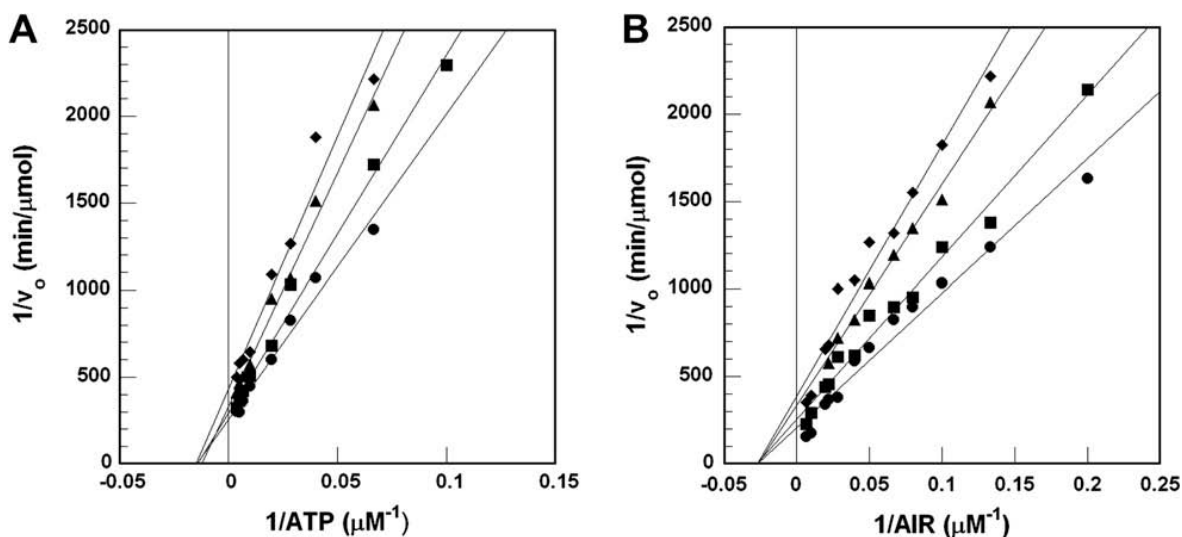


**Figure 18.** Kinetic characterization of class II inhibitors with various concentrations of **7** ((●) 0 IM, (■) 5 IM, (▲) 10 IM, and (◆) 25 IM). A. Constant AIR and varying ATP; B. Constant ATP and varying AIR.

### 2. 2. 3. C. Investigation of class III compounds

We have identified two compounds that are chemically unrelated to any other hits identified in the screen. Steady-state kinetics of **13** (Figure 19) indicates that the compound is competitive with AIR, but uncompetitive with ATP. This result suggests that the compound binds to the AIR-binding site of the enzyme only after ATP binds to the enzyme.

Compound **14** is riboflavin. Although this compound is unlikely to be a lead agent, we conducted kinetic analysis to determine the mechanism of inhibition. Steady-state kinetic analysis indicates that riboflavin is noncompetitive with both AIR and ATP as shown in Figure 20.

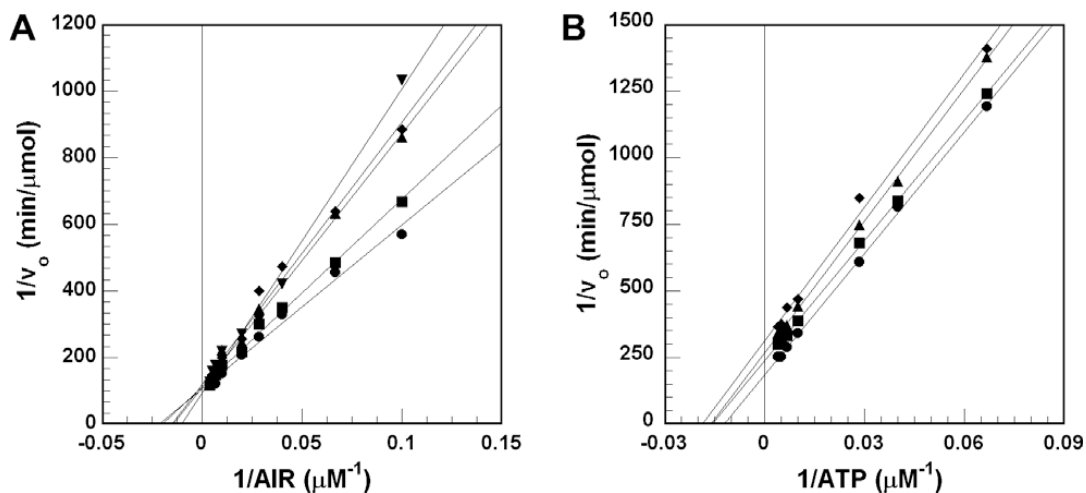


**Figure 19.** Kinetic characterization of compound **13** various concentrations ((●) 0 IM, (■) 5 IM, (▲) 10 IM, and (◆) 25 IM). A. Constant ATP and varying AIR; B. constant AIR and varying ATP

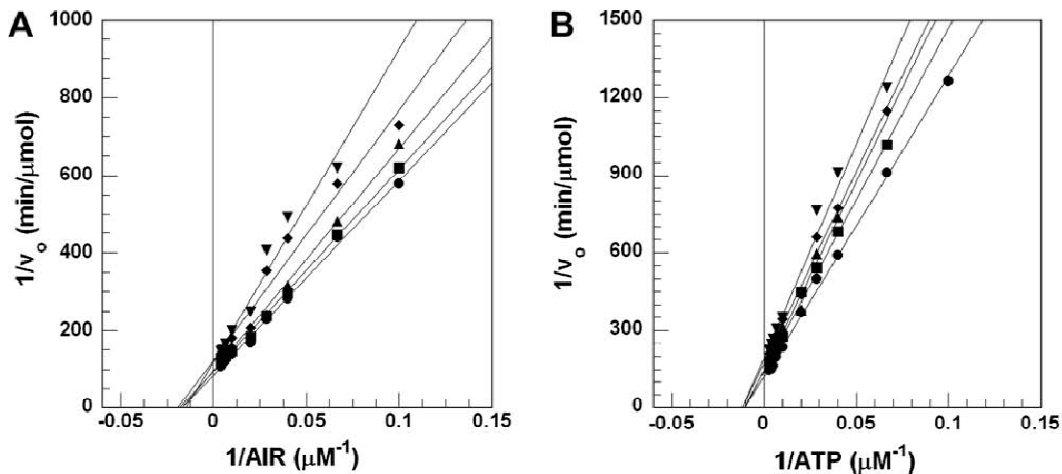


**Figure 20.** Kinetic characterization of compound **14** with various concentrations ((●) 0 IM, (■) 5 IM, (▲) 10 IM, and (◆) 25 IM). A. Constant ATP and varying AIR; B. constant AIR and varying ATP

### 2. 2. 3. D. Class II compounds do not inhibit AIR carboxylase or SAICAR

#### synthetase:

We assayed compounds **7**, **13** and **14** against the human bifunctional enzyme AIR carboxylase:SAICAR synthetase. We found that at a concentration of

up to 200  $\mu\text{M}$  of **7**, **13**, or **14**, no inhibition of either enzymatic activity was observed. Incubation of the enzymes with higher concentrations of the **7**, **13**, or **14** resulted in precipitation of the compounds. These results indicate that these agents are selective inhibitors of the microbial enzyme.

#### 2. 2. 4. Class II compounds inhibit *E. coli* growth:

Class II compounds were tested for their ability to inhibit *E. coli* cell growth in liquid cultures. We found that compounds **7** and **11** have minimum inhibitory concentrations of 64 mg/L and 256 mg/L, respectively. Most importantly, inhibition by either compound can be rescued by the addition of adenine, indicating that inhibition of bacterial growth is predominantly due to inhibition of purine biosynthesis.

In conclusion, we have found that class II inhibitors are novel allosteric inhibitors of N5-CAIR synthetase, they do not inhibit the human enzyme, AIR carboxylase, and they display antibacterial activity against Gram-negative bacteria.

#### 2. 2. 5. Design and synthesis of a class II based photoreactive agent:

The promising kinetic and antibacterial properties of the class II agents prompted us to initiate a study aimed at determining the structure of the enzyme:inhibitor complex. Such information would be invaluable for future drug design studies. Unfortunately, our cocrystallization efforts were unsuccessful because of the poor aqueous solubility of the class II inhibitors. As an alternative, we sought to identify the binding site of the class II inhibitors by crosslinking

studies. To accomplish this, we began a study to create a photoreactive crosslinker analog of **7** with the goal of identifying the binding site of **7** by proteomic analysis.

Using the structure-activity relationships observed in our HTS hits, we reasoned that there were two locations on the core chemical structure that could be modified. The first was the nitrogen atom on the isatin nucleus since a wide variety of substituents appeared to be tolerated at this location. The second location was on the phenyl ring of the isatin core. Given the synthetic ease of preparing N-substituted derivatives, we choose this location. For the photoreactive moiety we choose to use a diazirine group. Diazirines are extremely stable under non-UV conditions, yet these groups can be activated by irradiating at 360 nm<sup>59-62</sup> UV irradiation converts diazirines into reactive carbenes, which can non-specifically react with any neighboring amino acids. Diazirines are also small and offer limited steric hindrance.

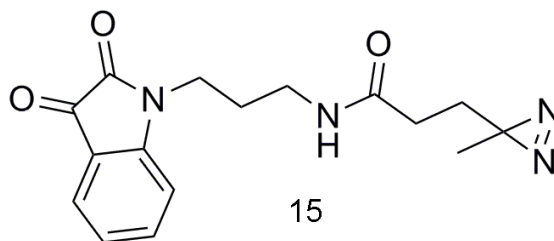
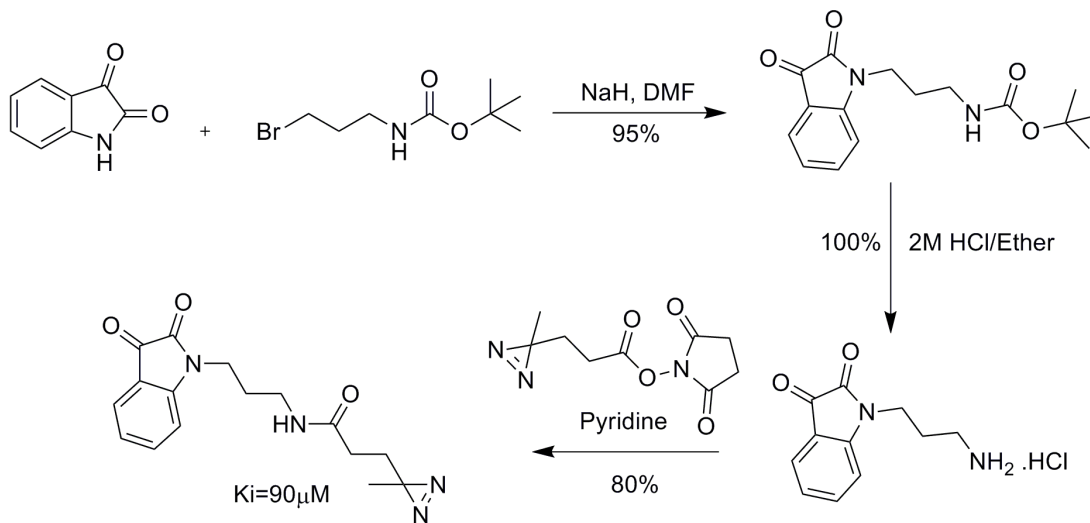


**Figure 21.** (left) Designed class II diazirine based photoreactive agent.

Based upon these finding, we designed compound **15** as our photocrosslinker (Figure 21). The synthesis of this molecule was accomplished according to Scheme 5.

**Scheme 5. Synthesis of compound 15.**



2. 2. 5. A. Kinetic characterization of the photoreactive agent:

We determined whether compound **15** could inhibit N<sup>5</sup>-CAIR synthetase using a dose-response curve. The resulting dose-response curve was used to determine the  $K_i$  value according to the equation  $K_i = (V_{\text{maxapp}} * [I]) / V_{\text{max}}$ , where  $V_{\text{maxapp}}$  is the apparent  $V_{\text{max}}$  obtained from the dose-response curve,  $V_{\text{max}}$  is the maximal velocity obtained from the uninhibited curve, and  $[I]$  is the inhibitor concentration. Using this analysis, we found that **15** was a non-competitive inhibitor with a  $K_i$  of 90  $\mu$ M.

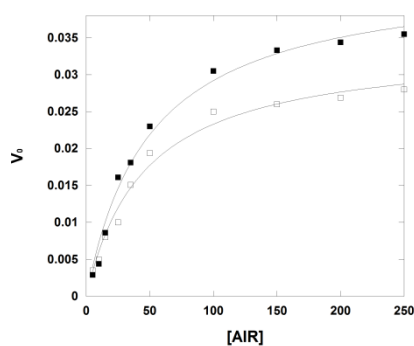


**Figure 22.** Kinetic characterization of **15**. (■) 0  $\mu$ M drug and (○) 90 $\mu$ M drug.

### 2. 2. 6. Photocrosslinking studies:

Photocrosslinking studies were performed in phosphate buffered saline. N<sup>5</sup>-CAIR synthetase (PurK) was incubated with 450 μM of **15** in the presence and absence of AIR and ATP. Control experiments conducted with the known inhibitor, **7**, were also conducted. A control reaction containing no **15** was also performed. All the samples were irradiated with UV light using a 100 watt UV lamp, emitting radiation between 340-370 nm. SDS-PAGE analysis of the reactions is shown in Figure 22. The data revealed the presence of a 84 kDa band in addition to the 42kDa band expected for N<sup>5</sup>-CAIR synthetase. The intensity of 84 kDa band was diminished in the presence of compound **7** (lane 3, Figure 22) indicating that compound **7** can compete with the photocrosslinker. This suggests that the crosslinker and **7** bind to the same site.

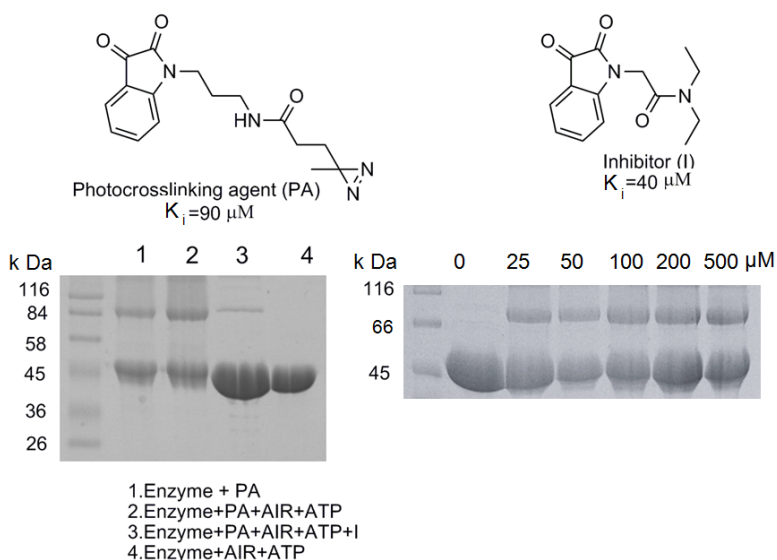


**Figure 23.** Photocrosslinking studies of N<sup>5</sup>-CAIR synthetase with compound **15**. A. Photocrosslinking studies in presence of inhibitor **7**, ATP and AIR; B. Photocrosslinking studies in presence of **15** at 0, 10, 25, 50, 75 and 100μm concentrations. Note: Denaturing gel.

In another experiment, we incubated N<sup>5</sup>-CAIR synthetase with compound **15** at concentrations 0, 10, 25, 50, 75 and 100 μM. Analysis of these reactions reveal that the 84 kDa band increases in intensity with the increase in compound **15** concentration. This result indicates that there is a direct relationship between the formation of the 84 kDa band and the concentration of **15**.

The presence of the 84 kDa band suggested that **15** caused the formation of stable, covalent dimers of N<sup>5</sup>-CAIR synthetase. Solution and crystallographic studies have shown that the synthetase exists as a dimer in solution. The data suggests that **15** is crosslinking two monomers together. How does this occur? Compound **15** contains a diazirine, which is a known photoactivable linker. However, the other end of the molecule is isatin, which is not known to be an activatable, reactive group. Our data suggests that the isatin region of **15** is converted to a reactive species during UV irradiation. The resulting reactive group then covalently modifies the protein generating crosslinked N<sup>5</sup>-CAIR synthetase. Given this unexpected behavior, we initiated a study on the photochemical properties of isatin and its derivatives.

#### 2. 2. 7. Study of photochemical properties of Isatin:

If isatin is converted into a reactive species by UV irradiation, we predicted that irradiation of **7** would lead to the generation of a time-dependent inactivation agent for N<sup>5</sup>-CAIR synthetase. Two experiments were conducted. In the first experiment, 1 mM of **7** in dimethylformamide (DMF) was incubated with 20 μM of N<sup>5</sup>-CAIR synthetase. At various timepoints during the incubation period, the

amount of remaining enzyme activity was determined by diluting the enzyme and assaying for N<sup>5</sup>-CAIR synthetase activity.

In the second experiment, a DMF solution of **7** was irradiated for 2 hours. A 1 mM solution of the UV-irradiated solution was incubated with N<sup>5</sup>-CAIR synthetase and the remaining enzyme activity was assayed over two hours. The percentage of enzyme activity remaining was plotted against time to determine whether there was time-dependent enzyme inactivation.

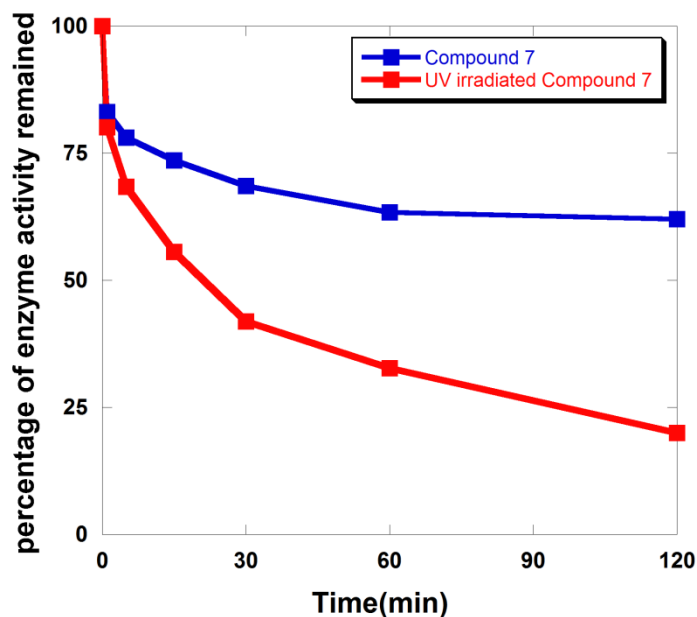


**Figure 24.** Time-dependent enzyme inactivation by **7** (blue) and UV irradiated **7** (red).

As shown in the Figure 23, **7** did result in the loss of approximately 35 percent of the enzyme activity; however, UV-irradiated **7** inhibited 85 percent of the enzyme. This suggests that UV irradiation changes **7** into a more reactive species, which modifies the enzyme. To determine if the inactivation was



reversible or irreversible, we dialyzed the enzyme:7 (both non-UV and UV treated) samples for 5 hours and then assayed the samples to determine if N<sup>5</sup>-CAIR synthetase activity was recovered. We observed that for the non-UV irradiated 7:enzyme sample, completely activity was recovered after dialysis; however, for the UV-irradiated 7:enzyme sample, no activity was restored upon dialysis.

#### 2. 2. 8. HPLC and GC/MS analysis of UV irradiated isatin and understanding the isatin photochemistry:

To identify the chemical change that is taking place upon UV irradiation, we conducted a GC/MS study on *N*-methyl isatin. We choose to use *N*-methyl isatin for this studies since the compound is simpler and cheaper than 7 and is readily available. *N*-methyl isatin in water was exposed to UV irradiation for 6 hours at a distance of 2 cm and set aside for another 9 hours. The resulting UV irradiated material was subjected to HPLC and GC/MS analysis to identify the chemical species created upon irradiation.

The HPLC chromatogram of *N*-methyl isatin and the irradiated sample are shown in Figure 22. As shown, *N*-methyl isatin had a retention time of 20 minutes by HPLC. HPLC of the irradiated sample showed two peaks with retention times of 20 and 22 minutes, respectively, as shown in Figure 24. The peak at 20 minutes represented unreacted *N*-methyl isatin, whereas the peak at 22 minutes represented a new compound.

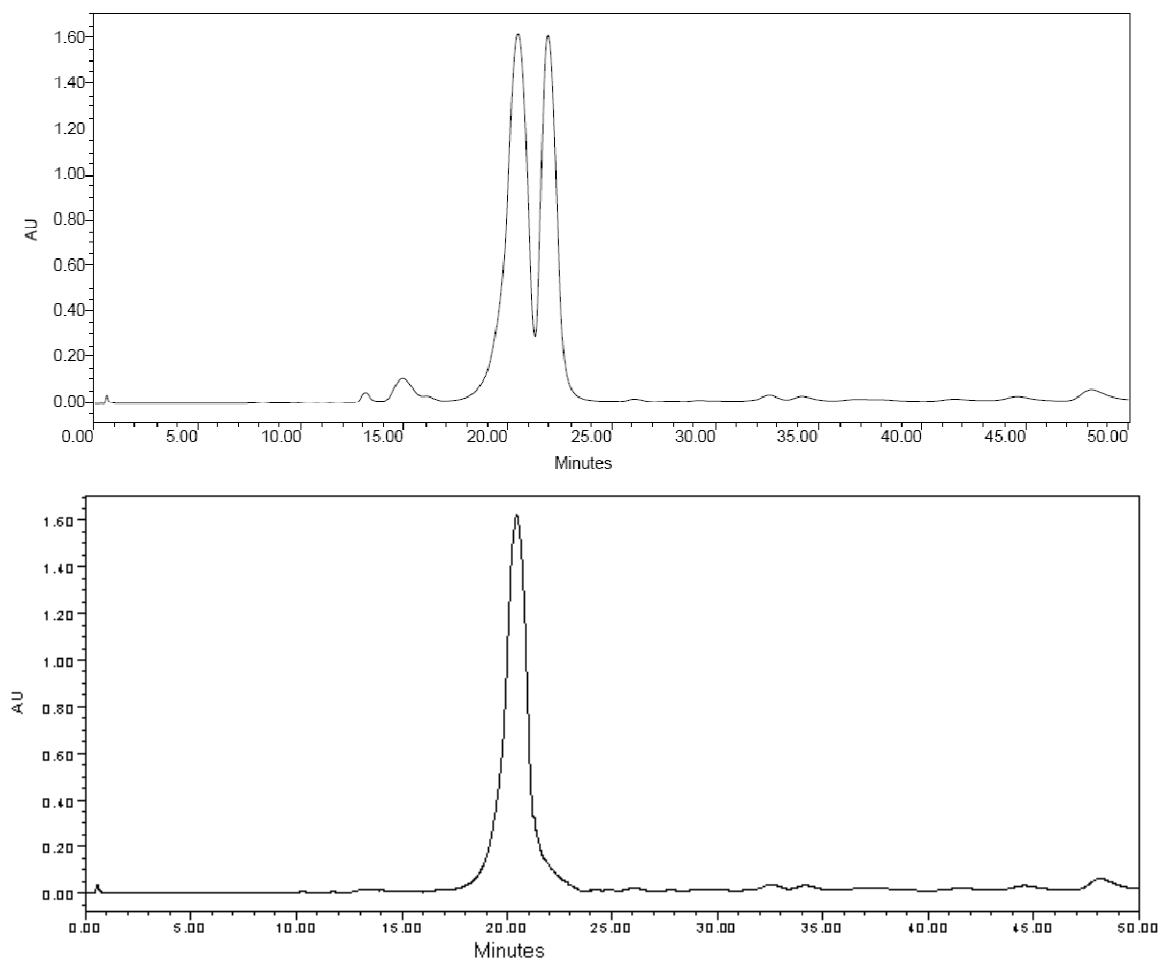


**Figure 25:** Top: HPLC analysis of the UV irradiated *N*-methyl isatin. The peak at 20 minutes is *N*-methyl isatin and the peak at 22 minutes corresponds to *N*-methyl isatoic anhydride. Bottom: HPLC chromatogram showing pure, authentic *N*-methyl isatin.

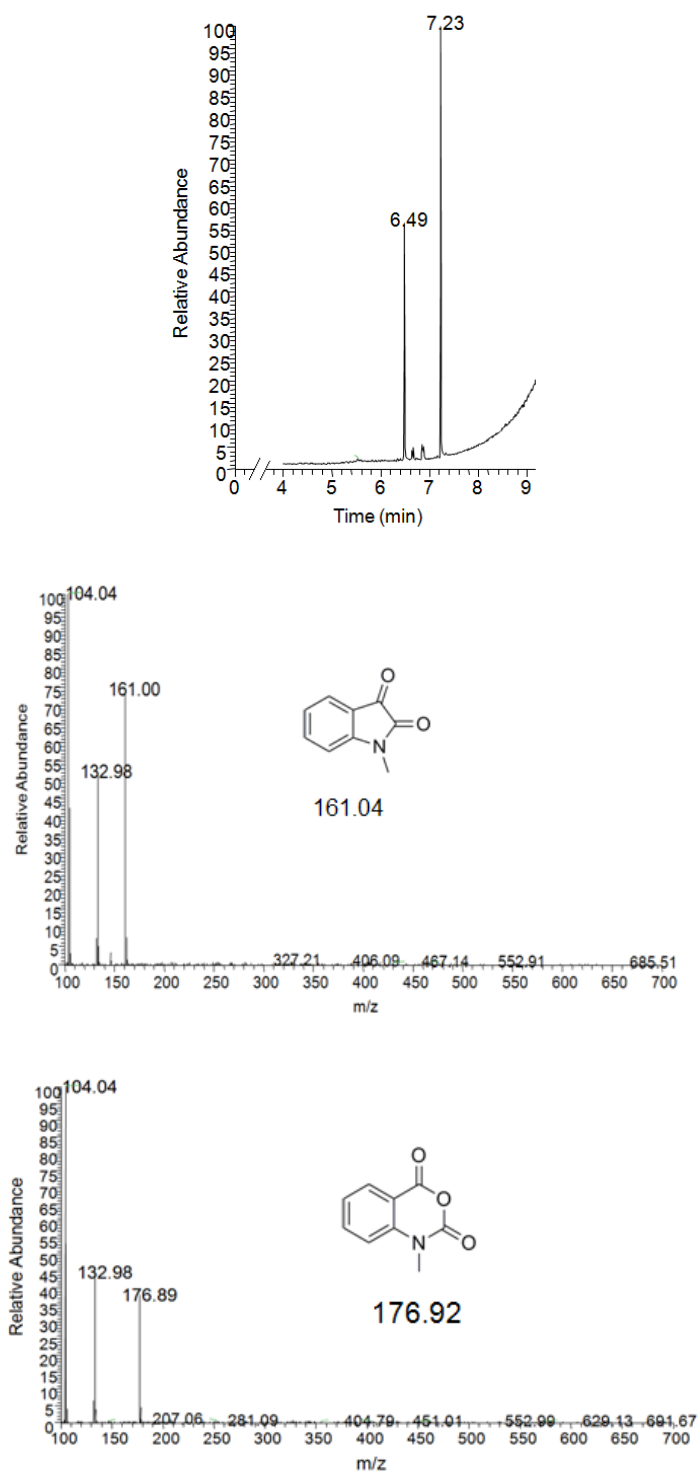


**Figure 26.** (Top) Gas chromatogram of UV irradiated *N*-methyl isatin; (Middle) Mass spectra of 6.49 peak; (Bottom) Mass spectra of 7.23 peak.

To determine the chemical composition of the new material, we conducted a GC/MS analysis (Figure 25) of the irradiated sample. Once again, two peaks were observed. Mass spectrometric analysis and GC analysis with an authentic sample, revealed that the peak at 6.49 minutes is *N*-methyl isatin and the peak at 7.23 minutes is *N*-methyl isatoic anhydride (see Figure 25). To examine the rate of formation of *N*-methyl isatoic anhydride from *N*-methyl isatin, we conducted a kinetic study. Irradiation of *N*-methyl isatin in THF followed by analyzes of the samples at 2-3 hour intervals revealed the slow increase in the 7.2 minute peak. Clearly, the rate of formation of the anhydride in THF is much slower than that observed for the reaction in water.

In addition to the slow rate of formation, we also observed that the concentration of the anhydride (as measured by the intensity of the 7.2 minute peak) is smaller than when *N*-methyl isatin was irradiated in water (compare figures 25 and 26). This result suggests that water and dissolved oxygen in the water may play a role in the formation of the *N*-methyl isatoic anhydride. To investigate this hypothesis, we conducted an UV-irradiation experiment of *N*-methyl isatin in freshly distilled THF in a sealed PCR tube. Irradiation over 6 hours did not result in the formation of any *N*-methyl isatoic anhydride (Figure 26). This experiment indicates that water and oxygen are likely involved in the conversion of isatin to isatoic anhydride in presence of UV radiation.

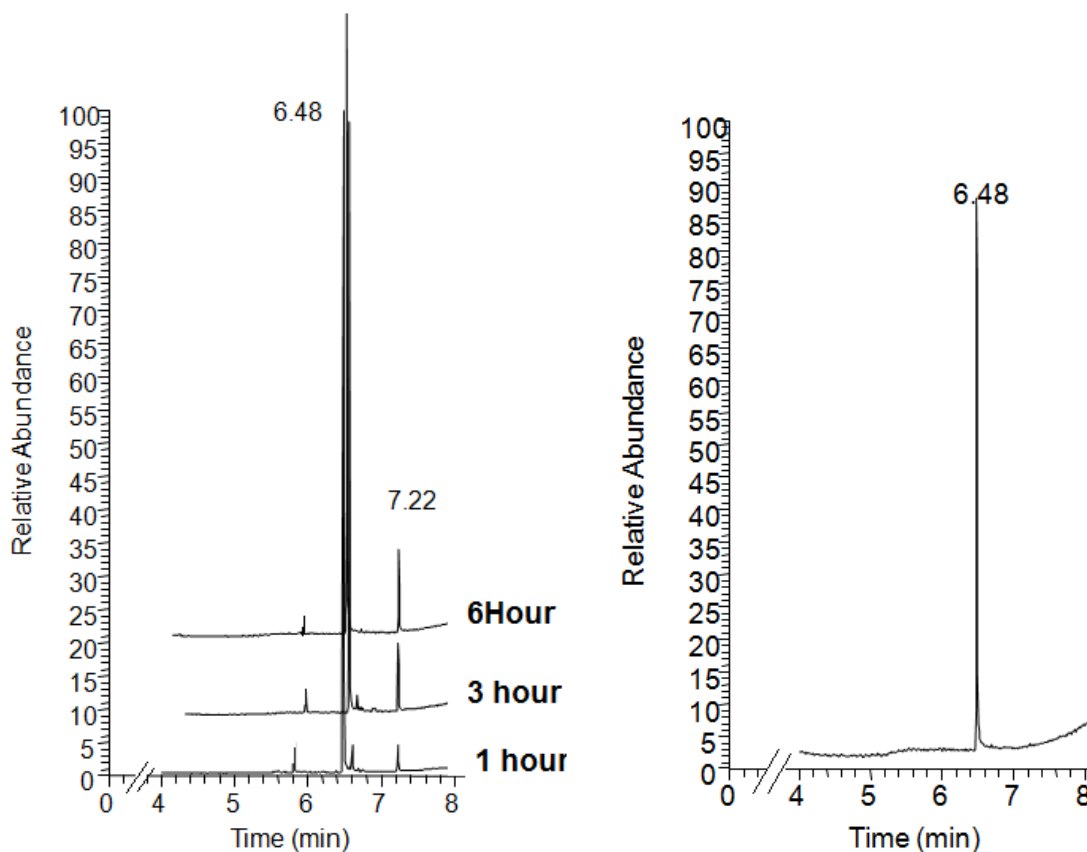
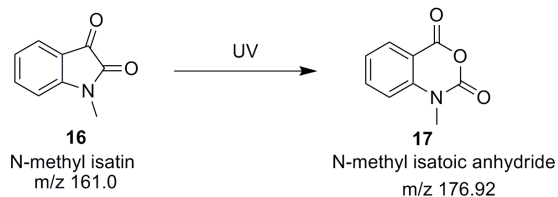


**Figure 27.** Left: *N*-methyl isatin was irradiated in wet THF. The gradual increase in the 7.2 peak (due to *N*-methyl isatoic anhydride) with increase in time of exposure to UV radiation indicating the formation of isatoic anhydride is time dependent.

Right: GC/MS chromatogram of UV irradiation of *N*-methyl isatin in freshly distilled THF. The chromatogram shows no peak at 7.2 corresponding to *N*-methyl isatoic anhydride after 6 hours of UV exposure.

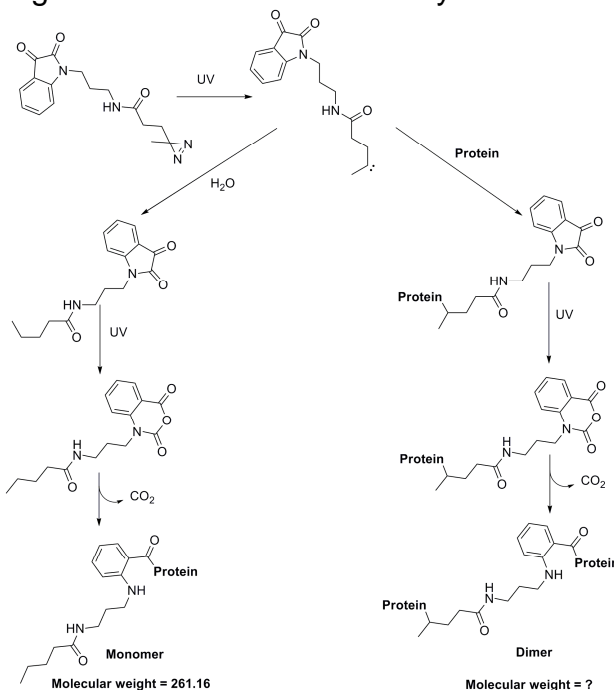
Based on the above experiments, we conclude that UV irradiation converts isatin to isatoic anhydride (Scheme 9).

**Scheme 6.** Photochemical turnover of *N*-methyl isatin to *N*-methyl isatoic anhydride



Given the above data, we propose that **15** is transformed into the highly reactive anhydride (**15b**) as shown in Scheme 7. By dissolving compound **15** in water and upon UV irradiation, the diazirine moiety converts into a carbene. The carbene is highly reactive and unstable. The carbene reacts with the surrounding protein. Then, after some time, the isatin moiety of **15** undergoes transformation into isatoic anhydride as shown in Scheme 7. Once the anhydride is made, it reacts with the protein to generate crosslinked protein.

**Scheme 7.** Proposed transformation of **15**. Upon UV irradiation of **15** in water. The generated carbene and isatoic anhydride might have involved intercrosslinking of monomers of N<sup>5</sup>-CAIR synthetase.



Previous researchers who have investigated isatoic anhydride and related molecules have shown that these molecules can readily react with lysine, serine and cysteine residues.<sup>63-66</sup> In order to verify this chemistry, we conducted a model reaction with isatoic anhydride and benzyl alcohol (Scheme 8). We observed **21** as the sole product in the reaction (Figure 27). This model reaction indicates that isatoic anhydride readily reacts with alcohols and further supports the role of isatoic anhydride as a reactive group capable of participating in the crosslinking of N<sup>5</sup>-CAIR synthetase monomers.

**Scheme 8.** Reaction of isatoic anhydride with benzyl alcohol

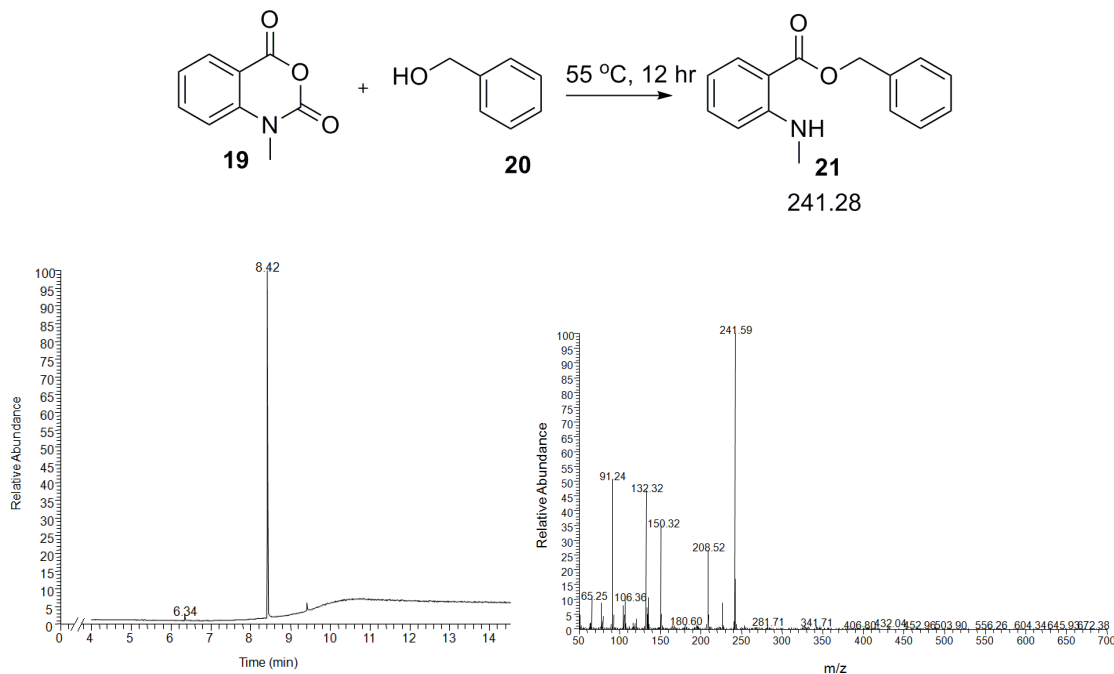


**Figure 28.** Left: GC analysis of the reaction shown in scheme 8. The anhydride (**19**) is completely consumed and the peak at 6.34 corresponds to benzyl alcohol (**20**). Right: Mass spectra of 8.42 peak showing m/z 241.59, corresponding to **21**.

### 2. 2. 9. LC-MS/MS analysis of the photocrosslinked protein

With an understanding of the photochemistry of **15**, we next sought to determine the binding site of **15**, and by extension, **7**. To do this, we turned to proteomic studies on the crosslinked N<sup>5</sup>-CAIR synthetase. N<sup>5</sup>-CAIR synthetase was treated with **15**, irradiated by UV light and then purified by SDS-PAGE. The individual 84 and 42 kDa bands from the gel were excised, treated with iodoacetamide to modify cysteine residues and then digested with either trypsin or and chymotrypsin. The digested samples were subjected to LC-MS/MS analysis (Proteomic Core Facility, Wayne State University). An examination of the proteomic data indicates that we have 80 to 95 percent coverage (depending upon the protease used) of the protein in all samples. Based on our understanding of the photochemistry and reactivity of **15**, we searched the proteomic data for a 261.16 modification. This modification represents an instance in which the anhydride reacts with the protein, but the carbene has been quenched with water. We found 73 separate instances where Ser227 was modified in the peptide NVSDAINQKAQEL. This result suggests that Ser227 may be in the allosteric binding site.

The above analysis does not explain the observed dimerization by **15** nor does it indicate if the Ser227 modification is due to a non-specific reaction with **15**. To gain knowledge of the binding site of **15** and the peptides responsible for the dimerization, we compared all experimentally determined peptides that we obtained through proteolysis of the 42 kDa and 84 kDa bands. Surprisingly, we



have found that only two peptides were missing in the 84 kDa band. All other peptides from the N- to the C-terminus could be accounted for. Interestingly, the two peptides were located in the same region as serine227. The two peptides are KAQELARKAVAAFDGKG and KLVYAPARNVSDAINQKA.

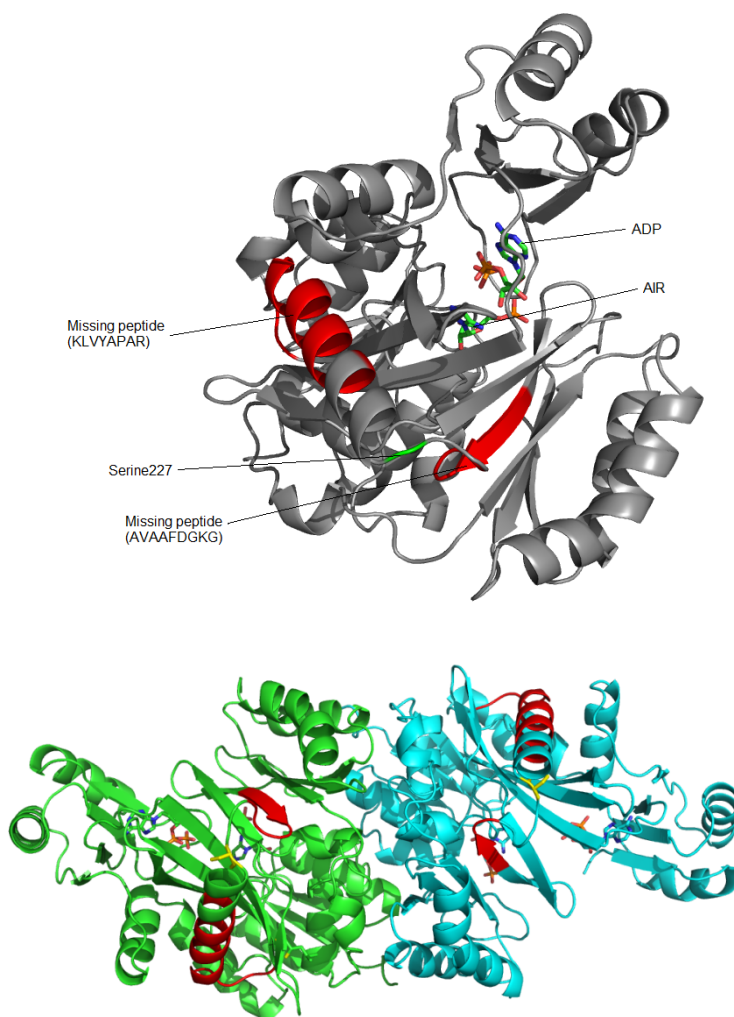


**Figure 29.** Top: N<sup>5</sup>-CAIR synthetase with the missing peptides shown in red. Ser 227 is shown in green. Bottom: N<sup>5</sup>-CAIR synthetase shown as dimer with the missing peptides shown in red. The two monomers of the enzyme are shown in green and cyan. The modified serine residue is shown in yellow. It is evident from this picture that the proposed binding site for **15** is not located at the dimer interface.

An examination of the location of these missing peptides in the crystal structure of *Aspergillus* N<sup>5</sup>-CAIR synthetase reveals that there is no obvious reason for the formation of a dimer during the photocrosslinking studies (Figure 28). The two missing peptides are 20 Å away from the dimer interface and the linker on **15** is too short to span this distance. Thus, the only way for dimers of the synthetase to form is the crosslinker bound to this site, would be if the enzyme existed in a different dimer conformation than the one observed in the crystal structure. This result hints at the existence of multiple conformations in the dimer formation of the synthetase. Others have observed conformational crosstalk between distal sites on ATP-grasp enzymes and the active site.<sup>45</sup> Given this, it is possible that **7** functions by binding to and stabilizing an alternative conformation which is inactive. Additional studies will have to be conducted to validate or refute this hypothesis.

## Chapter 3

### Discussion

#### 3.1. Structural and functional studies on N<sup>5</sup>-CAIR synthetase:

Previous NMR, biochemical and kinetic studies demonstrated that N<sup>5</sup>-CAIR synthetase generated the unstable product N<sup>5</sup>-CAIR from AIR using ATP and bicarbonate.<sup>23</sup> Based upon literature precedence for ATP-utilizing carboxylation enzymes, Stubbe and coworkers proposed that N<sup>5</sup>-CAIR synthetase proceeds through the formation of the highly unstable intermediate carboxyphosphate.<sup>23</sup> Subsequent positional isotope incorporation studies supported this hypothesis.<sup>23, 67, 68</sup>

The formation of carboxyphosphate has been proposed for other ATP-grasp enzymes that utilize bicarbonate as a one-carbon substrate. The two best studied examples are biotin carboxylase<sup>69</sup> and carbamoyl phosphate synthetase<sup>70, 71</sup> (Figure 29). Both enzymes catalyze a reaction that is analogous to that conducted by N<sup>5</sup>-CAIR synthetase; namely, ATP reacts with bicarbonate to generate carboxyphosphate, which is either directly attacked by a nucleophile or decomposes to CO<sub>2</sub> before attack by a nucleophile onto the generated CO<sub>2</sub>.

One approach towards understanding the chemistry of these enzymes is to examine their half-reactions (Figure 8). The first half reaction is the reaction between ATP and bicarbonate to generate carboxyphosphate and ADP. Both biotin carboxylase and carbamoyl phosphate synthetase are able to catalyze the transfer of phosphate to the carboxylic acid in the absence of the nucleophilic

substrate.<sup>50, 57, 69</sup> In keeping with the expected similarities between these enzymes and N<sup>5</sup>-CAIR synthetase, we have found that N<sup>5</sup>-CAIR synthetase will catalyze the bicarbonate-dependent hydrolysis of ATP in the absence of AIR. This result, in conjunction with the results published from the laboratory of Professor Stubbe, support the hypothesis that carboxyphosphate is an intermediate in the reaction.

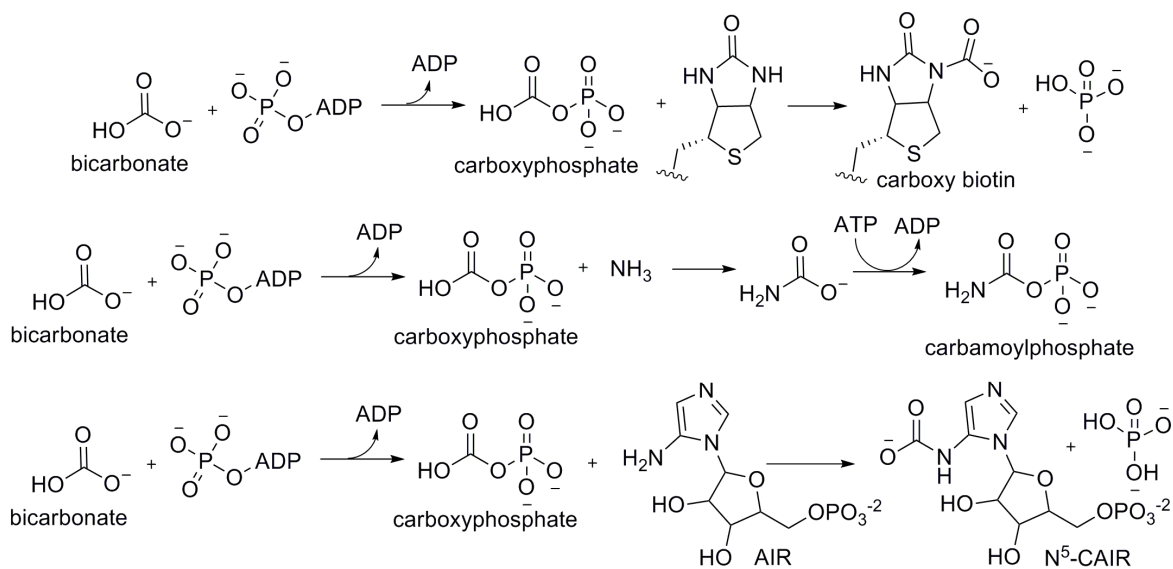


**Figure 30.** Top: mechanism of biotin carboxylase; Middle: Mechanism of carbamoyl phosphate synthetase; Bottom: Mechanism of N<sup>5</sup>-CAIR synthetase. All the three enzymes show production of carboxyphosphate intermediate.

The second half-reaction deals with the fate of carboxyphosphate. There is much debate regarding this question and two mechanisms have been proposed.<sup>69, 72</sup> The first proposed mechanism is that carboxyphosphate is the electrophile for the carboxylation reaction and is directly attacked by the nucleophilic substrate. The second proposed mechanism is that carboxyphosphate dissociates to CO<sub>2</sub>, which is the true electrophile in the reaction.

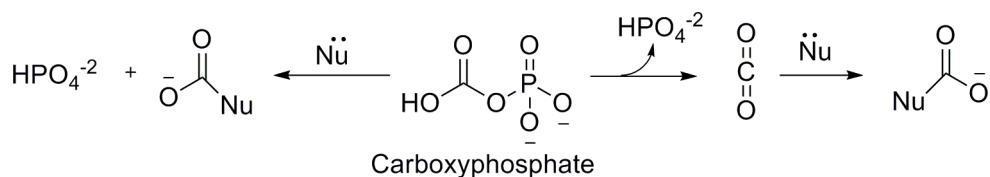


**Figure 31.** Possible fate of carboxyphosphate during carboxylation reaction.

We have initiated a variety of studies to attempt to address this issue for N<sup>5</sup>-CAIR synthetase. We began with an exploration of the structures N<sup>5</sup>-CAIR synthetase containing various ligands. Of particular interest were the structures of N<sup>5</sup>-CAIR synthetase in the presence of ATP and ADP:Pi since these structures provide information on the active-site architectures before and after ATP hydrolysis. The location of the inorganic phosphate provides a good approximation of the location of the carboxyphosphate binding site and we next attempted to model carboxyphosphate into this location.

Although carboxyphosphate has been postulated as a key intermediate in a number of reactions, few computational studies have been done on this compound. The first step in the formation of carboxyphosphate is the attack of bicarbonate on the  $\gamma$ -phosphorus atom of ATP. Herschlag *et al* studied phosphoryl-transfer reactions to bicarbonate and indicated that an intermolecular hydrogen bond between the proton on bicarbonate and one of the oxygen atoms of phosphate stabilized the transition state.<sup>53</sup> This suggests that the transition state and carboxyphosphate likely exists in a pseudo-chair conformation (Scheme 6), which is stabilized by a hydrogen bond between the proton on the acid and one of the oxygens on the phosphate. To investigate the stability of this conformation, we

initiated quantum mechanical calculations on various conformations of carboxyphosphate. We found that the pseudo chair conformation was 13 kcal/mol more stable than the extended conformation. This suggests that carboxyphosphate likely adopts a pseudo-chair conformation in the active site.

The next question deals with the fate of the proton on bicarbonate. It is important to recall that N<sup>5</sup>-CAIR synthetase utilizes bicarbonate and not carbonate and thus the proton on bicarbonate must be removed. The pseudo-chair conformation of carboxyphosphate suggests an answer to this problem. In the pseudo-chair conformation, it is possible that the phosphate group on carboxyphosphate can act as intramolecular base to remove the proton from the carbonyl carbon. Such an intramolecular proton transfer has been observed in the decomposition of carbamoylphosphate.<sup>56</sup> Quantum mechanical calculations on the proton-transfer reaction reveal that the proton prefers to be located on the phosphate group by about 4 kcal/mol. If such a proton transfer were to occur, one would expect that the leaving group would be HPO<sub>4</sub><sup>-2</sup> instead of PO<sub>4</sub><sup>-3</sup>. While we do not know whether this is the case for N<sup>5</sup>-CAIR synthetase, previous studies on biotin carboxylase indicates that HPO<sub>4</sub><sup>-2</sup> is indeed the product that is released from the enzyme.<sup>57</sup>

With the above studies completed, we could now generate a model of carboxyphosphate bound to N<sup>5</sup>-CAIR synthetase. To do this, we superimposed the phosphate group of the pseudo-chair conformation of carboxyphosphate onto the experimentally observed inorganic phosphate in the ADP:Mg:Pi structure of N<sup>5</sup>-

CAIR synthetase from *E. coli*. To generate a model of carboxyphosphate with AIR bound, we took the carboxyphosphate modeled structure and superimposed the *Aspergillus clavatus* ADP:AIR crystal structure to generate the final ADP:Mg:carboxyphosphate:AIR model. It is important to note that in these models, the superimposed structures displayed less than a 1 Å difference for the alpha carbon atoms of the peptide backbone, and the superimposed structures of ADP were less than 0.5 Å different. Given these modest differences, we are confident that our model represents an accurate snapshot of the active site during catalysis.

According to our model, the carboxyl group of carboxyphosphate is approximately 4 Å away from N<sup>5</sup> of AIR. This distance is longer than would be expected for a direct attack on the carbonyl group. Furthermore, the angle of attack of the amine on the carboxyl group is not ideal. The attacking nucleophile, AIR, should come in at a 107° angle to the carbonyl carbon to maintain the tetrahedral transition state during reaction.<sup>73</sup> But in this model, the orientation of the carbonyl carbon of carboxyphosphate with respect amine of AIR is less than 90°. The interesting feature of this model is that the carbonyl oxygens of the carboxyphosphate were beautifully placed between Lys353 and Arg271, two conserved residues in the active site of N<sup>5</sup>-CAIR synthetase. These observations, in addition to the computational and quantum-mechanical studies on carboxyphosphate, suggested to us that it is unlikely that AIR directly attacks carboxyphosphate. Thus, we propose that carboxyphosphate decomposes to CO<sub>2</sub>

and  $\text{HPO}_3^{-2}$  and the resulting  $\text{CO}_2$  group is then in the correct position for favorable attack by AIR.

If this hypothesis is correct, the enzyme should stabilize  $\text{CO}_2$  within the active site and should catalyze the reaction between  $\text{CO}_2$  and AIR. Experiments to investigate this hypothesis reveal the turnover of AIR by  $\text{N}^5$ -CAIR synthetase in the presence of high bicarbonate concentrations (to generate  $\text{CO}_2$ ) but in the absence of ATP. This experiment demonstrates the second half-reaction of the enzyme, namely AIR and  $\text{CO}_2$  to generate  $\text{N}^5$ -CAIR. This experiment is important because it directly addresses a key mechanistic issue and such a reaction has not been demonstrated for the other ATP-grasp carboxylation enzymes.

To gain more information on the mechanism of the reaction and on the binding site for AIR, we initiated site-directed mutagenesis experiments. The availability of the crystal structures of  $\text{N}^5$ -CAIR synthetase from *Aspergillus clavatus* and *E. coli* provided us with a good platform to start these studies. We mutated five residues (D153, R155, Y152, E73, and K353) to alanine and in all cases, the mutant enzymes displayed decreased catalytic proficiency. The  $K_m$  for AIR for the mutant proteins increased, but surprisingly, for most, the  $K_d$  for AIR remained either unchanged or decreased.

A mutant which is of interest is Glu73. Glu73 makes hydrogen bonding interactions with the 2' and 3' hydroxyl groups of AIR and is away from the catalytic site. Mutation of Glu73 resulted in decrease in  $K_d$  and 1,400-fold decrease in  $k_{\text{cat}}$ . We were surprised to see this result. Careful evaluation of the



crystal structure reveals that Glu73 lies in the same loop as Glu75. Glu75 in turn makes hydrogen-bonding interactions with Arg271, which lies in the active site. As mentioned above, we believe that Arg271 plays an important role in binding and stabilization of carboxyphosphate. We speculate that in the absence of Glu73, the orientation adopted by Glu75 might not be optimal for hydrogen bonding to Arg271. This, in turn, alters the conformation of Arg271, which disrupts the interactions made by this residue with carboxyphosphate.

One of the objectives of the site-directed mutagenesis study was to identify the active-site base used in catalysis. Based upon our model presented above, either Asp153 or Lys353 could function as the base. Both residues are strictly conserved in 100 aligned N<sup>5</sup>-CAIR synthetase amino acid sequences deposited in databanks to date<sup>40</sup>. Structural information from the Mg:ADP:AIR crystal structure shows that Lys353 is approximately 4 Å away from the exocyclic amine of AIR, whereas Asp153 lies less than 3 Å away and is hydrogen bonded to the exocyclic amine of AIR. Mutation of Asp153 results in an enzyme with essentially the same  $K_m$  and  $K_d$  as the wild-type enzyme, but with a  $k_{cat}$  value more than 1,600-fold lower. It is evident from this result that Asp153 is involved in catalysis, but not in binding. Mutation of the Lys353 resulted in an inactive protein that was still capable of binding AIR with the same affinity as the wild-type enzyme. According to our model, Lys353 should play an important role either in the formation or decomposition of carboxyphosphate. Given this important function, it is not surprising that loss of Lys353 may lead to an inactive enzyme. Thus, we propose

that Lys353 is not the active-site base and suggest that Asp153 assumes this function during catalysis.

Taken together, we propose the following mechanism for N<sup>5</sup>-CAIR synthetase (Figure 13). Bicarbonate reacts with ATP to generate carboxyphosphate. Carboxyphosphate, with the aid of Lys353 and Arg271 decomposes to CO<sub>2</sub> and HPO<sub>4</sub><sup>-2</sup>. These same residues serve to hold CO<sub>2</sub> near the site of attack and activate it. In a concerted reaction, the N5 of AIR is deprotonated by Asp153 as it attacks CO<sub>2</sub> to generate the product N<sup>5</sup>-CAIR. The resulting negative charge on the carbamate is neutralized by either Lys353 or Arg271.

Our proposed mechanism is similar to that suggested for other ATP-grasp carboxylases. Kinetic experiments conducted by Tipton *et al.*, showed bicarbonate-dependent and biotin independent activity for biotin carboxylase<sup>57</sup>, which indicates that bicarbonate attacks ATP and forms a carboxyphosphate intermediate. They also showed that the dianion of phosphate is released from the enzymatic reaction, which is consistent with our computational studies of the pseudo-chair conformation of carboxyphosphate and subsequent release of carbon dioxide from carboxyphosphate. Recently, Chou *et al* determined the crystal structure of biotin carboxylase with bicarbonate bound in the active site.<sup>74</sup> In the crystal structure (PDB: 3G8C), one of the oxygen atoms of bicarbonate is located in the correct position to initiate a nucleophilic attack on ATP to form the carboxyphosphate intermediate and the bicarbonate is in hydrogen bonding distance with Lys238 and Arg292.<sup>74</sup> It is important to point out that both biotin

carboxylase and N<sup>5</sup>-CAIR synthetase utilize a lysine and arginine in the bicarbonate site. At physiological pH both of these residues exist as positively charged species and may promote the dissociation of carboxyphosphate intermediate, as we proposed in the case of N<sup>5</sup>-CAIR synthetase (Figure 31).

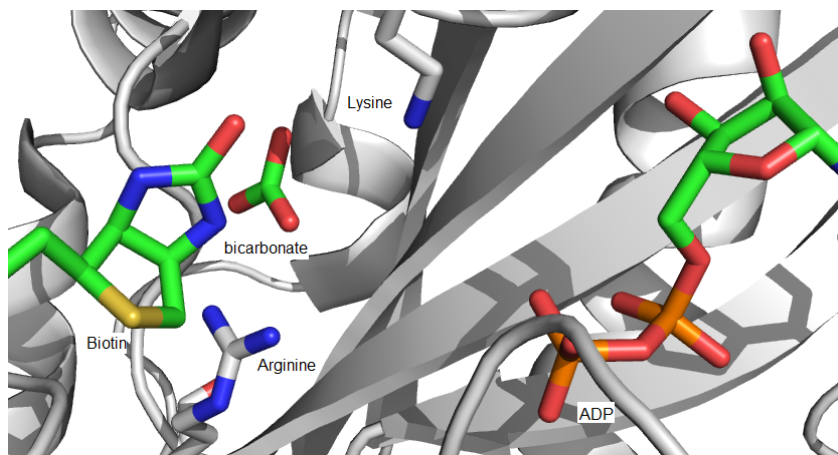


**Figure 32.** Biotin carboxylase with bicarbonate and ADP in the crystal structure.<sup>74</sup> The protein is shown in grey ribbon representation while biotin, bicarbonate and ADP is shown in stick representation with green carbons.

In reactions catalyzed by the carbamoyl phosphate synthetase, after formation of carboxyphosphate, ammonia (derived from glutamine) is carboxylated to form carbamate. Another ATP then phosphorylates the carbamate to form carbamoyl phosphate<sup>50</sup>. Like the biotin carboxylase reaction, it is uncertain whether carboxyphosphate or CO<sub>2</sub> is the carboxylating species. Gibson *et al.* studied the bicarbonate-dependent ATPase reaction catalyzed by carbamoyl phosphate synthetase in the absence of glutamine/ammonia. They showed that the initial rate of bicarbonate-dependent ATP cleavage was faster than the nonenzymatic rate of CO<sub>2</sub> hydration.<sup>72</sup> Given this, these investigators believed that if CO<sub>2</sub> was liberated during catalysis, it should be observable. A variety of

experiments including pH sensitive and  $^{13}\text{C}$ -NMR experiments failed to detect the presence of enzyme-generated carbon dioxide.<sup>72</sup> Based upon this negative result, the investigators concluded that carboxyphosphate must be the carboxylating species in carbamoyl phosphate synthetase. However, since they were studying only the half reaction, the ammonia channel in the enzyme active site could be occupied by water and the rate of hydration of  $\text{CO}_2$  might be enhanced because it occurred in the active site. If this happened, then it is unlikely that there would have been sufficient  $\text{CO}_2$  available for detection.

Taken together our structural, functional, kinetic and computational studies suggest that  $\text{N}^5$ -CAIR synthetase proceeds through carboxyphosphate. We suggested that carboxyphosphate predominantly exists in a pseudo-chair conformation and that this intermediate dissociates to  $\text{CO}_2$  by intramolecular proton transfer from carbonyl carbon to phosphoryl oxygen. The released  $\text{CO}_2$  is stabilized by Lys353 and Arg271.

### 3.2. Identification of inhibitors for $\text{N}^5$ -CAIR synthetase through HTS:

One potential, but unexplored, target in antimicrobial drug design is de novo purine biosynthesis. Since all cells require nucleic acids, growth of rapidly dividing cells can be inhibited by preventing the production of nucleotides.<sup>75, 76</sup> Biochemical and genetic studies have shown that de novo purine biosynthesis is different in microbes than in humans.<sup>23</sup> The divergence in the pathway is centered on the synthesis of CAIR. In microorganisms, purine biosynthesis requires the enzyme,  $\text{N}^5$ -CAIR synthetase. This enzyme is absent in humans.<sup>23</sup> Genetic studies support

the critical role of this enzyme in microbial growth. The enzyme has been identified as a virulence factor and mutations that inactivate the enzyme renders microbes nonvirulent.<sup>28, 33</sup> The uniqueness of N<sup>5</sup>-CAIR synthetase suggests that it is a safe target for the design of antimicrobial agents.

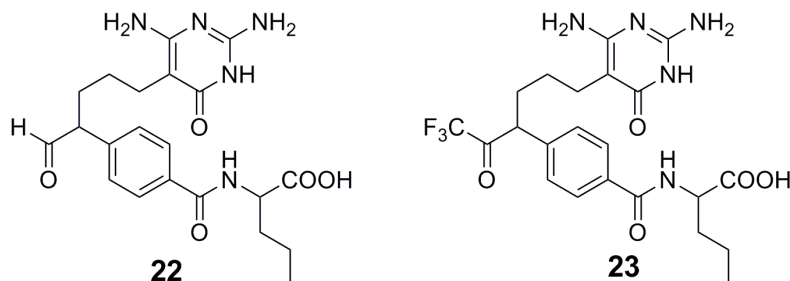
Despite the biochemical rationale for targeting biosynthesis, does inhibiting this pathway make sense? As noted in the introduction, there are two pathways for the synthesis of purines in most microorganisms. These pathways are the salvage pathway and the de novo pathway. Previous biochemical studies have shown that in the absence of de novo purine biosynthesis, microbes usually operate under salvage pathway.<sup>77</sup> However, the salvage pathway produces only a small amount of the total quantity of purine nucleotides within the cell (less than 1%) and it is highly dependent upon an exogenous source of purines. While the exact concentration of purines in different tissues is difficult to know, it is generally believed that the concentration is below 1.5  $\mu\text{M}$ .<sup>78, 79</sup> Thus, biochemical systems that require a large amount of nucleotides (*i.e.* DNA and RNA synthesis), would be rendered inactive due to the lack of basic “building” materials. However, it is important to recognize that inhibition of de novo purine biosynthetic pathway would provide only a bacteriostatic affect to the microorganism. It is also crucial to point out that not all microbes depend on the de novo purine biosynthetic pathway for their nucleotide requirements. For example *Mycobacterium*<sup>80</sup> and *Plasmodium*<sup>81</sup> species do not have the pathway and they largely depend upon the salvage

pathway and exogenous purines for their survival. Thus, in these cases, purine biosynthetic pathway inhibitors would be ineffective in controlling these infections.

The utility of targeting the *de novo* purine pathway can be demonstrated by agents that inhibit other enzymes within the pathway. The first efforts to inhibit the purine biosynthetic pathway were started in 1948 by Elion and coworkers.<sup>75</sup> This group designed 2,6-diaminopurine as an antimetabolite for the purine biosynthetic pathway and they found that the compound strongly inhibited the growth of *L. casei*.<sup>76</sup> They also found that the inhibition was reversed by the addition of adenine to the growing cultures. Excited by this finding, the Elion group intensified the search for more potent inhibitors of the pathway and discovered 6-mercaptopurine.<sup>75</sup> Studies revealed that 6-mercaptopurine was an antimetabolite of hypoxanthine and is a substrate for the enzyme hypoxanthine phosphoribosyltransferase.<sup>75</sup> The principal sites of action appear to be feedback inhibition of *de novo* purine synthesis, inhibition of inosine dehydrogenase, and incorporation into DNA in the form of thioguanine.

*De novo* purine biosynthesis contains two folate-utilizing enzymes. Inhibitors of folate utilizing and metabolizing enzymes are well known and these agents have provided the foundation for the development of inhibitors for the formyl-transfer reactions found in purine biosynthesis. In an effort to inhibit the N<sup>10</sup>-formyltetrahydrofolate-dependent GAR transformylase, Marsilje and Cheng *et al.* designed and synthesized N<sup>10</sup>-formyltetrahydrofolate-mimicking agents (**22** and **23**). These agents are potent inhibitors of the human GAR transformylase and

display exceptional cytotoxic activity.<sup>82-85</sup> To date, there have been no selective inhibitors of microbial transformylase enzymes.<sup>82, 85</sup>



At the beginning of this project, there were no known, small molecule inhibitors of N<sup>5</sup>-CAIR synthetase. To identify inhibitors, we screened 48,000 drug-like compounds using a phosphate-sensitive molybdate assay. This assay is based on the reaction of phosphomolybdate with the dye malachite green, and has been used previously to assay protein tyrosine phosphatase<sup>86</sup>, phosphoinositide phosphatases<sup>87</sup>, and myosin ATPase.<sup>88</sup> Our work is the first to report the use of this assay to screen a compound collection for inhibitors of N<sup>5</sup>-CAIR synthetase. The assay was reproducible ( $Z' > 0.7$ ), cost effective, suitable for automation, and easily converted from 96- to 384-well plates.

Using the above assay, we identified the first selective, non-nucleotide inhibitors of N<sup>5</sup>-CAIR synthetase. These compounds inhibited the enzyme in the range of 30–120  $\mu$ M and follow Lipinski's rules. The compounds were classified into three distinct classes based on structural similarity. Members of class I contained an indenedione group, which upon incubation in water resulted in the production of ninhydrin that reacted with the substrate AIR. Since these compounds are present in commercial chemical libraries, researchers conducting

HTS should be aware of the potential of these compounds to decompose and react with amines present in the substrate.

Compounds belonging to class II are ideal lead agents in that they display non-competitive kinetics with respect to both AIR and ATP. Such a feature is necessary for agents targeting an enzyme in the middle of a biosynthetic pathway since increases in the concentration of the substrate could not overcome inhibition by the drug. Class II compounds are small (approximately 250 atomic mass units) and thus provide flexibility to build additional binding features into the molecule to enhance potency. For example, we have successfully introduced a diazirine moiety into these molecules without losing inhibitory activity (compound **15**).

The non-competitive kinetics of class II molecules could indicate that these agents recognize a unique binding pocket on the enzyme. Interestingly, HTS of other members of the N<sup>5</sup>-CAIR synthetase superfamily (ATP-grasp superfamily) has identified compounds that regulate activity and bind to sites distinct from the active site. For example, the natural product soraphen A inhibits acetyl-CoA carboxylase by binding to a pocket some 25 Å away from the active site.<sup>45</sup> Binding to this location is thought to disrupt protein dimer formation resulting in inactivation of the enzyme. HTS against *S. aureus* Dala:D-ala ligase also identified a non-competitive inhibitor that bound very near the active site and precluded binding of both ATP and D-alanine<sup>58</sup>, respectively.

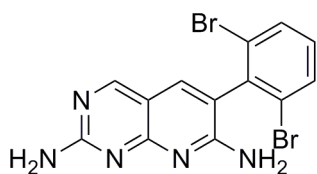
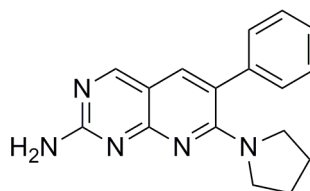
Compound **13**, which belongs to class III inhibitors, displays competitive kinetics with respect to AIR. This suggests that **13** binds at or near the AIR-binding



site. The uncompetitive nature of **13** with respect to ATP is interesting because it indicates that the inhibitor binds only to the enzyme:ATP complex. Given that **13** is competitive with AIR and thus likely binds to the AIR binding site, this suggests that N<sup>5</sup>-CAIR synthetase may function via an ordered kinetic mechanism with ATP binding first followed by AIR. Once both substrates are bound, catalysis occurs. Additional kinetic studies are necessary to validate or refute this conclusion.

In our HTS, we purposely kept the concentration of ATP high to prevent the identification of inhibitors that bound to the ATP site. We reasoned that compounds that competed with ATP would be non-selective. However, a recent study conducted by Miller *et al.* suggests that this hypothesis may be incorrect<sup>89</sup>. Miller *et al.* conducted a bacterial whole-cell screening study to identify compounds with antibacterial properties. They screened a library based upon a protein kinase pharmacophore and found a series of antibacterial pyridopyrimidines. The pyridopyrimidines were effective *in vitro* and *in vivo* against fastidious Gram-negative pathogens including *Haemophilus influenzae*.<sup>89</sup> Subsequent studies on one of the pyridopyrimidines (**24** and **25**) found that **24** and **25** targeted the ATP binding site of biotin carboxylase.<sup>89-91</sup> As we have mentioned previously, biotin carboxylase is a member of the ATP-grasp superfamily and is related to N<sup>5</sup>-CAIR synthetase. The identification of potent and selective inhibitors of biotin carboxylase is important, because it indicates that the ATP-binding site of the ATP-grasp superfamily of enzymes is distinct from that of other ATP-binding sites found in eukaryotic protein kinases and other ATP-utilizing enzymes. Given

this discovery, it is easy to envision efforts to target the ATP-binding site of N<sup>5</sup>-CAIR synthetase as a means to develop new antimicrobial agents targeting purine biosynthesis.

**24****25**

### 3.3. Identification of the binding site for class II inhibitors:

Kinetic studies on class II inhibitors, typified by **7**, revealed that these agents displayed non-competitive kinetics with respect to both AIR and ATP. The non-competitive nature of these inhibitors makes them attractive lead agents because they are immune to the increase in substrate concentration that would be expected when inhibiting an enzyme in the middle of a biosynthetic pathway. However, since non-competitive inhibitors frequently do not bind to the active site, structural studies become necessary to aid optimization of the inhibitor. Thus, it became a priority to determine the binding site for class II inhibitors.

Given the fact that the structure of N<sup>5</sup>-CAIR synthetase has been solved, we initiated a project that attempted to determine the structure of the inhibitor:enzyme complex. Unfortunately, the poor aqueous solubility of the class II inhibitors prevented the determination of the structure. To circumvent this problem, we chose to use a photoreactive derivative of the class II inhibitor, **7**, to label the binding site. Once this was accomplished, the location of the binding site could be determined by LC/MS/MS methods. The use of photoaffinity molecules to

modify the site of interaction has been very effective in providing information about the location of binding sites.<sup>60</sup> We synthesized **15** and conducted photocrosslinking studies with N<sup>5</sup>-CAIR synthetase. SDS-PAGE analysis of these studies revealed the presence of an 84 kDa band in addition to the expected 42 kDa band. Protein sequence analysis of the 84 kDa band demonstrated that it was N<sup>5</sup>-CAIR synthetase. Thus, two monomers of N<sup>5</sup>-CAIR synthetase were crosslinked. In order for this to occur, two photoactive groups must be present in **15**. Subsequent experiments showed that the istatin group in **15** was converted into isatoic anhydride, which presumably reacted with the protein.

The conversion of isatin into isatoic anhydride has been demonstrated in the literature using a variety of conditions containing either peroxide or chromium oxidants.<sup>92, 93</sup> However, there has been little mention of the photochemical conversion of isatin into the anhydride. Previous researchers who have investigated the photochemistry of isatin reported the photodecomposition of isatin in benzene with the subsequent detection of very small amounts of isatoic anhydride.<sup>94</sup> These researchers proposed that isatin might be converted to a diradical species that reacts with another isatin molecule to form isatoic anhydride. In another report, the photoreaction of isatin resulted in the formation of isatic acid (2-amino-phenylglyoxalic acid)<sup>95</sup> and not isatoic anhydride.<sup>94</sup>

To resolve these issues and to understand the photochemistry of isatin, we irradiated *N*-methyl isatin in water. We found that *N*-methyl isatin is cleanly converted to isatoic anhydride as shown in Figure 23. Additional experiments in

both “wet” and dry THF revealed that isatoic anhydride formed only in the presence of water. We have not done definitive experiments excluding molecular oxygen, but we believe that oxygen also plays a role in the conversion. Our mechanism for the synthesis of isatoic anhydride from isatin is shown in Figure 32. In this radical mechanism, UV light generates an isatic radical that then attacks oxygen. The resulting intermediate then undergoes ring expansion in a manner similar to that for the Baeyer-Villiger reaction to generate the anhydride.<sup>92</sup> This mechanism also posits that hydrogen peroxide is formed, and previous investigators have shown that hydrogen peroxide catalyzes the conversion of isatin to isatoic anhydride.<sup>92</sup>

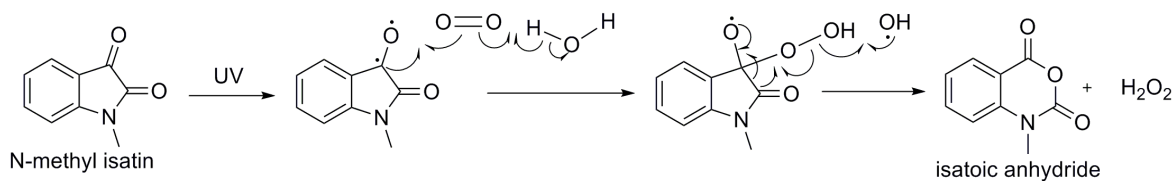


**Figure 33.** Proposed mechanism for the formation of isatoic anhydride from isatin

Once isatoic anhydride is formed, it must react with the protein for crosslinking of the monomers to occur. Previous researchers have reported that isatoic anhydride and its derivatives are reactive towards, lysine, serine and tyrosine derivatives<sup>63, 64</sup> and Zhang *et al.* have used a fluoros-tagged isatoic anhydride as a scavenger for amines in solution phase parallel syntheses.<sup>96</sup> All of these results are consistent with our studies regarding the reaction between isatoic anhydride and benzyl alcohol.

With our understanding of the photochemistry of isatin, we searched for peptides in our LC/MS/MS data that had an increase in molecular weight of 261. This molecular weight corresponds to a reaction with the protein at the isatin side of the molecule and the reaction of water with the diazirine side. Examination of the proteomic data revealed that serine 227 was modified several times indicating that this residue may be in the binding site of the class II inhibitors. However, serine 227 is not located at the dimer interface and thus cannot easily explain the formation of the dimer. The distance between serine 227 and the dimer interface of N<sup>5</sup>-CAIR synthetase is greater than 20 Å, yet the linker length of **15** is only 6 Å. Examination of the peptides determined from the LC/MS/MS experiments revealed that two peptides, KLVYAPAR and AVAAFDGKG are missing in the crosslinked protein. Interestingly, Ser227 is located in the sequence, KLVYAPARNVSDAINQKA, which contains one of the missing peptides. Mapping of these missing peptides onto the crystal structure of N<sup>5</sup>-CAIR synthetase reveals that neither peptide is near the dimer interface (Figure 28). If these peptides are from the class II binding site, this would indicate that N<sup>5</sup>-CAIR synthetase exists in multiple dimer conformations, only one of which has been crystallized. The existence of multiple dimer conformations is well documented for other proteins. For example, the transcriptional protein AraC undergoes dramatic dimer reorganization upon binding of the sugar arabinose.<sup>97, 98</sup>

The possibility of multiple conformations for the synthetase could also be important for the interaction of this protein with other enzymes in the purine

biosynthetic pathway. Recent work by the Benkovic laboratory has demonstrated the presence of a purisome complex in eukaryotic cells.<sup>25</sup> The formation of a multi-enzyme complex in purine biosynthesis has been speculated for years because of the instability of many of the intermediates in purine biosynthesis.<sup>25</sup> While the presence of the purisome has not been demonstrated in microorganisms, there is a compelling argument for why it should exist. N<sup>5</sup>-CAIR is one of the most unstable intermediates in purine biosynthesis. This compound has a half-life of approximately one minute under physiological conditions and decomposes to generate AIR.<sup>23</sup> Thus, if the synthesis of N<sup>5</sup>-CAIR is not tightly regulated, uncontrolled consumption of ATP occur. The presence of alternative conformations of N<sup>5</sup>-CAIR synthetase, some of which are inactive, could provide a solution to this problem. The presence of regulatory sites on N<sup>5</sup>-CAIR synthetase is also supported by studies on other ATP-grasp enzymes. For example, the polyketide, soraphen A, was discovered to be an allosteric inhibitor of biotin carboxylase<sup>45</sup>. Interestingly, soraphen A inhibits the activity of the enzyme despite the fact that it binds to the enzyme at a site that is ~20 Å away from the active site. This observation supports the contention that there are conformational changes, which regulate enzyme activity in ATP-grasp enzymes.

## Chapter 4.

### CONCLUSION AND FUTURE DIRECTIONS

In this dissertation we have conducted studies aimed at understanding the mechanism of N<sup>5</sup>-CAIR synthetase and identifying inhibitors of the enzyme. We initiated this study because N<sup>5</sup>-CAIR synthetase is found only in bacteria, yeast, and fungi, and thus is a ideal target for developing antimicrobial agents. Given the critical need for novel antibacterial and antifungal drugs, we believe that studies on this enzyme are needed to aid in the identification of agents that can inhibit this enzyme.

We began our studies with collaboration with Dr. Hazel Holden on the determination of the crystal structure of the enzyme from bacteria and fungi. These studies provided important information on the active-site architecture in the presence of various substrates and products. However, one critical intermediate could not be experimentally determined. N<sup>5</sup>-CAIR synthetase, like all ATP-grasp carboxylation enzymes is believed to proceed through formation of a carboxyphosphate. The instability of this intermediate required that we generate a molecular model of carboxyphosphate bound to the active site. However, once carboxyphosphate has been formed, its fate is unclear. Some researchers believe that carboxyphosphate dissociates to produce CO<sub>2</sub>, which is the true electrophile of the reaction. Others believe that carboxyphosphate itself is the electrophile. For N<sup>5</sup>-CAIR synthetase, a combination of structural, computational, and biochemical experiments have lead us to conclude that CO<sub>2</sub> is the electrophile in the reaction.

Once carbon dioxide is generated, the exocyclic amine of AIR attacks it to generate the product N<sup>5</sup>-CAIR.

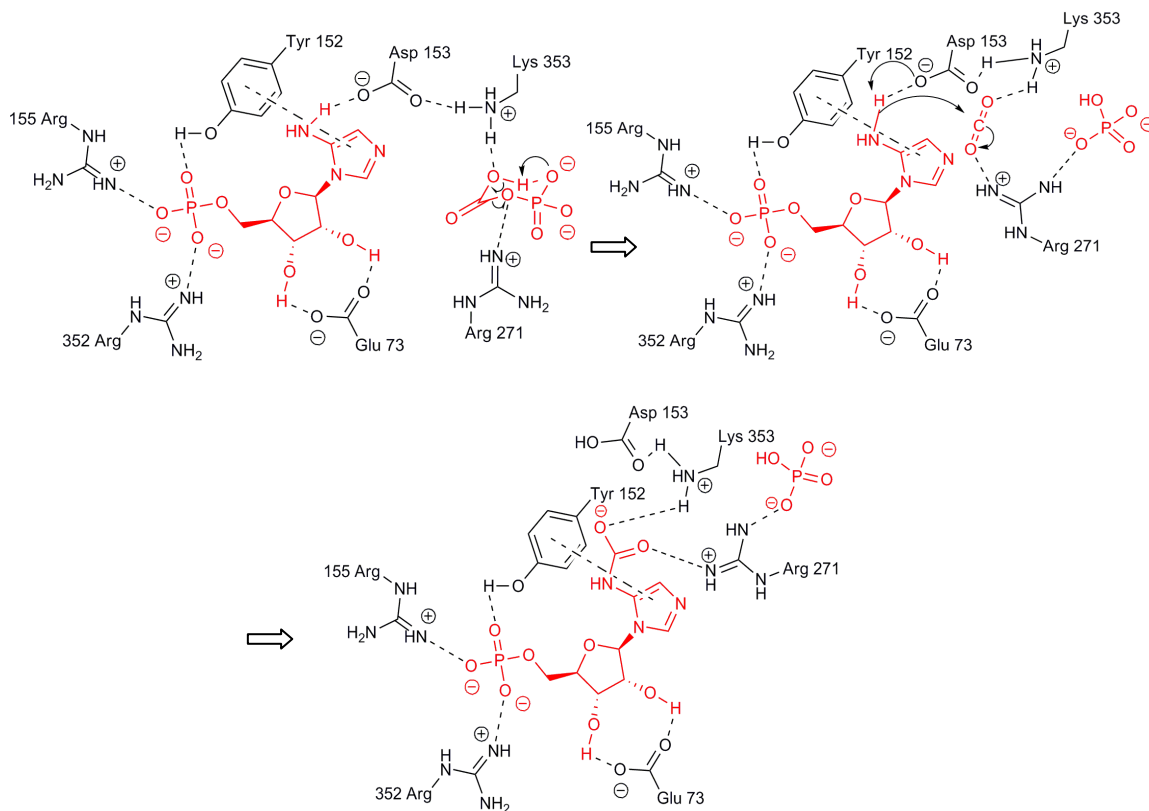


**Figure 15.** Proposed mechanism for N<sup>5</sup>-CAIR synthetase. AIR and carboxyphosphate are shown in red. The functional groups of the side chains of amino acids believed to be involved in the mechanism are shown along with the residue number.

Our second objective in this work was to identify inhibitors of N<sup>5</sup>-CAIR synthetase. In order to accomplish this, we conducted high-throughput screening on commercially available compound libraries at the Center for Chemical Genomics located at the University of Michigan. We identified three classes of inhibitors for the enzyme; however, only two sets of inhibitors turned out to have properties useful for drug-discovery studies. One compound was competitive with



AIR, and thus likely bound to the substrate-binding site of the enzyme. While interesting, we chose not to focus on this compound because of potential substrate competition issues. The remaining inhibitors were non-competitive with both AIR and ATP. These inhibitors were also selective in that they do not inhibit human AIR carboxylase, an enzyme evolutionarily related to the bacterial system. To determine the allosteric binding site of these inhibitors, we synthesized a diazirine photocrosslinking derivative and used this molecule to identify the binding site by proteomic analysis. Interestingly, our data showed dimerization of N<sup>5</sup>-CAIR synthetase in presence of the photo crosslinking agent. Subsequent photochemical studies revealed that isatin in presence of water and dissolved oxygen is converted to isatoic anhydride in the presence of UV light. This result is a new finding for isatin chemistry.

The proteomic analysis of the photo crosslinked protein revealed that serine 227 was the residue modified by the photocrosslinking agent. Additional studies on the photocrosslinked dimer revealed that only two peptides were missing in the dimerized protein indicating that these peptides might have in the binding site for the inhibitor. However, examination of the location of these two peptides in the crystal structure showed that the peptides are far away from the dimer interface of the enzyme. Thus, if these two peptides are indeed in the inhibitor binding site, N<sup>5</sup>-CAIR synthetase must exist in multiple dimer conformations.

### Areas of future research

The proposed mechanism for N<sup>5</sup>-CAIR synthetase is based upon indirect evidence. To gather direct evidence, direct detection of CO<sub>2</sub> released from the carboxyphosphate will need to be done. Examples of direct experimental approaches include NMR and IR measurements. Both have been applied to the study of carbon dioxide generating or utilizing enzymes.<sup>23, 72, 99</sup> Other approaches would include the use of CO<sub>2</sub> mimics (*i.e.* COS, etc) to determine if these agents inhibit the reaction or attempts to react various agents with CO<sub>2</sub> to trap this intermediate on the enzyme.

Future studies will also be needed to validate the binding site for the class II inhibitors. One possible approach would be to utilize site-directed mutagenesis to alter the binding site of the inhibitor. Mutants that prevent the ability of the class II inhibitors from inhibiting the enzyme would suggest the binding site for the compounds.

Future work can also be done on creating inhibitors of the ATP-binding site of N<sup>5</sup>-CAIR synthetase. As noted in the discussion, recent research on inhibitors of biotin carboxylase found a set of compounds which inhibit the enzyme while binding to the ATP site. These studies suggest that the ATP-binding site of ATP-grasp enzymes may be fundamentally different than sites found in other classes of enzymes. Studies on the ability of pyridopyrimidines to inhibit N<sup>5</sup>-CAIR synthetase may be useful future investigations.

## Chapter 5

### MATERIALS AND METHODS

All chemicals, unless otherwise indicated were purchased from Thermo Fischer Scientific, Aldrich or Sigma. N<sup>5</sup>-CAIR synthetase was obtained from Professor Hazel Holden (University of Wisconsin, Madison) and stored at -80 °C. The PurE and ADE2 genes were obtained from Professor Vincent Jo Davisson (Purdue University, West Lafayette). Unless otherwise stated, all solutions were stored at -20 °C. During all measurements, reagents and enzyme solutions were stored in crushed ice. Measurements of pH were done using an Acumet basic AB15 pH meter from Fischer Scientific. HPLC was conducted on a Waters 600 HPLC instrument using a PRP-1 column (Hamilton). Gas phase chromatographic analysis was done using a Trace GC Ultra instrument with mass spectrometry detection conducted with an ITQ900 instrument. Both instruments were obtained from Thermo Scientific. Enzymatic assays were performed on a Varian Cary 3 UV-vis spectrophotometer equipped with a temperature controller. All curve fitting was conducted using the software, Kaleidagraph. NMR spectra were recorded using a Varian 400 MHz spectrometer with deuterated solvents obtained from Cambridge Isotopes.

#### 5.1. Cloning, expression, and purification of human AIR carboxylase and bacterial N<sup>5</sup>-CAIR mutase:

The cloning of human AIR carboxylase and bacterial N<sup>5</sup>-CAIR mutase was accomplished as follows. The human gene was amplified by PCR using primer I

(5'-GGAATTCCATATGGCGACAGCTGAG-3'), which contains a NdeI site and primer II (5'-GGGCTCGAGTAAATTACATTCTCTG-3'), which contains a XhoI site. The bacterial gene was also amplified by PCR using primer III (5'-GGGAATTCCATATGGTCTTCCCGCA-3') which contains an NdeI site and primer IV (5'-GGGCTCGAGTGCCGCACCTCGCGG-3'), which contains an XhoI site. The purified PCR products were ligated into separate pGEM-T (Promega) vectors for screening and sequencing. Both pGEM vectors were digested with NdeI and XhoI to excise the N<sup>5</sup>-CAIR mutase and AIR carboxylase genes. Each gene was ligated into a pET22b (Novagen) plasmid for protein expression. Expression from this vector generated an N-terminal His-tag which contained the sequence MGSSHHHHHSSENLYFQGH at the beginning of the protein.

To express and purify the protein, each vector was transformed into *E. coli* DE3 cells. A colony from each transformation was grown overnight in lysogeny broth media at 37 °C. The overnight culture was used to inoculate a 500 mL culture and the culture was grown at 37 °C with shaking until an optical density of ~0.6 was measured at 600 nm. Protein expression was induced by the addition of 1 mM isopropyl β-D-1-thiogalactopyranoside and the induction was allowed to proceed for 2 hours. The cultures were cooled to 4 °C, the cells were collected by centrifugation at 4 °C and the cell pellets were stored frozen until use. To purify the protein, cells were lysed with B-PER cell lysing reagent (Thermo Scientific) and the resulting cellular debris was removed by centrifugation. The resulting supernatant was loaded onto a cobalt nitrilotriacetic acid resin column (Thermo

Scientific) and the column was washed with wash buffer (50 mM sodium phosphate, 300 mM sodium chloride, 10 mM imidazole; pH 7.4). The protein was then eluted with elution buffer (50 mM sodium phosphate, 300 mM sodium chloride, 150 mM imidazole; pH 7.4). Purified N<sup>5</sup>-CAIR mutase and AIR carboxylase were dialyzed against 10 mM Tris-HCl and 200 mM NaCl (pH 8). Following dialysis, the sample was concentrated to ~15 mg/mL and frozen in -80 °C freezer.

## 5.2. Kinetic analyses of wild-type and mutant N<sup>5</sup>-CAIR synthetase:

The steady-state kinetic parameters for the wild-type and mutant enzymes were determined using the ATP-coupled assay system as previously described<sup>43, 100</sup>. In a 1 mL cuvette, buffer (50 mM HEPES (pH 7.5), 20 mM KCl, and 6.0 mM MgCl<sub>2</sub>), 0.2 mM NADH, 2.0 mM phosphoenolpyruvate, 1.0 mM NaHCO<sub>3</sub>, 4 units of pyruvate kinase, and 17 units of lactate dehydrogenase were added. After the cuvette was equilibrated to 37 °C, N<sup>5</sup>-CAIR synthetase was added (the amount varied depending upon the mutant protein) followed by 1.1 mM ATP. Background levels of ATP hydrolysis were measured, and the reaction was initiated by the addition of AIR (concentration varied from 5 to 500 μM). NADH oxidation was monitored at 340 nm, and the concentration of AIR consumed was calculated using the extinction coefficient for NADH (6200 M<sup>-1</sup> cm<sup>-1</sup>). The background ATPase activity was very low (<0.5%) and thus was not subtracted from the initial velocity. The initial velocity of each reaction was determined during the first 2 min, and a plot of initial velocity versus AIR concentration was generated. Kinetic parameters

were determined by fitting multiple data sets to the Michaelis-Menten equation using KaleidaGraph.

### 5.3. Equilibrium dialysis of wild-type and mutant enzymes with substrate AIR:

The dissociation constant for AIR was determined by equilibrium dialysis. To conduct these experiments, 200  $\mu\text{L}$  of enzyme (final concentration of 10-12  $\mu\text{M}$  based upon a dimer molecular weight) in 50 mM HEPES (pH 7.5), 20 mM KCl, and 6.0 mM  $\text{MgCl}_2$  buffer was added to six dialysis tubes (MWC of 8,000). Simultaneously, six glass vials containing 1.5 mL of one of six AIR concentrations (from 1 to 300  $\mu\text{M}$  in the same buffer as the enzyme) were prepared, and the absorbance of each solution was determined at 250 nm. The concentration of AIR was determined using the published extinction coefficient of  $3,270 \text{ M}^{-1} \text{ cm}^{-1}$ . One dialysis tube was added to each vial, and the vials were gently shaken for 16 h at room temperature. After dialysis, the concentration of free AIR was determined by the absorbance at 250 nm using the extinction coefficient listed above. The concentration of bound AIR was determined by subtracting the amount of free AIR from the total amount of AIR added at the beginning of the experiment. Control experiments conducted in the absence of enzyme revealed no change in AIR concentration, indicating that the substrate was stable over the course of the experiment. Control experiments of the enzymes in the absence of substrate revealed that they lost 10-20 % of their activity during shaking at room temperature over the 16 h period. The dissociation constants and enzyme concentrations were

determined by fitting the data from a plot of the total amount of AIR versus the amount of bound AIR to the quadratic equation (Equation 1).

#### 5.4. Bicarbonate-dependent ATPase activity of N<sup>5</sup>-CAIR synthetase:

The bicarbonate-dependent ATPase activity was measured as follows. In a 1 mL cuvette, buffer (50 mM HEPES (pH 7.5), 20 mM KCl, and 6.0 mM MgCl<sub>2</sub>), 0.2 mM NADH, 2.0 mM phosphoenolpyruvate, 4 units of pyruvate kinase, and 17 units of lactate dehydrogenase were added. After the cuvette was equilibrated to 37 °C, 28 µg of N<sup>5</sup>-CAIR synthetase was added followed by 1.1 mM ATP. Background levels of ATP hydrolysis were measured, and the reaction was initiated by the addition of NaHCO<sub>3</sub> (concentration varied from 0 to 60 mM; the background value of bicarbonate in solution was not considered). NADH oxidation was monitored at 340 nm, and the concentration of ATP consumed was calculated using the extinction coefficient for NADH (6,200 M<sup>-1</sup> cm<sup>-1</sup>).

#### 5.5. Synthesis of N<sup>5</sup>-CAIR by N<sup>5</sup>-CAIR synthetase in the absence of ATP:

In a 1 ml total volume, buffer (HEPES 50 mM, KCl 20 mM, pH 7.8), 20 mM HCO<sub>3</sub><sup>-</sup>, 112 µg of enzyme were added. The reaction was incubated at 10 °C for 3 minutes and background absorptions were measured. The reaction was initiated by the addition of 0.5 mM AIR. The decrease in absorbance at 250nm was monitored for the consumption of AIR. Control reactions consisted of AIR and bicarbonate in the absence of enzyme and AIR and bicarbonate in the presence of 112 µg of bovine serum albumin (BSA).

#### 5.6. Molecular modeling for determining CO<sub>2</sub> binding site:

The location of AIR and ADP were experimentally determined from the *Aspergillus clavatus* N<sup>5</sup>-CAIR synthetase crystal structure (PDB: 3K5I). *E. coli* N<sup>5</sup>-CAIR synthetase (PDB: 3ETJ) was superposed on *Aspergillus* enzyme to generate inorganic phosphate on the *Aspergillus* enzyme. The inorganic phosphate binding site is the presumed binding site of carboxyphosphate. So, the modeled carboxyphosphate was superposed on inorganic phosphate to generate carboxyphosphate model in the active site.

#### 5.7. High-throughput screening of chemical libraries for inhibitors of N<sup>5</sup>-CAIR synthetase:

High-throughput screening was conducted at the Center for Chemical Genomics at the University of Michigan, Ann Arbor. The screening was conducted as follows. Buffer was added to each well of a 384-well plate (50 mM HEPES, pH 7.5, 20 mM KCl, 6.0 mM MgCl<sub>2</sub>, 100 mM ATP, supplemented with a 1/100 dilution of saturated NaHCO<sub>3</sub>) and 0.2 μL of a DMSO stock of each compound was added to the plate using a Biomek FX pin tool such that the final concentration of the compound in each well was between 5 and 27 μM. Each plate contained a column of positive controls (enzyme + AIR + 0.2 μL of DMSO) and negative controls (enzyme - AIR + 0.2 μL of DMSO). AIR (50 μM) was added to the appropriate wells using a Thermo Labsystems Multidrop Micro plate dispenser followed by 168 ng of N<sup>5</sup>-CAIR synthetase. The reaction mixture was incubated at room temperature for 5 min and was quenched by the addition of 6 μL of the malachite



green reagent (Bioassay Systems) to each well. The plates were incubated at room temperature for at least 15 min and then the absorbance (600 nm) of each well was determined using a PHERA star (BMG Labs) plate reader.

#### 5.8. Dose-response analysis of hits from the high-throughput screen:

The dose response assays were conducted at the Center for Chemical Genomics at the University of Michigan, Ann Arbor. The eight-point dose-response assay uses the same protocol as the high-throughput assay except that the concentration of each compound assayed was varied from 0.78 to 100  $\mu\text{M}$ . Each assay contained the same positive and negative controls used for the high-throughput screen. Data for compounds displaying a dose-response relationship were curve fitted using the following equation (Equation 2) to determine the  $\text{IC}_{50}$  value.

$$R = \frac{P-N}{(1+p\text{IC}_{50}-\text{Dose})^{\times H}} \quad (2)$$

For equation 2, R is the response, N is the value of the negative control, P is the value of the positive control, H is the Hill slope, and  $p\text{IC}_{50}$  is the negative logarithm of the  $\text{IC}_{50}$ .

#### 5.9. Kinetic analysis of inhibitors against $\text{N}^5$ -CAIR synthetase:

In a 1-mL cuvette, 50 mM HEPES, pH 7.5 buffer, containing 20 mM KCl and 6.0 mM  $\text{MgCl}_2$ , was added followed by 0.2 mM NADH, 2.0 mM PEP, 1.0 mM  $\text{NaHCO}_3$ , 4 units of pyruvate kinase, and 17 units of lactate dehydrogenase. To the cuvette, 168 ng of  $\text{N}^5$ -CAIR synthetase was added, followed by ATP and the cuvette was incubated at 37  $^{\circ}\text{C}$  for 3 min. For experiments in which ATP was held

constant, the ATP concentration was 1.1 mM while the concentration of AIR was varied from 5 to 250  $\mu\text{M}$ . For experiments in which AIR was held constant, the AIR concentration was held at 100  $\mu\text{M}$  while ATP was varied from 5 to 250  $\mu\text{M}$ . Background levels of ATP hydrolysis were measured, and the reaction was initiated by the addition of AIR and the inhibitor to be tested (0–50  $\mu\text{M}$ ). The reaction mixture was incubated at 37 °C and NADH oxidation was monitored at 340 nm. The background ATPase activity was very low (<0.5%) and thus was not subtracted from the initial velocity. The initial velocity of each reaction was determined during the first 2 min, and a plot of initial velocity versus varied substrate was generated. Lineweaver–Burke plots of each experiment were constructed to determine the likely mode of inhibition. Secondary plots of the slope versus inhibitor concentration were used to determine the  $K_i$  value for each inhibitor. All graphing and curve fitting was done using KaleidaGraph.

#### 5.10. Measurement of Minimum Inhibitory Concentrations (MICs):

MICs were determined in a liquid assay with *E. coli* NEB-5 cells growing in variant bacterial (VB) medium. Exponential-phase cultures of *E. coli* (5 $\mu\text{L}$ ) were distributed in a 96 well plate containing 200  $\mu\text{L}$  of VB medium. Each well was treated with one drug concentration (0.1, 0.5, 1, 2, 4, 8, 16, 32, 64, 128, 256, 512  $\mu\text{g/ml}$ ). In another well, ampicillin (100  $\mu\text{g/ml}$ ) was added as control. The plate was incubated at 37 °C for 12 hours and then observed to determine cell growth. The lowest concentration of drug that resulted in no visible growth was taken as the MICs of the compound. To determine if growth inhibition could be rescued,

cultures which were inhibited by the compound were treated with 1 mM of adenine in water and incubated at 37 °C for 12 hours. Recovery of growth was again determined visually.

#### 5.11. Kinetic analysis of inhibitors against human AIR carboxylase:

Compounds **7**, **13**, and **14** were analyzed as inhibitors against the human bifunctional enzyme using the coupled assay as previously described for the *Gallus gallus* bifunctional AIR carboxylase:SAICAR synthetase<sup>100</sup>. In a 1 mL total volume, 50 mM HEPES, pH 7.8, 0.05 µg of enzyme, and 25 mM MgCl<sub>2</sub> were preincubated for 5 min at room temperature. To the solution, 100 mM KHCO<sub>3</sub>, 2.0 mM PEP, 1.0 mM ATP, 4.0 units of pyruvate kinase, 10 mM aspartic acid, and 0.24 unit of human bifunctional enzyme carboxylase:SAICAR synthetase were added. The reaction was incubated at 37°C and was initiated by the addition of 0.5 mM AIR. After 1 minute monitoring the reaction 200 µL of **7**, **13**, and **14** were added to the reaction and the reaction was continued to monitor at 282 nm for the production of SAICAR.

AIR carboxylase was assayed as follows.<sup>43</sup> In a 1 ml total volume, buffer (Hepes 50 mM, KCl 20 mM, pH 7.8) and 0.05 µg of enzyme were added. The reaction was incubated at 37 °C and the inhibitor to be tested was added (200 µM). The reaction was initiated by the addition of 0.5 mM CAIR and the conversion of CAIR to AIR was monitored at 260 nm.

#### 5.12. Synthesis of the photocrosslinker **15**:

1.10. A. tert-Butyl 3-(2,3-dioxindolin-1-yl)propylcarbamate (**16**):

To a stirred solution of isatin (2.71 mmol, 400 mg) and NaH (2.71 mM, 65 mg) in dry dimethylformamide, tert-butyl 3-bromopropylcarbamate (2.71 mM, 647 mg) was added dropwise under argon atmosphere. The reaction was stirred for 16 hours until TLC analysis (10% acetone in dichloromethane as the mobile phase) revealed the disappearance of the starting materials. The reaction was evaporated to dryness under reduced pressure and the solid residue was treated with water to quench the reaction. The aqueous mixture was extracted with dichloromethane to isolate compound **16**. Compound **16** was purified by silica column chromatography using 10% acetone in dichloromethane as the mobile phase. The appropriate fractions were isolated, evaporated to dryness to generate a solid (yield: 95%). <sup>1</sup>H NMR (400 MHz, CDCl<sub>3</sub>) δ 1.405 (s, 3H), 1.415 (s, 3H), 1.437 (s, 3H), 1.880 (t, 2H, *J* = 12 Hz), 3.159 (d, 2H, *J* = 5.2Hz), 3.775 (q, 2H, *J* = 6.4 Hz), 5.019 (s, 1H), 6.89 (m, 1H), 7.12 (m, 1H), 7.58 (m, 2H). <sup>13</sup>C NMR (100 MHz, CDCl<sub>3</sub>), δ 180.1, 161.9, 155.9, 148.1, 134.7, 117.7, 116.2, 125.7, 134.7, 79.5, 39.8, 37.4, 28.4. Ms calculated for C<sub>16</sub>H<sub>20</sub>N<sub>2</sub>O<sub>4</sub> is (M+H) is 305.14, fond 305.13

1.10.B. *N*-(3-(2,3-Dioxoindolin-1-yl)propyl)-3-(3-methyl-3H-diazirin-3-yl)propanamide (**15**):

Compound **16** was added to a solution of HCl in ether (2 M, 2 ml) and the resulting deprotection was allowed to run at room temperature for 10 hours. The reaction was then evaporated under reduced pressure to generate the crude, orange colored salt of 1-(3-aminopropyl) indoline-2, 3-dione. A small portion of the material was kept aside for NMR analysis and the rest of the compound was

utilized for the coupling of diazirine moiety without further purification. The salt of 1-(3-aminopropyl) indoline-2, 3-dione (0.2 mM, 50 mg) was added to 1 ml of dry pyridine and stirred for 15 minutes. To the pyridine solution under argon atmosphere, 2,5-dioxopyrrolidin-1-yl 3-(3-methyl-3H-diazirin-3-yl) propanoate (0.2 mM, 45 mg, Pierce Biotechnology) was added. The reaction mixture was stirred for 16 hours and then evaporated under reduced pressure. The resulting residue was washed with 1 N HCl to remove pyridine and the remaining crude material was subjected to silica column chromatography using 10% acetone in dichloromethane as the mobile phase. The product **15** was isolated in 80% yield.  $^1\text{H}$  NMR (400 MHz,  $\text{CDCl}_3$ ):  $\delta$  1.043 (s, 3H), 1.785 (t, 2H,  $J = 7.2\text{Hz}$ ), 1.925 (q, 2H, 5.6Hz), 2.061 (t, 2H,  $J = 7.6\text{Hz}$ ), 3.26 (q, 2H,  $J = 6.4\text{Hz}$ ), 3.825 (q, 2H,  $J = 6.4$ ), 6.92 (d, 1H,  $J = 7.6\text{Hz}$ ), 7.159 (m, 1H), 7.625 (m, 2H).  $^{13}\text{C}$  NMR (100 MHz,  $\text{CDCl}_3$ ):  $\delta$  179.9, 172.6, 160.1, 148.1, 134.7, 129.9, 125.7, 116.7, 68.9, 44.8, 37.7, 39.8, 26.3, 26.1. MS calculated for  $\text{C}_{16}\text{H}_{19}\text{N}_4\text{O}_3$  is (M+H) 315.13, found 315.14.

### 5.13. Kinetic analysis of **15** against $\text{N}^5$ -CAIR synthetase:

In a 1-mL cuvette, 50 mM HEPES, pH 7.5 buffer, containing 20 mM KCl and 6.0 mM  $\text{MgCl}_2$ , was added followed by 0.2 mM NADH, 2.0 mM PEP, 1.0 mM  $\text{NaHCO}_3$ , 4 units of pyruvate kinase, and 17 units of lactate dehydrogenase. To the cuvette, 168 ng of  $\text{N}^5$ -CAIR synthetase was added, followed by ATP and the cuvette was incubated at  $37^\circ\text{C}$  for 3 min. Background levels of ATP hydrolysis were measured, and the reaction was initiated by the addition of AIR and the inhibitor to be tested (0 and 90  $\mu\text{M}$ ). The reaction mixture was incubated at  $37^\circ\text{C}$

and NADH oxidation was monitored at 340 nm. The background ATPase activity was very low (<0.5%) and thus was not subtracted from the initial velocity. The initial velocity of each reaction was determined during the first 2 min, and a plot of initial velocity versus varied substrate was generated. Lineweaver–Burke plots of each experiment were constructed to determine the  $V_{\max}$  and  $V_{\max \text{ app}}$ . The  $K_i$  value was determined using equation 3 in which  $V_{\max \text{ app}}$  is the maximal velocity obtained from dose-response curve,  $V_{\max}$  is obtained from uninhibited curve and  $[I]$  is inhibitor concentration.

$$K_i = (V_{\max \text{ app}} \times [I]) / V_{\max} \quad (3)$$

#### 5.14. Photocrosslinking experiments with **15** and N<sup>5</sup>-CAIR synthetase:

To examine the ability of **15** to crosslink N<sup>5</sup>-CAIR synthetase, the following experiment was performed. Into 3 separate PCR tubes, a 100  $\mu\text{l}$  total of a solution of phosphate buffered saline (50  $\mu\text{L}$  of 0.1 M sodium phosphate, 0.15 M sodium chloride, pH 7.2), N<sup>5</sup>-CAIR synthetase (100  $\mu\text{M}$ ), ATP (100  $\mu\text{M}$ ), and AIR (100  $\mu\text{M}$ ) was added. One tube was set aside as a negative control. To another tube, **15** (100  $\mu\text{M}$ ) was added. To a third tube, **15** and **7** (100  $\mu\text{M}$  each) were added. A fourth tube containing phosphate buffer saline, enzyme and **15** was prepared. All tubes were UV irradiated with an 110V UV lamp (model: B100AP, manufactured by UVP Inc.) emitting radiation between 340-360 nm for 20 minutes. The distance between the light source and the reaction was 5 cm. The reaction was analyzed on a 12% SDS-PAGE gel and visualized by staining with Commassie Blue.

5.15. Dose-dependent photocrosslinking studies of **15** with N<sup>5</sup>-CAIR synthetase:

In a 100  $\mu$ L solution contained in PCR tubes, phosphate buffered saline (50  $\mu$ L of 0.1 M sodium phosphate, 0.15 M sodium chloride, pH 7.2), N<sup>5</sup>-CAIR synthetase (100  $\mu$ M), ATP (100  $\mu$ M), and AIR (100  $\mu$ M), various concentrations of **15** (10  $\mu$ M, 25, 50, 75 and 100  $\mu$ M) were added. The PCR tubes were UV irradiated with a 110 V UV lamp (model: B100AP, manufactured by UVP Inc.) emitting radiation between 340-360 nm for 20 minutes. The distance between the light source and the reaction was 5 cm. After UV irradiation, the reaction was analyzed on a 12% SDS-PAGE gel and visualized by staining with Commaassie Blue.

5.16. Time-dependent inactivation kinetics of N<sup>5</sup>-CAIR synthetase with **7**:

A solution of **7** (0.01 mmol, 5 mg) in DMF and subjected to UV irradiation with a 110 V UV lamp (model: B100AP, manufactured by UVP Inc.) emitting radiation between 340-360 nm for 2 hours. The distance between the light source and the reaction was 5 cm. N<sup>5</sup>-CAIR synthetase (20  $\mu$ M) was incubated on ice with either the non-UV irradiated or the UV irradiated **7** (100  $\mu$ M). Enzyme samples from the two preparations were withdrawn at 1, 5, 15, 30, 60 and 120 minutes and analyzed for the activity of the enzyme using the pyruvate kinase and lactate dehydrogenase coupled assay system. The resulting enzyme activity was compared to an enzyme control which did not contain any **7**. The percent activity was calculated at each time point by taking the ratio of the activity of the treated sample versus the untreated sample.

5.17. Reversibility of the time-dependent inactivation of 7:

Solutions of either the non-UV irradiated or the UV irradiated **7** (100  $\mu\text{M}$ ) incubated with  $\text{N}^5\text{-CAIR}$  synthetase (20  $\mu\text{M}$ ) were incubated for 2 hours on ice. The resulting solutions were then dialyzed for 5 hours against 10mM Tris-HCl, 200 mM NaCl (pH 7.2) buffer. After dialysis, the activity of the enzyme was determined by the standard pyruvate kinase/lactate dehydrogenase assay system.

5.18. Photochemistry of N-methyl isatin:

N-methyl isatin (0.124 mmol, 20 mg) was dissolved in 3 ml of THF in a beaker. The beaker was UV irradiated for 2 hours from a distance of 3 cm with an 110 V UV lamp emitting radiation between 340-360 nm. After UV irradiation the compound was analyzed by HPLC and GC/MS. HPLC separation of the UV treated *N*-methyl isatin was done with a PRP-1 column (Hamilton) using a gradient of water:acetonitrile such that the gradient started at 0% acetonitrile and proceeded to 100% acetonitrile over a period of 50 minutes. For GC/MS analysis 0.1  $\mu\text{g}$  the compound was dissolved in 5ml  $\text{CH}_2\text{Cl}_2$  and 1 $\mu\text{L}$  of the solution was injected on to a GC column of Trace GC Ultra. The sample was vaporized at 250  $^\circ\text{C}$  and the column was ramped from 80 to 300  $^\circ\text{C}$  over 15 minutes. The peaks obtained by GC analysis were identified by mass analysis using the ITQ900 detector. The identification of the new peaks was determined by comparison to authentic samples.

5.19. Reaction of N-methyl isatoic anhydride with benzyl alcohol:



*N*-Methyl isatoic anhydride (0.28 mmol, 50 mg) was dissolved in dry DMF and treated with benzyl alcohol (0.28 mmol, 30 mg) under argon atmosphere. The reaction mixture was stirred at 55 °C for 12 hours. After 12 hours, the DMF was removed under reduced pressure by a rotary evaporator. The resulting residue was washed with water and dried under vacuum. A sample of the material was dissolved in dichloromethane and subjected to GC/MS analysis. The remainder of the material was purified by silica column chromatography using 10% acetone in dichloromethane as a mobile phase. The major material was isolated and dried in vacuum to give a straw color liquid in 95% yield. <sup>1</sup>H NMR (400 MHz, CDCl<sub>3</sub>): 2.914 (s, 3H), 4.638 (s, 1H), 5.331 (s, 2H), 6.65 (m, 2H), 7.44 (m, 6H), 8.013 (d, 1H, *J* = 8.4Hz). <sup>13</sup>C NMR (100 MHz, CDCl<sub>3</sub>): 165.9, 152.3, 136.1, 133.8, 130.7, 128.9, 127.6, 127, 113.2, 110.9, 65.7, 30.1. MS calculated for C<sub>15</sub>H<sub>15</sub>NO<sub>2</sub> is (M+) 241.48, found 241.59.

#### 5.20. LC-MS/MS analysis of photocrosslinked proteins:

Proteomic analysis of the crosslinked proteins was conducted at the proteomics core facility at Wayne State University. The appropriate band from the SDS-PAGE gel was excised, reduced (DTT), alkylated (iodoacetamide) and digested (trypsin or chymotrypsin) by an automated process (ProGest, Genomic Solutions). The resulting peptides were dried and resuspended in a 5% acetonitrile, 0.1% TFA solution. Peptides were purified with a CapTrap (Michrom) and separated with an in-line Magic C18AQ 200A 3u 100Ux150mm nano-flow column. Peptides were ionized with the ADVANCE ion source (Michrom) and

introduced into an LTQ-XL mass spectrometer (Thermo Fisher Scientific). Abundant species were fragmented with either collision-induced dissociation (CID) or electron transfer dissociation (ETD). Data analyses were performed using BioWorks (Thermo), and Scaffold (Proteome Software) software that incorporated SEQUEST, X!Tandem and ProteinProphet algorithms.

**APPENDIX: LIST OF ABBREVIATIONS**

°C	degrees centigrade
AIR	5-aminoimidazole ribonucleotide
ATP	adenosine triphosphate
CAIR	4-carboxy-5-aminoimidazole ribonucleotide
HEPES	N-(2-hydroxyethyl)-piperazine-N-(2-ethanesulfonic acid)
HPLC	high-performance liquid chromatography
LB	Luria-Bertani media
min	minute
mL	millilitre
NADH	dihyronicotinamide adenine dinucleotide
N <sup>5</sup> -CAIR	N <sup>5</sup> -carboxyaminoimidazole ribonucleotide
NMR	nuclear magnetic resonance
PAGE	polyacrylamide gel electrophoresis
PEP	phosphoenolpyruvate
PK	pyruvate kinase
s	second
SAICAR	4-[(N-succinylamino) carbonyl]-5-aminoimidazole
SDS	sodium dodecyl sulfate
TLC	thin-layer chromatography
Tris	tris-(hydroxymethyl)aminomethane
UV	ultraviolet

## REFERENCES

1. Ellis, V. H., The Classic - Penicillin - Its Practical Application in Orthopedic-Surgery and Fractures (Reprinted). *Clinical Orthopaedics and Related Research* **1984**, (190), 3-10.
2. Stewart, W. H., Securing Health in Our Urban Future: A Report to the Surgeon General *The Reports of the Surgeon General* **1967**.
3. Walsh, C., Where will new antibiotics come from? *Nature Reviews Microbiology* **2003**, 1, 65-70.
4. Klevens, R. M.; Morrison, M. A.; Nadle, J.; Petit, S.; Gershman, K.; Ray, S.; Harrison, L. H.; Lynfield, R.; Dumyati, G.; Townes, J. M.; Craig, A. S.; Zell, E. R.; Fosheim, G. E.; McDougal, L. K.; Carey, R. B.; Fridkin, S. K.; Investigators, A. M., Invasive methicillin-resistant *Staphylococcus aureus* infections in the United States. *Jama-Journal of the American Medical Association* **2007**, 298 (15), 1763-1771.
5. Lodise, T. P.; McKinnon, P. S., Clinical and economic impact of methicillin resistance in patients with *Staphylococcus aureus* bacteremia. *Diagnostic Microbiology and Infectious Disease* **2005**, 52 (2), 113-122.
6. Matthew E. Falagas, P. K. K. a. I. A. B., The diversity of definitions of multidrug-resistant (MDR) and pandrug-resistant (PDR) *Acinetobacter baumannii* and *Pseudomonas aeruginosa* *J Med Microbiol* **2006**, 55, 1619-1629.

7. Fischbach, M. A.; Walsh, C. T., Antibiotics for Emerging Pathogens. *Science* **2009**, 325 (5944), 1089-1093.
8. Walsh, C. T.; Wright, G. D., Antimicrobials. *Current Opinion in Microbiology* **2009**, 12 (5), 473-475.
9. Kainer, M. A.; Devasia, R. A.; Jones, T. F.; Simmons, B. P.; Melton, K.; Chow, S.; Broyles, J.; Moore, K. L.; Craig, A. S.; Schaffner, W., Response to emerging infection leading to outbreak of linezolid-resistant enterococci. *Emerging Infectious Diseases* **2007**, 13 (7), 1024-1030.
10. Schoen, C.; Unzicker, C.; Stuhler, G.; Elias, J.; Einsele, H.; Ulrich, G.; Abele-Horn, M.; Mielke, S., Life-Threatening Infection Caused by Daptomycin-Resistant *Corynebacterium jeikeium* in a Neutropenic Patient. *Journal of Clinical Microbiology* **2009**, 47 (7), 2328-2331.
11. Z Su, J. H., Emerging bacterial enzyme targets. *Current Opinion in Investigational Drugs* **2007**, 8, 140-149.
12. Gerdes, S. Y.; Scholle, M. D.; D'Souza, M.; Bernal, A.; Baev, M. V.; Farrell, M.; Kurnasov, O. V.; Daugherty, M. D.; Mseeh, F.; Polanuyer, B. M.; Campbell, J. W.; Anantha, S.; Shatalin, K. Y.; Chowdhury, S. A. K.; Fonstein, M. Y.; Osterman, A. L., From genetic footprinting to antimicrobial drug targets: Examples in cofactor biosynthetic pathways. *Journal of Bacteriology* **2002**, 184 (16), 4555-4572.
13. Ali, S. T.; Gill, A. E.; Lewendon, A., Novel targets for antibiotic drug design. *Curr Opin Investig Drugs* **2002**, 3 (12), 1712-7.

14. Isaacson, R. E., Novel targets for antibiotics. *Expert Opin. Invest. Drugs* **1994**, 3 (2), 83-91.
15. Buchanan, B. L. a. J. M., Biosynthesis of Purines. *Journal of Biological Chemistry* **1956**, 1005-1018.
16. Murray, A. W., The Biological Significance of Purine Salvage. *Annu. Rev. Biochem.* **1971**, 40, 811-826.
17. Zhang, Y.; Morar, M.; Ealick, S. E., Structural biology of the purine biosynthetic pathway. *Cellular and Molecular Life Sciences* **2008**, 65 (23), 3699-3724.
18. Berg, J. M.; Tymoczko, J. L.; Stryer, L., *Biochemistry*. 6th ed.; W. H. Freeman: New York, 2007; p 1 v. (various pagings).
19. Wakako Watanabe, G.-i. S., Atsu Aiba, Kiyoshi Mizobuchi, Identification and Sequence Analysis of Escherichia coli purE and purK Genes Encoding 5'-Phosphoribosyl-5-Amino-4-Imidazole Carboxylase for De Novo Purine Biosynthesis. *Journal of Bacteriology* **1989**, 171 (1), 198-204.
20. Chen, Z. D.; Dixon, J. E.; Zalkin, H., Cloning of a Chicken Liver Cdna- Encoding 5-Aminoimidazole Ribonucleotide Carboxylase and 5-Aminoimidazole-4-N-Succinocarboxamide Ribonucleotide Synthetase by Functional Complementation of Escherichia-Coli Pur Mutants. *Proceedings of the National Academy of Sciences of the United States of America* **1990**, 87 (8), 3097-3101.

21. Mueller, E.; Meyer, E.; Rudolph, J.; Stubbe, J., A New Intermediate in the Purine Biosynthetic-Pathway. *Abstracts of Papers of the American Chemical Society* **1993**, 206, 155-ORGN.
22. Firestine, S. M.; Davisson, V. J., A Comparative-Study of the Escherichia-Coli and Avian Forms of the Enzyme 5-Aminoimidazole Ribonucleotide Carboxylase. *Abstracts of Papers of the American Chemical Society* **1994**, 208, 27-Biol.
23. Mueller, E. J.; Meyer, E.; Rudolph, J.; Davisson, V. J.; Stubbe, J., N-5-Carboxyaminoimidazole Ribonucleotide - Evidence for a New Intermediate and 2 New Enzymatic-Activities in the De-Novo Purine Biosynthetic-Pathway of Escherichia-Coli. *Biochemistry* **1994**, 33 (8), 2269-2278.
24. Alenin, V. V.; Kostikova, T. R.; Domkin, V. D., Chemical Synthesis of N1-Substituted 5-Aminoimidazoles and the Formation of N-Carboxylation Products in Aqueous-Solutions of Potassium Bicarbonate. *Zhurnal Obshchei Khimii* **1987**, 57 (3), 692-701.
25. An, S. G.; Kumar, R.; Sheets, E. D.; Benkovic, S. J., Reversible compartmentalization of de novo purine biosynthetic complexes in living cells. *Science* **2008**, 320 (5872), 103-106.
26. Firestine, S. M.; Davisson, V. J., Carboxylases in De-Novo Purine Biosynthesis - Characterization of the Gallus-Gallus Bifunctional Enzyme. *Biochemistry* **1994**, 33 (39), 11917-11926.

27. Mcfarland, W. C.; Stocker, B. A. D., Effect of Different Purine Auxotrophic Mutations on Mouse-Virulence of a Vi-Positive Strain of Salmonella-Dublin and of 2 Strains of Salmonella-Typhimurium. *Microbial Pathogenesis* **1987**, 3 (2), 129-141.
28. Kirsch, D. R.; Whitney, R. R., Pathogenicity of Candida-Albicans Auxotrophic Mutants in Experimental Infections. *Infection and Immunity* **1991**, 59 (9), 3297-3300.
29. Perfect, J. R.; Toffaletti, D. L.; Rude, T. H., The Gene Encoding Phosphoribosylaminoimidazole Carboxylase (Ade2) Is Essential for Growth of Cryptococcus-Neoformans in Cerebrospinal-Fluid. *Infection and Immunity* **1993**, 61 (10), 4446-4451.
30. Bacon, G. A.; Burrows T. W.; Yates., M., The effects of biochemical mutation on the virulence of Bacterium typhosum:the virulence of mutants. *Journal of Experimental Pathology* **1950**, 31, 714-724.
31. Garber, E. D., A. J. Hackett, and R. Franklin., The virulence of biochemical mutants of Klebsiella pneumoniae. *Genetics* **1952**, 38, 693-697.
32. Ivanovics, G., E. Marjai, and A. Dobozy., The growth of purine mutants of Bacillus anthracis in the body of the mouse. *J. Gen. Microbiol.* **1968**, 53, 147-162.
33. Straley, S. C.; Harmon, P. A., Growth in Mouse Peritoneal-Macrophages of Yersinia-Pestis Lacking Established Virulence Determinants. *Infection and Immunity* **1984**, 45 (3), 649-654.



34. Finlay, B. B.; Falkow, S., Common Themes in Microbial Pathogenicity. *Microbiological Reviews* **1989**, *53* (2), 210-230.
35. Saracheck, A., Restriction fragment polymorphism in mitochondrial DNA of *Cryptococcus neoformans*. *J. Gen. Microbiol.* **1964**, *135*, 3353-3362.
36. Polissi, A.; Pontiggia, A.; Feger, G.; Altieri, M.; Mottl, H.; Ferrari, L.; Simon, D., Large-scale identification of virulence genes from *Streptococcus pneumoniae*. *Infection and Immunity* **1998**, *66* (12), 5620-5629.
37. Donovan, M.; Schumuke, J. J.; Fonzi, W. A.; Bonar, S. L.; Gheesling-Mullis, K.; Jacob, G. S.; Davisson, V. J.; Dotson, S. B., Virulence of a phosphoribosylaminoimidazole carboxylase-deficient *Candida albicans* strain in an immunosuppressed murine model of systemic candidiasis. *Infection and Immunity* **2001**, *69* (4), 2542-2548.
38. Cersini, A.; Martino, M. C.; Martini, I.; Rossi, G.; Bernardini, M. L., Analysis of virulence and inflammatory potential of *Shigella flexneri* purine biosynthesis mutants. *Infection and Immunity* **2003**, *71* (12), 7002-7013.
39. Wang, J. Y.; Mushegian, A.; Lory, S.; Jin, S. G., Large-scale isolation of candidate virulence genes of *Pseudomonas aeruginosa* by in vivo selection. *Proceedings of the National Academy of Sciences of the United States of America* **1996**, *93* (19), 10434-10439.
40. Thoden, J. B.; Holden, H. M.; Firestine, S. M., Structural Analysis of the Active Site Geometry of N-5-Carboxyaminoimidazole Ribonucleotide

- Synthetase from *Escherichia coli*. *Biochemistry* **2008**, *47* (50), 13346-13353.
41. Thoden, J. B.; Holden, H. M.; Paritala, H.; Firestine, S. M., Structural and Functional Studies of *Aspergillus clavatus* N-5-Carboxyaminoimidazole Ribonucleotide Synthetase. *Biochemistry* **2010**, *49* (4), 752-760.
42. Thoden, J. B.; Kappock, T. J.; Stubbe, J.; Holden, H. M., Three-dimensional structure of N-5-carboxyaminoimidazole ribonucleotide synthetase: A member of the ATP grasp protein superfamily. *Biochemistry* **1999**, *38* (47), 15480-15492.
43. Meyer, E.; Leonard, N. J.; Bhat, B.; Stubbe, J.; Smith, J. M., Purification and Characterization of the *PurK* and *PurC* Gene-Products - Identification of a Previously Unrecognized Energy Requirement in the Purine Biosynthetic-Pathway. *Biochemistry* **1992**, *31* (21), 5022-5032.
44. Li, H.; Fast, W.; Benkovic, S. J., Structural and functional modularity of proteins in the de novo purine biosynthetic pathway. *Protein Science* **2009**, *18* (5), 881-892.
45. Y. Shen, S. L. V., S.C. Weatherly, T.D. Elich & L. Tong., A mechanism for the potent inhibition of eukaryotic acetyl coenzyme A carboxylase by soraphen A, a macrocyclic polyketide natural product. *Mol. Cell* **2004**, *16*, 881-891.

46. Waldrop, G. L.; Rayment, I.; Holden, H. M., 3-Dimensional Structure of the Biotin Carboxylase Subunit of Acetyl-Coa Carboxylase. *Biochemistry* **1994**, 33 (34), 10249-10256.
47. Waldrop, G.; Holden, H. M.; Rayment, I., Preliminary-X-Ray Crystallographic Analysis of Biotin Carboxylase Isolated from Escherichia-Coli. *Journal of Molecular Biology* **1994**, 235 (1), 367-369.
48. Thoden, J. B.; Holden, H. M.; Wesenberg, G.; Raushel, F. M.; Rayment, I., Structure of carbamoyl phosphate synthetase: A journey of 96 angstrom from substrate to product. *Biochemistry* **1997**, 36 (21), 6305-6316.
49. Thoden, J. B.; Huang, X. Y.; Raushel, F. M.; Holden, H. M., The small subunit of carbamoyl phosphate synthetase: Snapshots along the reaction pathway. *Biochemistry* **1999**, 38 (49), 16158-16166.
50. Holden, H. M.; Thoden, J. B.; Raushel, F. M., Carbamoyl phosphate synthetase: an amazing biochemical odyssey from substrate to product. *Cellular and Molecular Life Sciences* **1999**, 56 (5-6), 507-522.
51. Mary J. Wimmer, I. A. R., Sue G. Powers, Alton Meister, Evidence That Carboxyphosphate Is a Kinetically Competent Intermediate in the Carbamyl Phosphate Synthetase Reaction. *The Journal of Biological Chemistry* **1979**, 254 (6), 1854-1859.
52. Herschlag, D.; Jencks, W. P., Nucleophiles of High Reactivity in Phosphoryl Transfer-Reactions - Alpha-Effect Compounds and Fluoride-Ion. *Journal of the American Chemical Society* **1990**, 112 (5), 1951-1956.

53. Herschlag, D.; Jencks, W. P., The Effects of Mg-2+, Hydrogen-Bonding, and Steric Factors on Rate and Equilibrium-Constants for Phosphoryl Transfer between Carboxylate Ions and Pyridines. *Journal of the American Chemical Society* **1990**, *112* (5), 1942-1950.
54. Herschlag, D.; Jencks, W. P., Catalysis of the Hydrolysis of Phosphorylated Pyridines by Mg(OH)<sup>+</sup> - a Possible Model for Enzymatic Phosphoryl Transfer. *Biochemistry* **1990**, *29* (21), 5172-5179.
55. Firestine, S. M.; Wu, W. D.; Youn, H.; Davisson, V. J., Interrogating the mechanism of a tight binding inhibitor of AIR carboxylase. *Bioorganic & Medicinal Chemistry* **2009**, *17* (2), 794-803.
56. Waldrop, G. L.; Turnbull, J. L.; Parmentier, L. E.; Oleary, M. H.; Cleland, W. W.; Schachman, H. K., Steady-State Kinetics and Isotope Effects on the Mutant Catalytic Trimer of Aspartate Transcarbamoylase Containing the Replacement of Histidine-134 by Alanine. *Biochemistry* **1992**, *31* (28), 6585-6591.
57. Tipton, P. A.; Cleland, W. W., Catalytic Mechanism of Biotin Carboxylase - Steady-State Kinetic Investigations. *Biochemistry* **1988**, *27* (12), 4317-4325.
58. Liu, S. P.; Chang, J. S.; Herberg, J. T.; Horng, M. M.; Tomich, P. K.; Lin, A. H.; Marotti, K. R., Allosteric inhibition of Staphylococcus aureus D-alanine : D-alanine ligase revealed by crystallographic studies. *Proceedings of the National Academy of Sciences of the United States of America* **2006**, *103* (41), 15178-15183.

59. Winnacker, M.; Breeger, S.; Strasser, R.; Carell, T., Novel Diazirine-Containing DNA Photoaffinity Probes for the Investigation of DNA-Protein-Interactions. *Chembiochem* **2009**, *10* (1), 109-118.
60. Brunner, J., New Photolabeling and Cross-Linking Methods. *Annual Review of Biochemistry* **1993**, *62*, 483-514.
61. Blencowe, A.; Blencowe, C.; Cosstick, K.; Hayes, W., A carbene insertion approach to functionalised poly(ethylene oxide)-based gels. *Reactive & Functional Polymers* **2008**, *68* (4), 868-875.
62. Blencowe, A.; Fagour, W.; Blencowe, C.; Cosstick, K.; Hayes, W., Synthesis of hyperbranched poly(aryl amine)s via a carbene insertion approach. *Organic & Biomolecular Chemistry* **2008**, *6* (13), 2327-2333.
63. Moorman, A. R.; Abeles, R. H., A New Class of Serine Protease Inactivators Based on Isatoic Anhydride. *Journal of the American Chemical Society* **1982**, *104* (24), 6785-6786.
64. Jing, H.; Babu, Y. S.; Moore, D.; Kilpatrick, J. M.; Liu, X. Y.; Volanakis, J. E.; Narayana, S. V. L., Structures of native and complexed complement factor D: Implications of the atypical His57 conformation and self-inhibitory loop in the regulation of specific serine protease activity. *Journal of Molecular Biology* **1998**, *282* (5), 1061-1081.
65. Harper, J. W.; Powers, J. C., Reaction of Serine Proteases with Substituted 3-Alkoxy-4-Chloroisocoumarins and 3-Alkoxy-7-Amino-4-

Chloroisocoumarins - New Reactive Mechanism-Based Inhibitors.

*Biochemistry* **1985**, 24 (25), 7200-7213.

66. Harper, J. W.; Hemmi, K.; Powers, J. C., Reaction of Serine Proteases with Substituted Isocoumarins - Discovery of 3,4-Dichloroisocoumarin, a New General Mechanism Based Serine Protease Inhibitor. *Biochemistry* **1985**, 24 (8), 1831-1841.
67. Jones, M. E., and Spector, L., The pathway of carbonate in the biosynthesis of carbamyl phosphate. *Journal of Biological Chemistry* **1960**, 285, 2897-2901.
68. Ogita, T.; Knowles, J. R., Role of Biotin in Enzyme-Catalyzed Carboxylation Reactions. *Biochemistry* **1988**, 27 (8), 3077-3077.
69. Attwood, P. V.; Wallace, J. C., Chemical and catalytic mechanisms of carboxyl transfer reactions in biotin-dependent enzymes. *Accounts of Chemical Research* **2002**, 35 (2), 113-120.
70. Paul M. Andersoni, A. M., Evidence for an Activated Form of Carbon Dioxide in the Reaction Catalyzed by *Escherichia coli* Carbamyl Phosphate Synthetase. *Biochemistry* **1965**, 4 (12), 2803-2809.
71. Holden, H. M.; Thoden, J. B.; Raushel, F. M., Carbamoyl phosphate synthetase: a tunnel runs through it. *Current Opinion in Structural Biology* **1998**, 8 (6), 679-685.

72. Gibson G.E., M. L. S., Raushel F.M., Carbamoyl Phosphate Synthetase from *Escherichia coli* Does Not Catalyze the Dehydration of Bicarbonate to Carbon Dioxide. *Bioorganic Chemistry* **1998**, 26 (5), 255-268.
73. H. B. Borgi, J. D. D., J. M. Lehn, G. Wipff, Stereo Chemistry of reaction Paths at Carbonyl Centres. *Tetrahedron* **1974**, 30, 1563-1572.
74. Chou, C. Y.; Yu, L. P. C.; Tong, L., Crystal Structure of Biotin Carboxylase in Complex with Substrates and Implications for Its Catalytic Mechanism. *Journal of Biological Chemistry* **2009**, 284 (17), 11690-11697.
75. G.B. Elion, G. H. H., H. VanderWerff, Antagonists of Nucleic acid derivatives: VI. Purines. *Journal of Biological Chemistry* **1951**, 192, 505-518.
76. Elion, G. B., The Purine Path to Chemotherapy. *Physiology of Medicine: Nobel Lecture* **1988**, 448-468.
77. Murray, A. W., The Biological Significance of Purine Salvage. *Annual review of Biochemistry* **1971**, 40, 811-826.
78. Zarzeczny, R.; Brault, J. J.; Abraham, K. A.; Hancock, C. R.; Terjung, R. L., Influence of ribose on adenine salvage after intense muscle contractions. *Journal of Applied Physiology* **2001**, 91 (4), 1775-1781.
79. Brault, J. J.; Terjung, R. L., Purine salvage to adenine nucleotides in different skeletal muscle fiber types. *Journal of Applied Physiology* **2001**, 91 (1), 231-238.

80. Mary Jackson, F.-X. B., Isabel Ota, Jean Rauzier,; Carlos Martin, B. G. a. C. G., The *Mycobacterium tuberculosis* purine biosynthetic pathway: isolation and characterization of the *purC* and *purI* genes. **1996**, *142*, 2439-2447.
81. Neils B. QUASHIE, D. D.-S., Patrick G. BRAY, Giancarlo A. BIAGINI‡, Christian DOERIG,; Lisa C. RANFORD-CARTWRIGHT, H. P. D. K., A comprehensive model of purine uptake by the malaria parasite *Plasmodium falciparum*: identification of four purine transport activities in intraerythrocytic parasites. **2008**, *411*, 287-295.
82. Marsilje, T. H.; Labroli, M. A.; Hedrick, M. P.; Jin, Q.; Desharnais, J.; Baker, S. J.; Gooljarsingh, L. T.; Ramcharan, J.; Tavassoli, A.; Zhang, Y.; Wilson, I. A.; Beardsley, G. P.; Benkovic, S. J.; Boger, D. L., 10-formyl-5,10-dideaza-acyclic-5,6,7,8-tetrahydrofolic acid (10-formyl-DDACTHF): A potent cytotoxic agent acting by selective inhibition of human GAR Tfase and the de novo purine biosynthetic pathway. *Bioorganic & Medicinal Chemistry* **2002**, *10* (8), 2739-2749.
83. Cheng, H.; Hwang, I.; Chong, Y. H.; Tavassoli, A.; Webb, M. E.; Zhang, Y.; Wilson, I. A.; Benkovic, S. J.; Boger, D. L., Synthesis and biological evaluation of N-{4-[5-(2,4-diamino-6-oxo-1,6-dihydropyrimidin-5-yl)-2-(2,2,2-trifluoroacetyl)pentyl]benzoyl}-L-glutamic acid as a potential inhibitor of GAR Tfase and the de novo purine biosynthetic pathway. *Bioorganic & Medicinal Chemistry* **2005**, *13* (10), 3593-3599.



84. Chong, Y.; Hwang, I.; Tavassoli, A.; Zhang, Y.; Wilson, I. A.; Benkovic, S. J.; Boger, D. L., Synthesis and biological evaluation of alpha- and gamma-carboxamide derivatives of 10-CF<sub>3</sub>CO-DDACTHF. *Bioorganic & Medicinal Chemistry* **2005**, *13* (10), 3587-3592.
85. Cheng, H.; Chong, Y. H.; Hwang, I.; Tavassoli, A.; Zhang, Y.; Wilson, I. A.; Benkovic, S. J.; Boger, D. L., Design, synthesis, and biological evaluation of 10-methanesulfonyl-DACTHF, 10-methanesulfonyl-5-DACTHF, and 10-methylthio-DDACTHF as potent inhibitors of GAR Tfase and the de novo purine biosynthetic pathway. *Bioorganic & Medicinal Chemistry* **2005**, *13* (10), 3577-3585.
86. Harder, K. W.; Owen, P.; Wong, L. K. H.; Aebersold, R.; Clarklewis, I.; Jirik, F. R., Characterization and Kinetic-Analysis of the Intracellular Domain of Human-Protein-Tyrosine-Phosphatase-Beta (Hptp-Beta) Using Synthetic Phosphopeptides. *Biochemical Journal* **1994**, *298*, 395-401.
87. Maehama, T.; Taylor, G. S.; Slama, J. T.; Dixon, J. E., A sensitive assay for phosphoinositide phosphatases. *Analytical Biochemistry* **2000**, *279* (2), 248-250.
88. R.D. Henkel, J. L. V., R.A. Walsh, A microassay for ATPase. *Anal. Biochem.* **1998**, *169*, 312-318.
89. Miller, J. R.; Dunham, S.; Mochalkin, I.; Banotai, C.; Bowman, M.; Buist, S.; Dunkle, B.; Hanna, D.; Harwood, H. J.; Huband, M. D.; Karnovsky, A.; Kuhn, M.; Limberakis, C.; Liu, J. Y.; Mehrens, S.; Mueller, W. T.;

- Narasimhan, L.; Ogden, A.; Ohren, J.; Prasad, J. V. N. V.; Shelly, J. A.; Skerlos, L.; Sulavik, M.; Thomas, V. H.; VanderRoest, S.; Wang, L. A.; Wang, Z. G.; Whitton, A.; Zhu, T.; Stover, C. K., A class of selective antibacterials derived from a protein kinase inhibitor pharmacophore. *Proceedings of the National Academy of Sciences of the United States of America* **2009**, *106* (6), 1737-1742.
90. Fischbach, C. T. W. a. M. A., Repurposing libraries of eukaryotic protein kinase inhibitors for antibiotic discovery. *Proceedings of National Academy of Science* **2009**, *106* (6), 1689-1690.
91. Igor Mochalkin†, J. R. M., Lakshmi Narasimhan, Venkataraman Thanabal,; Paul Erdman, P. B. C., J. V. N. Vara Prasad, Sandra Lightle, Michael D. Huband,; C. Kendall Stover, Discovery of Antibacterial Biotin Carboxylase Inhibitors by Virtual Screening and Fragment-Based Approaches. **2009**, *4* (6), 473-483.
92. Gernot Reissenweber, D. M., Oxidation of Isatins to Isatoic Anhydrides and 2,3-Dioxo-1,4-benzoxazines. *Angewandte Chemie-International Edition* **1980**, *19* (3), 222-223.
93. Deligeorgiev, T.; Vasilev, A.; Vaquero, J. J.; Alvarez-Builla, J., A green synthesis of isatoic anhydrides from isatins with urea-hydrogen peroxide complex and ultrasound. *Ultrasonics Sonochemistry* **2007**, *14* (5), 497-501.
94. Haucke, G.; Seidel, B.; Graness, A., The Photochemistry of Isatin. *Journal of Photochemistry* **1987**, *37* (1), 139-146.

95. Sharma I; Saxena A; Ojha C K; Pardasani P; Pardasani R T; T, M., A comprehensive approach to the photochemical synthesis of bioactive compounds by the reaction of oxazolidine, thiazolidine and pyrazolidine derivatives with indol-,3-diones. *Proceedings of Indian Academy of Science (Chemical Science)*, **2002**, 114 (6), 523-531.
96. Zhang, W.; Chen, C. H. T.; Nagashima, T., Fluorous electrophilic scavengers for solution-phase parallel synthesis. *Tetrahedron Letters* **2003**, 44 (10), 2065-2068.
97. Firestine, S. M.; Salinas, F.; Nixon, A. E.; Baker, S. J.; Benkovic, S. J., Using an AraC-based three-hybrid system to detect biocatalysts in vivo. *Nature Biotechnology* **2000**, 18 (5), 544-547.
98. Schleif, R., AraC protein: a love-hate relationship. *Bioessays* **2003**, 25 (3), 274-282.
99. Krebs, J. F.; Rana, F.; Dluhy, R. A.; Fierke, C. A., Kinetic and Spectroscopic Studies of Hydrophilic Amino-Acid Substitutions in the Hydrophobic Pocket of Human Carbonic Anhydrase-ii. *Biochemistry* **1993**, 32 (17), 4496-4505.
100. Firestine, S. M.; Poon, S. W.; Mueller, E. J.; Stubbe, J.; Davisson, V. J., Reactions Catalyzed by 5-Aminoimidazole Ribonucleotide Carboxylases from Escherichia-Coli and Gallus-Gallus - a Case for Divergent Catalytic Mechanisms. *Biochemistry* **1994**, 33 (39), 11927-11934.

**ABSTRACT****ENZYMOLGY AND MEDICINAL CHEMISTRY OF N<sup>5</sup>-  
CARBOXYAMINOIMIDAZOLE RIBONUCLEOTIDE SYNTHETASE:  
A NOVEL ANTIBACTERIAL TARGET**

by

**HANUMANTHARAO PARITALA****AUGUST 2010****Advisor:** Dr. Steven M. Firestine**Major:** Pharmaceutical Sciences**Degree:** Doctor of Philosophy

N<sup>5</sup>-Carboxyaminoimidazole ribonucleotide synthetase (N<sup>5</sup>-CAIR synthetase), a key enzyme in microbial de novo purine biosynthesis, catalyzes the conversion of aminoimidazole ribonucleotide (AIR) to N<sup>5</sup>-CAIR. To date, this enzyme has been observed only in microorganisms, and thus, it represents an ideal target for antimicrobial drug development. Here, we report structural and functional studies on the *Aspergillus clavatus* N<sup>5</sup>-CAIR synthetase and identification of inhibitors for the enzyme. In collaboration with Dr. Hazel Holden of the University of Wisconsin, the three-dimensional structure of *Aspergillus clavatus* N<sup>5</sup>-CAIR synthetase was solved in the presence of either Mg<sub>2</sub>ATP or MgADP and AIR. These structures, determined to 2.1 and 2.0 Å resolution, respectively, revealed that AIR binds in a pocket analogous to that observed for other ATP-grasp enzymes involved in purine metabolism. On the basis of these models, a site-directed mutagenesis study was subsequently conducted that focused on five

amino acid residues located in the active site region of the enzyme. These investigations demonstrated that Asp153 and Lys353 play critical roles in catalysis without affecting substrate binding. All other mutations affected substrate binding and, in some instances, catalysis as well. Taken together, the structural and kinetic data presented here suggest a catalytic mechanism whereby  $Mg_2ATP$  and bicarbonate first react to form the unstable intermediate carboxyphosphate. This intermediate subsequently decarboxylates to  $CO_2$  and inorganic phosphate, and the amino group of AIR, through general base assistance by Asp153, attacks  $CO_2$  to form  $N^5$ -CAIR.

To identify the inhibitors for this enzyme, we have conducted high-throughput screening (HTS) against *Escherichia coli*  $N^5$ -CAIR synthetase using a highly reproducible phosphate assay. HTS of 48,000 compounds identified 14 compounds that inhibited the enzyme. The hits identified could be classified into three classes based on chemical structure. Class I contains compounds with an indenedione core. Class II contains an indolinedione group, and class III contains compounds that are structurally unrelated to other inhibitors in the group. We determined the Michaelis–Menten kinetics for five compounds representing each of the classes. Examination of compounds belonging to class I indicates that these compounds do not follow normal Michaelis–Menten kinetics. Instead, these compounds inhibit  $N^5$ -CAIR synthetase by reacting with the substrate AIR. Kinetic analysis indicates that the class II families of compounds are non-competitive with both AIR and ATP. One compound in class III is competitive with AIR but

uncompetitive with ATP, whereas the other is non-competitive with both substrates. Finally, these compounds display no inhibition of human AIR carboxylase indicating that these agents are selective inhibitors of N<sup>5</sup>-CAIR synthetase.

Given the importance of the class II, non-competitive inhibitors, we developed a diazirine-based photocrosslinking agent to identify the binding site of these inhibitors. These studies revealed that the isatin core of class II inhibitors is capable of undergoing photochemical conversion to isatoic anhydride. Once formed, the anhydride is capable of reacting with the protein. Treatment of N<sup>5</sup>-CAIR synthetase with the photoreactive agent lead to the dimerization of two monomers of the synthetase. Proteomic analysis of the crosslinked protein identified serine 227 as a possible site of modification. These studies also revealed two peptides that were missing in the dimerized protein sample. These two peptides were located near serine 227. While compelling, the location of the missing peptides and serine 227 is 20 Å away from the dimerization interface observed in the crystal structure. Thus, our photocrosslinking studies suggest that N<sup>5</sup>-CAIR synthetase may exist in multiple dimer conformations.

## AUTOBIOGRAPHICAL STATEMENT

Hanumantharao Paritala was born in Gummalampadu village, Andhrapradesh state, India. He entered the University of Mysore, Mysore in 1995. Hanumantharao received his B. Pharm. (Bachelor of Pharmaceutical sciences) in 1999. He then joined S. G. S. institute of technology and science, Indore in M.Pharm. (Master of Pharmaceutical Sciences Program) under the supervision of Dr S. G. Kaskhedikar. Hanumantharao received Research Award for his work at Kaskhedikar laboratory from Indian Drug Manufacturers Association. Hanumantharao graduated from SGSITS and moved to United States to join Dr Steven Firestine laboratory at Wayne State University for pursuing graduate studies. In April 2008 Hanumantharao got married with Sireesha. Hanumantharao will graduate in August 2010 and will be pursuing postdoctoral research under the direction of Professor Kate Carroll at The Scripps Research Institute, Florida.

### Publications:

1. Thoden, James B.; Holden, Hazel M.; **Paritala, Hanumantharao**; Firestine, Steven M. "Structural and Functional Studies of Aspergillus clavatus N5-Carboxyaminoimidazole Ribonucleotide Synthetase". *Biochemistry*, **2010**, 49, 752-760.
2. **Paritala, Hanumantharao**; Firestine, Steven M. "Characterization of INS-VNTR Sequences for Their Ability to Adopt G-quadruplex Structures". *Nucleosides, Nucleotides and Nucleic Acids*, **2010**, 29(2), 81-90.
3. Firestine, Steven M.; **Paritala, Hanumantharao**; McDonnell, Jane E.; Thoden, James B.; Holden, Hazel M. "Identification of Inhibitors of N5-carboxyaminoimidazole Ribonucleotide Synthetase by High-throughput screening". *Bioorganic & Medicinal Chemistry* **2009**, 17(9), 3317-3323.
4. **Paritala, Hanumantharao**; Firestine, Steven M. "Benzo(h)quinoline Derivatives as G-quadruplex Binding Agents". *Bioorganic & Medicinal Chemistry Letters* **2009**, 19(6), 1584-1587.
5. Sambasivarao, S. V.; Soni, Love K.; Gupta, Arun K.; **Hanumantharao, P.**; Kaskhedikar, S. G. "Quantitative Structure-Activity Analysis of 5-arylidene-2, 4-thiazolidinediones as Aldose Reductase Inhibitors". *Bioorganic & Medicinal Chemistry Letters* **2006**, 16(3), 512-520.
6. **Hanumantharao, P.**; Sambasivarao, S. V.; Soni, L. K.; Gupta, A. K.; Kaskhedikar, S. G. "QSAR Analysis of Analogs of Bis[2-(acylamino) phenyl] disulfides, 2-(acylamino)benzenethiols and S-[2-(acylamino) phenyl] Alkanethioates as Antihyperlipidemic agents". *Indian Journal of Chemistry, Section B: Organic Chemistry Including Medicinal Chemistry* (**2005**), 44B (7), 1481-1486.
7. **Hanumantharao, P.**; Sambasivarao, S. V.; Soni, Love K.; Gupta, A. K.; Kaskhedikar, S. G. "QSAR Analysis of Thiazole Benzenesulfonamide Substituted 3-pyridylethanolamines as  $\beta$ 3-adrenergic Receptor Agonist". *Bioorganic & Medicinal Chemistry Letters* **2005**, 15(12), 3167-3173.
8. Sambasivarao, S. V.; **Hanumantharao, P.**; Kaskhedikar, S. G. "Status of Aldose reductase II inhibitors in Management of Non Insulin Dependent Diabetes Mellitus". *Indian Drugs* **2005**, 42(5), 261-267.
9. Gupta, A. K.; Soni, L. K.; **Hanumantharao, P.**; Sambasivarao, S. V.; Babu, M. Arockia; Kaskhedikar, S. G. "3D-QSAR Analysis of Some Cinnamic Acid Derivatives as Antimalarial Agents". *Asian Journal of Chemistry* **2004**, 16(1), 67-73.
10. Soni, L. K.; **Hanumantharao, P.**; Gupta, A. K.; Sambasivarao, S. V.; Kaskhedikar, S. G. "3D-QSAR Analysis of Oxadiazole Substituted Isopropoxyphenyl Propionic Acids as PPAR $\alpha$  and PPAR  $\gamma$  Agonists". *Indian Drugs* **2003**, 40(11), 627-635.